공학박사 학위논문

Highly Efficient Fluorescent Organic Light-Emitting Diodes using Delayed Fluorescence

지연형광을 이용한 고효율 형광 유기발광소자

2017년 8월

서울대학교 대학원

재료공학전공

선 진 원

Abstract

Highly Efficient Fluorescent Organic Light-Emitting Diodes using Delayed Fluorescence

Jin Won Sun
Department of Materials Science and Engineering
The Graduate School
Seoul National University

When organic light emitting diodes (OLEDs) appeared commercially aming to replace conventional display devices in early 2000s, it was not easy to guess OLEDs would become a dominant lighting source in display and lighting products industry. With ability of displaying colors in higher quality and wider viewing angle than those of liquid crystal display (LCD), and its adaptability to other technology from being able to be flexible and transparent, now OLEDs have become the ultimate display means. However, there are unsolved issues that need to draw our attention.

Competition rose between phosphorescent and fluorescent OLEDs especialy to take better position for the commercial blue OLED. Blue phosphorescent OLEDs exhibit highly efficient blue light, however the stability issue still need to be cleared and further, phosphorescent OLEDs are considered to be toxic for containing heavy metal complex. Therefore, blue fluorescent OLEDs are being used commercially in spite of their low EL efficiency from limitation of exciton production portion of singlet to ~25%.

Theoretically, if singlet-triplet splitting (ΔE_{ST}) is small enough, then reverse intersystem

crossing (RISC) can take place harvesting additional triplets in fluorescent OLEDs. In order to have small ΔE_{ST}, it is necessary to have spatial separation of the highly occupied molecular orbital (HOMO) and the lowest occupied molecular orbital (LUMO). Recently, by taking advantage of small ΔE_{ST}, efficient intra- and intermolecular charge transfer (CT) materials have been reported, which are referred to thermally activated delayed fluorescence (TADF) material and excited charge transfer complex (exciplex) system, respectively. Especially, OLEDs adopting exciplex system exhibit high EL efficiency from efficient energy transfer (ET) of host to dopant material and charge balance in emission layer (EML).

Further investigating into the method to boost EL efficiency in fluorescent OLEDs, there are sensitizing and heavy atom effect (HAE). Implementing phosphorescent or TADF material in EML working as assisted dopants in organized structure of cascading enegy levels of singlet and triplet among the constituents, improved EL efficiencies in fluorescent OLEDs were reported. Also, in CT type host material, HAE can be induced to improve EL efficiency of fluorescent OLED by enhancing mixing of singlet and triplet state taking advantage of both the sensitizing and HAE.

In this dissertation, the work is focused on the investigation of full potential of fluorescent OLEDs, especially blue fluorescent OLEDs, attempting to answer the series of questions: 1) Is it possible to turn all the triplets into light in fluorescent OLED? 2) Can there be efficient host system for blue fluorescent OLED? 3) Is it possible to achieve high EL efficiency and color purity in a same blue fluorescent OLED, simultaneously? 4) Is it possible to achieve high EL efficiency in conventional blue fluorescent OLEDs?

Starting from the first question of the possibility of achieving high EL efficiency in fluorescent OLED equivalent to that of phosphorescent OLED. In **Chapter 2**, 100% internal quantum efficiency (IQE) is achieved in a green fluorescent OLED exhibiting 30% external quantum efficiency (EQE) comparable to that of phosphorescent OLED. The OLED comprises an exciplex-forming cohost system doped with a fluorescent dye that has a strong delayed

fluorescence as a result of reverse intersystem crossing (RISC); the exciplex-forming cohosts contributed efficient ET and charge balance in the system. Large distribution of exciton in exciplex cohost lowered exciton density in EML resulting in the smallest efficiency roll-off among the other reported OLEDs using the same fluorescent emitter. The orientation of the transition dipole moment of the fluorescent dye is shown to have an influence on the EQE of the device.

Motivated by the result of the highly efficient green fluorescent OLED using exciplex cohost system in Chapter 2, the efficient mixed cohost system for blue fluorescent OLED was investigated in **Chapter 3**. Selecting host material for blue emitter is particulary difficult for the requirement of high triplet energy, therefore the majority of reported efficient blue fluorescent OLEDs have been dependent on the same single host material of high triplet energy, which arouse the second question for efficient host system for blue fluorescent OLEDs. The efficient mixed cohost suggested in this work boosted electorluminescence (EL) efficiency of the blue fluorescent OLED by fully utilizing the ability of blue TADF emitter. The EQE was increased from previously reported ~13% to 21.8% from perfect charge balance through bipolar character of the mixed cohost. The achieved EQE was the highest among the blue fluorescent OLEDs of the same emitting material in the single host. The achieved EQE was one of the highest EQEs in blue fluorescent OLEDs and identical to the theoretically achievable maximum EL efficiency using the emitter under consideration of none electrical loss.

Through the works in chapter 2 and 3, the fluorescent OLED was proven to be able to achieve the equivalent EL efficiency to that of phosphorescent OLED achieving 100% IQE, and highly efficient blue fluorescent OLED based on the mixed cohost was reported, therefore the motivation of further investigating into the potential of blue fluorescent OLEDs has risen. Despite of numerous reports on efficient blue fluorescent OLEDs, not many have achieved color purity and high EL efficiency at the same time. In **Chapter 4**, the mixed cohost was further utilized to realize deep blue emission and high EL efficiency at the same time using blue TADF emitter based on azasiline unit. For electroluminescence with delayed fluorescence, the azasiline unit has been

introduced for the first time as a donor in a TADF material. The TADF material of 5-(4-(4,6-diphenyl-1,3,5-triazin-2-yl)phenyl)-10,10-diphenyl-5,10-dihydrodibenzo[b,e][1,4]azasiline (DTPDDA) shows strong intramolecular CT character with large spatial separation with the acceptor of triazine leading to narrow splitting of singlet and triplet excited states for the efficient RISC. A blue OLED based on DTPDDA not only displayed deep blue emission in the Commission Internationale de L'Eclairage (CIE) coordinates of (0.149, 0.197) but also exhibited EQE of 22.3% which is the highest value ever reported for a blue fluorescent OLED. Theoretical prediction based on transient photoluminescence (PL) and optical simulation result agrees well with the achieved EQE indicating the successful conversion of triplet excitons to singlet in the blue fluorescent OLED by using DTPDDA.

In **Chapter 5**, further utilizing azasiline unit for blue TADF emitter, donor-connector-acceptor (D-C-A) and donor-acceptor-donor (D-A-D) type blue TADF emitters were implemented into the mixed cohost in order to investigate the full potential of blue fluorescent OLEDs based on azasilin unit. Utilizing the azasiline unit, 5-(4'-(4,6-diphenyl-1,3,5-triazin-2-yl)-[1,1'-biphenyl]-4-yl)-10,10- diphenyl-5,10-dihydrodibenzo[b,e][1,4]azasiline (DTPPDDA), the TADF blue emitter of D-C-A type resulted in deep blue emission with CIE coordinate of (0.151, 0.087), close to the blue standard of the National Television System Committee (NTSC) of (0.140, 0.080) with 4.7% EQE. In D–A–D type materials of bis(4-(10,10-diphenyldibenzo[b,e]-[1,4]azasilin-5(10H)-yl)phenyl)methanone (BDAPM) and 5,5'-(sulfonylbis(4,1-phenylene))bis(10,10-diphenyl-5,10-dihydro dibenzo[b,e][1,4]azasiline) (SPDDA), carbonyl and sulfone units were used as the acceptors where the azasiline moeity was used as the donor unit, respectively. The sulfonyl unit contributed to a large twist of the molecular structure while the carbonyl unit led to a small twist of the molecular structure. As a result, the blue fluorescent OLEDs containing BDAPM and SPDDA demonstrated 11.4% and 2.3% EQEs with CIE y-values of 0.310 and 0.107, respectively.

However, emitting from TADF material often shows broad EL spectrum due to strong CT state of the material, and the stability of the TADF based OLEDs still need to be improved. As an

alternative, conventional fluorophore can be used as an emitter, where assisted dopants either phosphorescent or TADF material is strategically implemented to enhance spin mixing of singlet and triplet excited states. Recently, the high EL efficiencies were reported from blue fluorescent OLEDs based on conventional blue fluorescent dye, taking advantage of TADF material as a sensitizer. With small ΔE_{ST} of TADF material, RISC can occur effectively harvesting additional triplet excitons. Also, adopting heavy metal compound of platinum or iridium enhances spin mixing of singlet and triplet from HAE, consequently EL efficiency of OLED can be improved. Even more, increased spin reversal of triplet to singlet was observed by taking advantage of CT state of host on the induction of HAE from iridium complex, eventually enhancing the singlet to triplet ratio ($\eta_{S/T}$). In **Chapter 6**, almost all the triplets were harvested in the conventional blue fluorescence OLED by promoting both sensitizing and HAE through co-doping TADF material and phosphorescent material into EML. Comparison of the theoretical and experimental data indicates that $\eta_{S/T}$ was increased from 0.23 to 0.94 with increased EQE from 5.6% to 12.3% in blue fluorescent OLED when the both TADF material and phosphorescent material were doped together as assisted dopants, indicating the nearly all the triplets harvested in the conventional blue fluorescent OLED.

Keywords: Organic light-emitting diodes, blue fluorescence, thermally activated delayed fluorescence, exciplex, triplet harvesting, reverse intersystem crossing, mixed cohost

Student Number: 2013-30181

Contents

Abstract ..... **i**

Contents ..... **vi**

List of Tables ..... **ix**

List of Figures ..... **x**

Chapter 1. Introduction **1**

1.1. Brief history of organic light-emitting diodes 1

1.2. Efficiency of OLEDs 3

1.3. Additional triplet harvest in fluorescent OLEDs 4

1.3.1. Thermally activated delayed fluorescence (TADF) 4

1.3.2. Intermolecular Charge Transfer complex (Exciplex) 7

1.4. Outline of the thesis 9

Chapter 2. A fluorescent organic light emitting diode with 30% external quantum efficiency **12**

2.1. Introduction 12

2.2. Experimental 13

2.3. Result and discussion 14

2.4. Conclusion 30

Chapter 3. Highly efficient sky-blue fluorescent organic light emitting diode based on mixed cohost system for thermally activated delayed fluorescence emitter (2CzPN) **31**

3.1. Introduction 31

3.2. Experimental.....33

3.3. Result and discussion.....34

3.4. Conclusion 46

Chapter 4. Thermally activated delayed fluorescence from azasiline based intramolecular charge-transfer emitter (DTPDDA) and a highly efficient blue light emitting diode 47

4.1. Introduction 47

4.2. Experimental.....49

4.3. Result and discussion.....51

4.4. Conclusion 69

Chapter 5. Azasiline-based thermally activated delayed fluorescence emitters for blue organic light emitting diodes 70

5.1. Introduction 70

5.2. Experimental.....72

5.3. Result and discussion.....74

5.4. Conclusion 103

Chapter 6. Almost all the triplets were harvested in conventional blue fluorescent organic light emitting diode 104

6.1. Introduction 104

6.2. Experimental.....106

6.3. Result and discussion.....107

6.4. Conclusion.....122

Chapter 7. Summary and Outlook.....123

Bibliography.....126

초록.....132

List of Publications.....135

List of Patents.....136

List of Awards.....137

List of Presentation.....138

List of Tables

Table 2.1 The voltage, current efficiency, EQE and power efficiency of the OLED. 21

Table 3.1 Voltage, current efficiency, current density, EQE, and power efficiency of the OLED. 45

Table 4.1 Comparison of LUMO and HOMO levels of DTPDDA and PXZ-TRZ through DFT calculations. 53

Table 4.2 X, Y, Z-Coordinates of DTPDDA with DFT calculation. 64

Table 4.3 The voltage, current efficiency, EQE, and power efficiency of the OLED. 68

Table 5.1 Device performances. $\eta_{S/T}$ indicates singlet-triplet factor. 83

Table 5.2 DFT Geometry of DTPPDDA. 84

Table 5.3 DFT Geometry of BDAPM. 89

Table 5.4 DFT Geometry of SPDDA. 94

Table 5.5 Max. EQEs of OLED devices of the TADF emitters in various doping ratios of 2, 8 and 16 wt% in the host of mCP:TSPO1. 99

Table 5.6 Singlet(S_1) & triplet(T_1) energy levels, Experimental and calculated singlet-triplet splittings($\triangle E_{ST}$) and prompt(τ_p) and delayed(τ_d) decay rates. 100

Table 5.7 Oscillator strength for the materials 101

Table 6.1 PLQYs, Estimated Singlet-triplet factors, Achieved and theoretical EQEs of the blue fluorescent OLEDs. 112

Table 6.2 Transient decay rates of the samples. 120

Table 6.3 Device performances of the blue fluorescent OLEDs of mCP:0.5 wt% TBPe, mCP:6 wt% DTPPDDA:0.5 wt% TBPe, mCP:8 wt% $(HFP)_2Ir(pic)$:0.5 wt%TBPe and mCP:6 wt% DTPPDDA:8 wt% $(HFP)_2Ir(pic)$:0.5 wt%TBPe. 121

List of Figures

Figure 1.1 Examples of commercial OLED devices; television (upper left; LG OLED TV), mobile phone adopting bendable OLED dispay (upper right; Samsung Galaxy S8), flexible OLED lighting and display devices are implemented for tail lamps in automobile (lower left; BMW M4, lower right; Audi) 2

Figure 1.2 Schematic representation of TADF mechanism.[3] 6

Figure 1.3 Potential energy diagram of exciplex formation and emission. 8

Figure 2.1 (a) Chemical structures of mCP, B3PYMPM and 4CzIPN. (b) Absorption spectrum of 4CzIPN and PL spectra of mCP:B3PYMPM film and mCP:B3PYMPM:5 wt% 4CzIPN film. 15

Figure 2.2 (a) Angle-dependent PL intensity of the *p*-polarized light from a 30-nm-thick film composed of mCP:B3PYMPM:5wt% 4CzIPN at 515 nm. Solid line represents the theoretical fit to the experimental data with the horizontal transition dipole ratio of 0.73. (b) Molecular structure of 4CzIPN. An arrow indicates the orientation of the transition dipole moment of the molecule. (c) Schematic diagram of the device structure and energy levels (eV) of the devices. (d) Contour plot of the predicted maximum EQEs as function of the thickness of HTL and ETL for green fluorescent OLEDs under the assumption of negligible electrical loss and both singlet and triplet excitons are havested as light in the OLEDs. A star represents the highest EQE of 29.6% achieved in this study where the thicknesses of HTL and ETL are 65 and 50 nm, respectively. 16

Figure 2.3 (a) Current density–voltage–luminance characteristics of the OLED. Inset: Angular distribution of the EL intensity of the OLED. The solid line represents the Lambertian distribution. (b) EQE and power efficiency of the optimized OLED with the thicknesses of HTL and ETL of 65 and 50 nm, respectively. 20

Figure 2.4. Current density–voltage–luminance characteristics of OLEDs (a) according to the thickness of ETL with the fixed thickness of HTL at 65nm and (b) according to the thickness of

HTL with the fixed thickness of ETL at 50nm. EQE and power efficiency of the OLEDs (c) according to the thickness of ETL with the fixed thickness of HTL at 65 nm and (d) according to the thickness of HTL with the fixed thickness of ETL at 50 nm. 24

Figure 2.5 Comparison of the experimental (circle) and simulated (dashed line) EQEs (a) as a function of the thickness of ETL with the fixed thickness of HTL at 65 nm, and (b) as a function of the thickness of HTL with the fixed thickness of ETL at 50 nm. 26

Figure 2.6 Efficiency roll-offs of the OLEDs in this work compared to the other reported OLEDs of 4CzIPN.[60-62] 27

Figure 2.7 Comparison of the experimental (dashed line) and the simulated (colored contour) angle dependent p-polarized PL spectrum of the mCP:B3PYMPM:5 wt% 4CzIPN film. 28

Figure 2.8 Optimized geometry and direction of transition dipole moment from S_1 to S_0 of 4CzIPN along (a) X, Y direction (b) Y, Z direction. 29

Figure 3.1 (a) Chemical structures of mCP, PO15 and 2CzPN. (b) The absorption and PL spectra of 2CzPN measured in methylene chloride and the PL spectra of mCP, PO15, mCP:PO15 and mCP:PO15:5 wt% 2CzPN were measured with 50 nm thick films on 1 mm thick fused silica. 35

Figure 3.2 (a). The film PL spectra of mCP, PO15, 2CzPN, 50 wt% mCP: 50 wt% 2CzPN, 50 wt% PO15 : 50 wt% 2CzPN, and mCP:5 wt% 2CzPN, and the EL spectrum of the blue OLED. (b) PL spectra of mCP:5 wt% 2CzPN, PBCB2CZ:5 wt% 2CzPN and TCTA:5 wt% 2CzPN. The film PL spectra were measured using 50 nm thick films deposited on precleaned fused silica substrates. Monochromatic light with the wavelength of 250 nm~330 nm, considering 2nd harmonic, from a Xenon lamp was used as the excitation source and a photomultiplier tube as the detector. (b) PL spectra of mCP:5 wt% 2CzPN, PBCB2CZ:5 wt% 2CzPN and TCTA:5 wt% 2CzPN. With the selection of different hosts for 2CzPN, the PL spectra were different from solvatochromic effect due to CT characteristics of the TADF material.

..... 36

Figure 3.3 (a) Angle-dependent PL intensity of the *p*-polarized light from a 30-nm-thick film

composed of mCP:PO15:5 wt% 2CzPN. Solid line represents the theoretical fit to the experimental data with the horizontal transition dipole ratio of 0.70. A continuous wave diode laser (405 nm, Edmund optics Inc.) was used as the excitation source and the incident angle of the excitation light was fixed at 45° from the plane normal direction of substrate and the *p*-polarized emitted light was detected at 480 nm. (b) Transient PL decays of mCP:PO15:5 wt% 2CzPN at room temperature. Inset: prompt fluorescence measured in the range of 0 to 10 ns after excitation. 39

Figure 3.4 (a) Schematic diagram of the device structure and energy levels (eV) of the device. (b) Contour plot of the predicted maximum EQE values as functions of the thickness of the p-HTL and n-ETL for blue fluorescent OLEDs under the assumption of negligible electrical loss and the assumption that both singlet and triplet excitons are harvested as light in the OLEDs. The star represents the highest EQE of 21.8% achieved in this study where the thicknesses of the HTL and ETL are 45 and 50 nm, respectively. 40

Figure 3.5 (a) Current density-voltage-luminance characteristics and (b) EQE of the blue fluorescent OLED. The reproducibility of the OLED is in the range of ±0.5 % EQE. Inset: EL spectrum of the OLED. (C) Comparison of the EQEs of the OLEDs of mCP:PO15:5 wt% 2CzPN (This Work), mCP:5 wt% 2CzPN (This Work) and PO15:5 wt% 2CzPN (This Work). The EQEs of previously reported OLEDs of mCP:5 wt% 2CzPN and PPT:5 wt% 2CzPN are added for comparison. The device structures for the EMLs evaluated in this work are identical to the one addressed in the manuscript, except the EMLs. 42

Figure 3.6 Angle-dependent PL intensities of the p-polarized light from a 30-nm-thick films of mCP:PO15:5 wt% 2CzPN and mCP:5 wt% 2CzPN. Solid line represents the theoretical fit to the experimental data with the horizontal transition dipole ratio of 0.70 and 0.69 for mCP:PO15:5 wt% 2CzPN and mCP:5 wt% 2CzPN, respectively. A continuous wave diode laser (405 nm, Edmund optics Inc.) was used as the excitation source and the incident angle of the excitation light was fixed at 45° from the plane normal direction of substrate and the p-polarized emitted light was detected at 480 nm. 44

Figure 4.1 (a) Chemical structure of DTPDDA. DFT calculation data: (b) Molecular structure of DTPDDA. (c) HOMO level at the phenyl-dibenzo azasiline unit. (d) LUMO level at the triphenyl triazine unit. 52

Figure 4.2 (a) The absorption spectrum of DTPDDA measured in toluene and PL spectra of DTPDDA in various solvents. Numbers in the brackets are the dielectric constants of the solvents. (b) The PL spectra of DTPDDA and TSPO1 measured in toluene and methylene chloride, espectively. The rest of the PL spectra of mCP, mCP:TSPO1, mCP:DTPDDA, TSPO1:DTPDDA and mCP:TSPO1:16 wt% DTPDDA were measured with 50 nm thick films on 1 mm thick fused silicas. Inset: the chemical structures of two hosts used for EML, mCP and TSPO1. mCP:DTPDDA, TSPO1:DTPDDA and mCP:TSPO1:16 wt% DTPDDA showed the emission solely from DTPDDA without the emission from the hosts, indicating that energy transfer from the host molecules to the dopant is efficient in this system. The photoluminescent quantum yield (PLQY) of the mCP:TSPO1:16 wt% DTPDDA film was 74 ± 2%. 56

Figure 4.3 (a) Prompt and delayed PL spectra of mCP:TSPO1: 16 wt% DTPDDA at 35 K. Prompt and delayed components were collected at 20 ns and 300 μs, respectively. (b) Transient PL decays of mCP:TSPO1:16 wt% DTPDDA film measured at 450 nm at temperature of 300 K and 35 K. Inset: Transient PL within the range of 0 to 50 ns after excitation. Red dotted line is the single exponential fitting with decay time of 11.8 ns for the prompt fluorescence. 58

Figure 4.4 (a) Schematic diagram of the device structure and energy levels (eV) of the device. (b) Contour plot of the predicted maximum EQEs as function of the thickness of HIL and EIL for blue fluorescent OLEDs. A star indicates the achieved EQE in this work. 59

Figure 4.5 (a) EL spectrum of the blue fluorescent OLED Inset : (top) the image of blue emission from the OLED. (bottom) A star denotes the CIE coordinate of the EL spectrum at (0.149, 0.197). (b) Current density-voltage-luminance characteristics of the OLED. Inset: Angular distribution of the EL intensity of the OLED. The solid line represents the Lambertian distribution. (c) EQE and power efficiency of the blue fluorescent OLED to current densities. 60

Figure 4.6 Angle-dependent PL intensities of the p-polarized light from 30-nm-thick films composed of mCP:TSPO1:16 wt% DTPDDA at 465nm. Solid lines represent theoretical fits to the experimental data. 63

Figure 5.1 Chemical structure, molecular structure, HOMO and LUMO of the emitters. 76

Figure 5.2 PL spectra of (a) DTPPDDA, (b) SPDDA and (c) BDAPM in various solvents. Numbers in the brackets are the dielectric constants of the solvents. (d) PL spectra of the host of mCP:TSPO1 and the emitters. Absorption and PL spectra of DTPPDDA, BDAPM and SPDDA were measured in toluene. PL spectra of mCP:TSPO1 and mCP:TSPO1:X wt% emitter were measured with 50 nm thick films on 1 mm thick fused silicas. Doping ratios were 8, 16 and 2 wt% for DTPPDDA, BDAPM and SPDDA, respectively. 77

Figure 5.3 Transient PL decays of (a) mCP:TSPO1: 8 wt% DTPPDDA, (b) mCP:TSPO1: 16 wt% BDAPM and (c) mCP:TSPO1: 2 wt% SPDDA films measured at the peak wavelengths of each materials at temperature of 300 K and 18 K. Insets : Prompt and delayed PL spectra measured at 18K for the estimation of S_1 and T_1. 78

Figure 5.4 (a) Schematic diagram of the device structure and energy levels (eV) of the device. (b) EL spectra of the blue fluorescent OLEDs Inset:CIE coordinates of the OLEDs in this work compared to that of NTSC. (c) Current density-voltage-luminance characteristics of the OLEDs. (d) EQEs of the blue fluorescent OLEDs to current densities. 81

Figure 5.5 Contour plot of the predicted maximum EQEs as a function of the thickness of HIL and EIL for OLED device of (a)DTPPDDA (b)BDAPM and (c)SPDDA. Stars indicate the achieved EQE in this work. 82

Figure 6.1 (a) Chemical structures of the materials used in this work. (b) Absorption and PL spectra of the materials. 109

Figure 6.2 (a) Time resolved PL spectra and (b) transient decays of all the samples for the EML. Inset of (b): transient decay mCP:0.5 wt% TBPe and mCP:6wt% DTPPDDA:0.5 wt% TBPe of

from excitation to 260 nm. 110

Figure 6.3 (a) Device structure, (b) EL spectra, (c) J-V-L and (d) EQEs of the blue fluorescent OLEDs. 111

Figure 6.4 (a) J-V-L and (b) EQEs of the OLEDs of mCP:B3PYMPM:0.5 wt% TBPe, mCP:B3PYMPM:10 wt% DTPPDDA:0.5 wt% TBPe, mCP:B3PYMPM:10 wt% Ir(ppz)3:0.5 wt% TBPe and mCP:B3PYMPM:10 wt% Ir(ppz)3:10 wt% DTPPDDA:0.5 wt% TBPe..... 113

Figure 6.5 Singlet and triplet energy levels of mCP,HFP_2(Ir)pic, DTPPDDA and TBPe..... 117

Figure 6.6 Transition dipole moment of TBPe measured with mCP:0.5 wt% TBPe film. 118

Figure 6.7 (a) singlet and triplet levels and (b) absorption and PL spectra of mCP: B3PYMPM, $Ir(ppz)_3$, DTPPDDA and TBPe. 119

Chapter 1. Introduction

1.1 Brief history of organic light-emitting diodes (OLEDs)

Organic light emitting diodes (OLEDs) are the device that converts electrical energy to light on the recombination of hole and electron injected from anode and cathode. OLEDs separate them from other display and lighting devices for their distinctive features of high color purity, fast response time and superior applicability. OLEDs can easily incorporate with various products from mobile phone, television and even automobile because depending on substrate, OLEDs can be transparent and flexible. (Figure 1.1) This year of 2017 marks the 30 years of anniversary since OLEDs based on heterojunction was firstly introduced by C. W. Tang et. al. in 1987, consisted of a hole-transport layer (HTL) and an electron-transport layer (ETL). He later discovered host-guest system in OLED devices using Alq3 as a host material, transferrering energy to dopant, however the electroluminescence efficiency was low from only ~25% of the excitons leading to optical emission in those fluorescent light-emitting materials.[1]

In 1998, M.A. Baldo et. al reported 100% internal quantum efficiency (IQE) from the OLED of phosphorescent material, where organometallic compound was utilized for harvesting triplet excitons from strong spin-orbit coupling. This research is often referred to create a base for commercializing OLEDs in industry.[2]

As the commercialization of OLEDs become successful, the need for high electroluminescence (EL) efficiency grew, especially in fluorescent OLEDs. One of the milestones in this era was C. Adachi et. al reported highly efficient fluorescent OLEDs based on thermally activated delayed fluorescence (TADF) where reverse intersystem crossing (RISC) takes place to harvest triplet excitons for light emission, from small singlet-triplet splitting (ΔE_{ST}).[3-4]

Figure 1.1 Examples of commercial OLED devices; television (upper left; LG OLED TV), mobile phone adopting bendable OLED dispay (upper right; Samsung Galaxy S8), flexible OLED lighting and display devices are implemented for tail lamps in automobile (lower left; BMW M4, lower right; Audi).

1.2 Efficiency of OLEDs

The efficiency of OLEDs can be judged by calculating photons per injected electrons, which is the external quantum efficiency (EQE) of OLEDs. The EQE can be described with internal quantum efficiency (IQE; η_{int}), and out-coupling efficiency (η_{out}), and can be defined as the equation below,[5]

$$\eta_{EQE} = \eta_{\text{int}} \times \eta_{out} = \gamma \times \eta_{S/T} \times q_{eff}(\phi_{PL}, \Gamma) \times \eta_{out}(\Theta, \Gamma) \quad (1)$$

,where γ is the charge balance factor, $\eta_{S/T}$ is the singlet-triplet exciton factor ($\eta_{S/T}$ =0.25 for fluorescent emitters and $\eta_{S/T}$ =1 for phosphorescent emitters), and q_{eff} is the effective radiative quantum yield of the emitter in the cavity structure. q_{eff} is a function of the photoluminescence quantum yield (PLQY) of the emitter (ϕ_{PL}), as well as the structure of the microcavity, including the position of the emission zone represented by Γ (a factor related to the device structure). The out-coupling efficiency η_{out} is a function of Γ and the proportion of horizontally oriented dipoles, $\Theta = (p_{\parallel} / p_{\parallel} + p_{\perp})$, where $p_{\parallel}$ and $p_{\perp}$ are the fractions of horizontal and vertical dipoles, respectively. As additional triplet takes part into emission process, $\eta_{S/T}$ can be increased, resulting in significant improvement of IQE in OLEDs.[3-4] Also, enhancing charge injection by *n*- or *p*- type dopants in the transport layers,[6-7] and achieving improved charge balance in emission layer (EML) can increase in charge balance leading to higher IQE.

1.3 Additional triplet harvest in fluorescent OLEDs

1.3.1 Thermally Activated Delayed Fluorescence (TADF)

On the electrical excitation, 25% of singlet and 75% of triplet excitons are formed on the recombination of injected charge carriers according to the spin statics. Therefore, phosphorescent material of metal-organic complex were used as sole means to harvest non-radiative triplet excitons.[2] However, even in metal-free fluorescent material, if singlet-triplet spitting (ΔE_{ST}) is small enough, then efficient spin-up conversion from non-radiative state to radiative singlet states can happen via reverse intersystem crossing (RISC) in thermally activated delayed fluorescence (TADF) material.[3] (see Figure 1.2)

The design rule for TADF material is the spatial separation of the highest occupied molecular orbital (HOMO) and the lowest unoccupied molecular orbital (LUMO), which forms intramolecular charge transfer (CT) state in a single molecule. Exchange energy decreases exponentially with increasing HOMO–LUMO separation distance. From strong CT character of the TADF material, TADF material typically shows linear solvatochromic shift in photoluminescence (PL) spectra to the increase of dielectric constants of adopted solvents. From RISC, delayed emission is usually observed from TADF material, increasing as the increase of temperature. However, for some cases, non-radiative transition from triplet state was larger than RISC rate, therefore delayed emission was increased in the lowest temperature from suppressing non-radiative transition from triplet state. TADF materials are not only being used as emitters but also used as assisted dopants even host materials, taking advtantage of their small ΔE_{ST}.[8]

Commercially, blue fluorescent OLEDs are being used in spite of low electroluminescence (EL) efficiency for poor stability and toxicity of blue phosphorescent OLEDs. Therefore, investigation of efficient blue TADF based OLEDs is necessary at this point. Recently, EQE over ~30% was reported in blue fluorescent OLED using TADF emitter, and separately deep blue emission was realized in the Commission Internationale de L'Eclairage (CIE) coordinates of (0.149, 0.197).[9-10] However, reports on simultaneously achieving both deep blue emission

(CIE(y)<0.2), and high EL efficiency in blue fluorescence OLEDs are scarce. Furthermore, emitting from TADF material expose drawbacks of broad EL spectrum deteriorating color purity and short device lifetime.

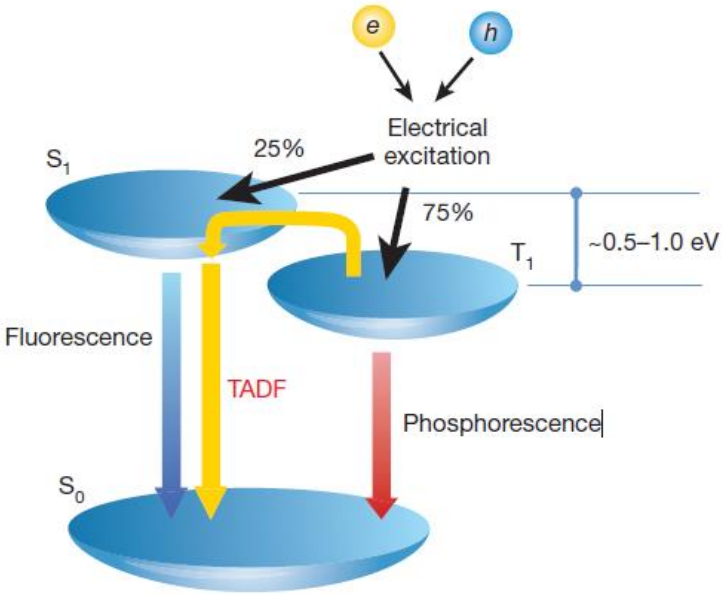

Figure 1.2 Schematic representation of TADF mechanism.[3]

1.3.2 Intermolecular charge transfer complex (Exciplex)

An excited intermolecular charge-transfer (CT) complex is the exciplex which is associated of differing molecule between electron-donating and electron-accepting molecules under photo- and electrical excitation. The CT state occurs with the independent excited donor (D*) and an excited acceptor (A*) molecues. Exciplex is repulsive in ground state and attractive in excited state as shown in Figure 1.3. For complex consisted of the sam molecules referred to excited state dimer (excimer) which is a common phenonmenon for aromatic molecules especially if the singlet state lifetime is long.

Since exciplex emission orginate from the lowest unoccupied molecular orbital (LUMO) of an acceptor and the highest occupied molecular orbital (HOMO) of a donor, newly formed HOMO-LUMO in exciplex contribute to small exchange energy which is proportional to the gap of singlet and triplet states (ΔE_{ST}). HOMO and LUMO of exciplex are located at two different molecules, therefore exciplex should have triplet level close to singlet level smaller than that of intramolecular CT material (TADF). Hence, reverse intersystem crossing (RISC) should be efficient in exciplex.

Exciplex emission occurs following Frank-Condon principle, from the minimum of excited state to ground state. Therefore, photoluminescence (PL) spectrum of exciplex is red-shifted to those of donor and acceptor molecules and featurless from indefinite vibrational character of the ground state.[11]

Previously reported OLEDs adopting exciplex system demonstrated efficient device performance in terms of external quantum efficiency (EQE), low driving voltage and efficiency roll-off from combined advantage of efficient energy transfer (ET) to dopant, charge balance and low exciton density due to broad recombination zone.[12-20]

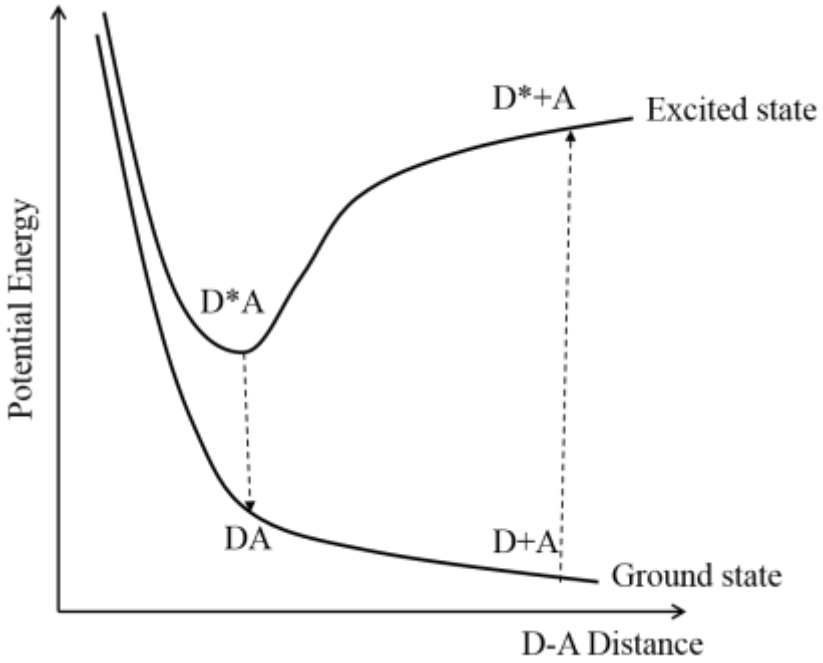

Figure 1.3 Potential energy diagram of exciplex formation and emission.

1.4 Outline of the thesis

In this thesis, we investigate fluorescent organic light emitting diodes (OLEDs) in order to realize high electroluminescence (EL) efficiency, especially blue fluorescent OLEDs.

100% internal quantum efficiency (IQE) was achieved with a green fluorescent OLED exhibiting 30% external quantum efficiency (EQE). The OLED comprises the exciplex-forming co-host system of N,N′-dicarbazolyl-3,5-benzene (mCP) and bis-4,6-(3,5-di-3-pyridylphenyl)-2-methylpyrimidine (B3PYMPM) doped with the fluorescent dye of (4s,6s)-2,4,5,6-tetra(9H-carbazol-9-yl)isophthalonitrile (4CzIPN) that has a strong delayed fluorescence as a result of reverse intersystem crossing (RISC). The exciplex-forming cohosts stimulate energy transfer and charge balance in the system. From using exciplex cohost, recombination zone was broad lowering exciton density, which showed the smallest efficiency roll-off among the OLEDs of 4CzIPN. The orientation of the transition dipole moment of the fluorescent dye was shown to have an influence on the EQE of the device. (Chapter 2)

The mixed cohosts of mcP and 2,8-bis(diphenylphosphoryl)dibenzothiophene (PO15) have been developed for a highly efficient blue fluorescent OLED doped with a thermally activated delayed fluorescence (TADF) emitter [4,5-di (9H-carbazol-9-yl) phthalonitrile (2CzPN)]. We have demonstrated one of the highest external quantum efficiency of 21.8% in blue fluorescent OLEDs, which is identical to the theoretically achievable maximum EL efficiency using the emitter. Interestingly, the efficiency roll-off is large even under the excellent charge balance in the device and almost the same as the single host based devices, indicating that the efficiency roll-off in 2CzPN based TADF host is related to the material characteristics, such as low reverse intesystem crossing rate rather than charge imbalance. (Chapter 3)

For electroluminescence with delayed fluorescence, the azasiline unit has been introduced for the first time as a donor in a TADF material. The TADF material of 5-(4-(4,6-diphenyl-1,3,5-triazin-2-yl)phenyl)-10,10-diphenyl-5,10-dihydrodibenzo[b,e][1,4]azasiline (DTPDDA) showed strong intramolecular charge transfer (CT) character with large spatial separation with the

acceptor of triazine leading to narrow splitting of singlet and triplet excited states for the efficient RISC. The blue organic light emitting diode (OLED) based on DTPDDA not only displays deep blue in the Commission Internationale de L'Eclairage (CIE) coordinates of (0.149, 0.197) but also exhibits a high EQE of 22.3% which is the highest value ever reported for a blue fluorescent OLED. Theoretical prediction based on transient photoluminescence (PL) and optical simulation result agrees well with the achieved EQE indicating the successful conversion of triplet excitons to singlet in the blue fluorescent OLED by using DTPDDA. (Chapter 4)

Further utilizing the azasiline unit, 5-(4′-(4,6-diphenyl-1,3,5-triazin-2-yl)-[1,1′-biphenyl]-4-yl)-10,10-diphenyl-5,10-dihydrodibenzo[b,e][1,4]azasiline (DTPPDDA) in the formation of donor–connector–acceptor (D–C–A) materials resulted in deep blue emission with CIE coordinate of (0.151, 0.087), close to the blue standard of the National Television System Committee (NTSC) of (0.140, 0.080) with 4.7% EQE. In the donor–acceptor–donor (D–A–D) type materials of bis(4-(10,10-diphenyldibenzo[b,e][1,4]azasilin-5(10H)-yl)phenyl)methanone (BDAPM) and 5,5′-(sulfonylbis(4,1-phenylene))bis(10,10-diphenyl-5,10-dihydrodibenzo[b,e][1,4]azasiline) (SPDDA), carbonyl and sulfone units were used as the acceptors, respectively. The sulfonyl unit contributed to a large twist of the molecular structure while the carbonyl unit led to a small twist of the molecular structure. As a result, the blue fluorescent OLEDs containing BDAPM and SPDDA demonstrated 11.4% and 2.3% EQEs with CIE y-values of 0.310 and 0.107, respectively. (Chapter 5)

Almost all the triplets were harvested in the conventional blue fluorescence OLED using a blue fluorophore of 2,5,8,11-tetra-tert-butylperylene (TBPe) as the emitter by promoting both sensitizing and heavy atom effect (HAE) through co-doping TADF material of DTPPDDA and phosphorescent material of bis-2-(2,4-difluoro-3-(perfluoropropyl)phenyl)-4-methylpyridine-Ir Ⅲ-picolinate ((HFP)2Ir(pic)) into emitting layer (EML). Comparison of the theoretical and experimental data indicates that the singlet to triplet ratio ($\eta_{S/T}$) was increased from 0.23 to 0.94 with increased EQE from 5.6% to 12.3% in blue fluorescent OLED when the both TADF material

of DTPPDDA and phosphorescent material of (HFP)2Ir(pic) were doped together as assisted dopants. (Chapter 6)

Chapter 2. A Fluorescent Organic Light-Emitting Diode with 30% External Quantum Efficiency

2.1 Introduction

Over the past two decades, phosphorescent organic light-emitting diodes (PhOLEDs) based on heavy metal complexes have been recognized as the sole solution for achieving 100% internal quantum efficiency (IQE) by harvesting both singlet and triplet excitons as light. Recently, however, fluorescent OLEDs showing a delayed emission without any heavy-metal complexes have attracted tremendous attention as a promising solution for simultaneously obtaining high external quantum efficiency (EQE), low cost, and stability of the device.[3-4,13,15,21-25] These fluorescent materials are able to harvest triplet excitons as well as singlet excitons under electrical excitation via reverse intersystem crossing (RISC) from the triplet (T_1) to singlet (S_1) state due to the low energy gap between the two states—normally below 0.1 eV. Ideally, 100% IQE can be achieved, leading to around 30% EQE in the fluorescent OLEDs, if the efficiency of the RISC is unity. However, the highest reported EQE of the fluorescent OLEDs is below 20%,[25] which is still much lower than the ~30–35% EQE achieved by PhOLEDs.[5,12,26-34]

In this article, a green fluorescent OLED with 30% EQE corresponding to almost 100% IQE is demonstrated. It comprises an exciplex-forming host doped with a fluorescent dye, (4*s*,6*s*)-2,4,5,6-tetra(*9H*-carbazol-9-yl)isophthalonitrile (4CzIPN), which shows strong delayed fluorescence through RISC. The exciplex-forming host was introduced to stimulate energy transfer and charge balance in the system.[5, 12,28-30, 32-34] In addition, the orientation of the transition dipole moment of the fluorescent dye influencing the EQE of the device will be discussed.

2.2 Experimental

The OLEDs were fabricated on clean glass substrates pre-patterned with 70-nm-thick ITO under a pressure of 5×10^{-7} Torr by thermal evaporation without breaking the vacuum. Before the deposition of organic layers, the ITO substrates were pre-cleaned with isopropyl alcohol and acetone, and then exposed to UV–ozone for 10 minutes. Organic layers were deposited at a rate of 1 Å/s, and the deposition rate of co-deposited layers was 1 Å/s in total.

Current density, luminance, and EL spectra were measured using a programmable source meter (Keithley 2400) and a spectrophotometer (Spectrascan CS100, Photo Research). The angular distribution of the EL was measured with a programmable source meter (Keithley 2400), goniometer, and fiber optic spectrometer (Ocean Optics S2000). The EQE and the power efficiency of the OLEDs were calculated from current density−voltage−luminance characteristics, EL spectra, and the angular distribution of the EL intensity.

Geometry optimizations and calculations of the transition dipole moments of 4CzIPN were performed using B3LYP-level theory and the 6–31G(d) basis set for all the other atoms with Gaussian09.[45]

Orientation of the transition dipole moments was measured using a continuous wave diode laser (405 nm, Edmund optics Inc.). The incident angle of the excitation light was fixed at 45° from the plane normal direction of the substrate, and the p-polarized emitted light was detected at 515 nm, which is close to the peak wavelength of the PL spectrum of the fluorescent dye.

Cyclic voltammetry was performed on a VSP versatile modular potentiostat, and data were analyzed using EC-LAB. A platinum wire was used as the counter-electrode, and a platinum disk was used as the working electrode.

2.3 Result and discussion

N,*N*′-dicarbazolyl-3,5-benzene (mCP) and bis-4,6-(3,5-di-3-pyridylphenyl)-2-methylpyrimidine (B3PYMPM) at a molar ratio of 1:1 were selected as the cohosts for 4CzIPN. Figure 2.1 shows the chemical structures of mCP, B3PYMPM, and 4CzIPN; the emission spectra of mCP:B3PYMPM and mCP:B3PYMPM:(5 wt% 4CzIPN) films; and the absorption spectrum of the 4CzIPN film. The cohost system efficiently formed an exciplex upon photo-excitation, manifested by a featureless photoluminescence (PL) spectrum, which was red-shifted from the spectra of mCP and B3PYMPM.[33] The normalized PL spectrum of the mCP:B3PYMPM film doped with 5 wt% 4CzIPN showed emission entirely from 4CzIPN with the peak position at 515 nm (optical energy gap of 2.58 eV),[3] indicating that the energy transfer from the exciplex to the fluorescent dopant is efficient. The efficient energy transfer is expected from the large spectral overlap between the exciplex emission and the absorption of 4CzIPN.

The photoluminescent quantum yield (PLQY) of the mCP:B3PYMPM:(5 wt% 4CzIPN) film was 97 ± 3%; it was measured in an integrating sphere using a He–Cd laser (325 nm) as an excitation source.[35] The PLQY value is close to that reported in the literature.[3] Almost 100% PLQY of the mCP:B3PYMPM:(5 wt% 4CzIPN) film is attributed to the efficient energy transfer from the host to 4CzIPN and the efficient blocking of the non-radiative decay processes of the excited states of 4CzIPN.

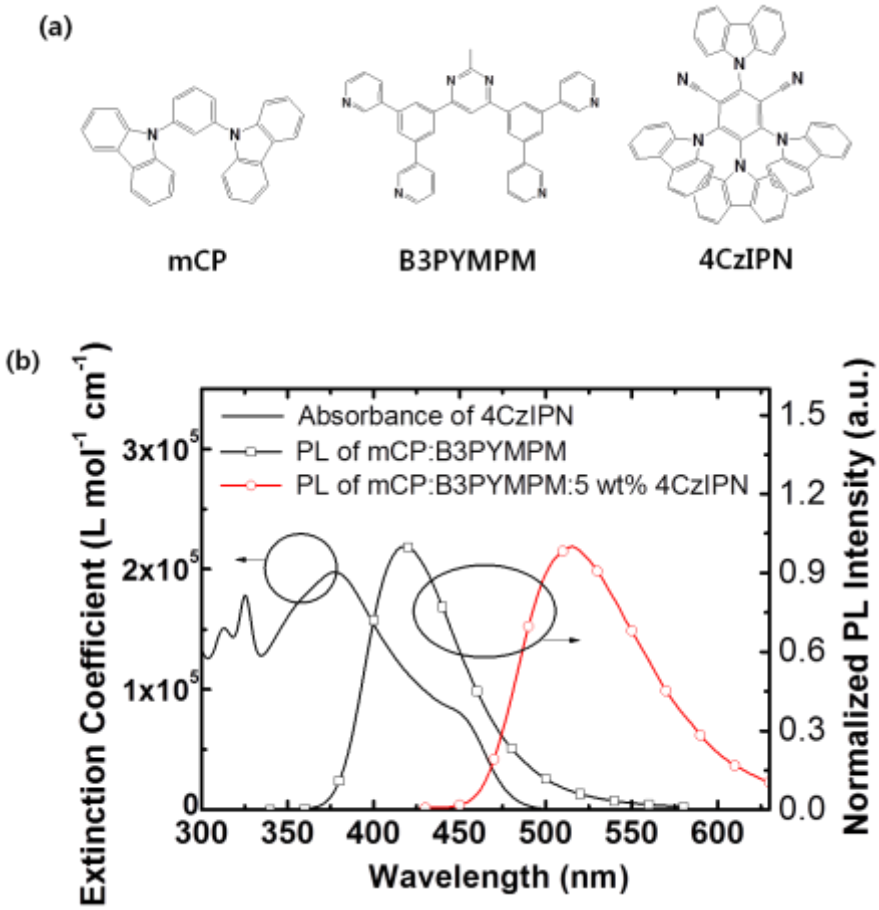

Figure 2.1 (a) Chemical structures of mCP, B3PYMPM and 4CzIPN. (b) Absorption spectrum of 4CzIPN and PL spectra of mCP:B3PYMPM film and mCP:B3PYMPM:5 wt% 4CzIPN film.

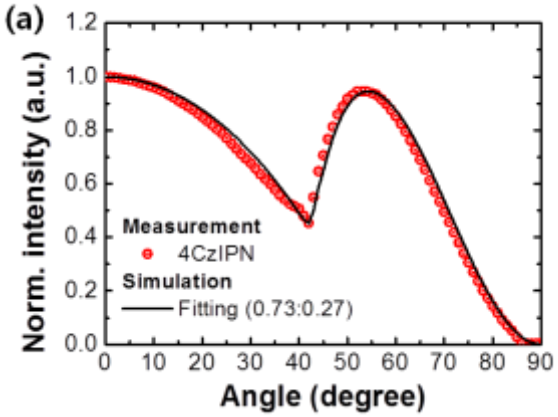
(a)
Norm. intensity (a.u.)
Angle (degree)
Measurement
4CzIPN
Simulation
Fitting (0.73:0.27)

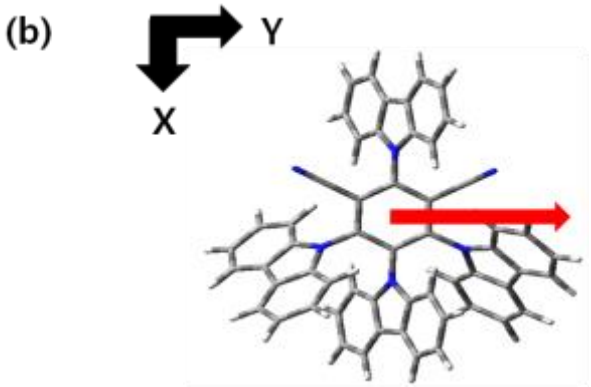
(b)
Y
X

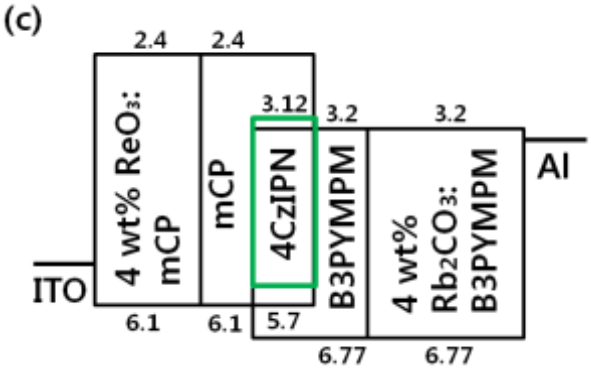
(c)
ITO
4 wt% ReO3: mCP
mCP
4CzIPN
B3PYMPM
4 wt% Rb2CO3: B3PYMPM
Al
2.4
2.4
3.12
3.2
3.2
6.1
6.1
5.7
6.77
6.77

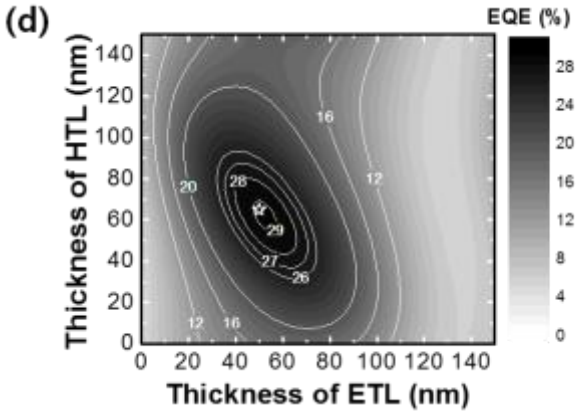
(d)
EQE (%)
Thickness of HTL (nm)
Thickness of ETL (nm)

Figure 2.2 (a) Angle-dependent PL intensity of the *p*-polarized light from a 30-nm-thick film composed of mCP:B3PYMPM:5wt% 4CzIPN at 515 nm. Solid line represents the theoretical fit to the experimental data with the horizontal transition dipole ratio of 0.73. (b) Molecular structure of 4CzIPN. An arrow indicates the orientation of the transition dipole moment of the molecule. (c) Schematic diagram of the device structure and energy levels (eV) of the devices. (d) Contour plot of the predicted maximum EQEs as function of the thickness of HTL and ETL for green fluorescent OLEDs under the assumption of negligible electrical loss and both singlet and triplet excitons are havested as light in the OLEDs. A star represents the highest EQE of 29.6% achieved in this study where the thicknesses of HTL and ETL are 65 and 50 nm, respectively.

Since 4CzIPN shows strong delayed fluorescence, efficient triplet harvesting is also expected by RISC with negligible triplet loss. The higher T_1 levels of mCP, B3PYMPM, and the exciplex of mCP:B3PYMPM—that is, 2.90, 2.68, and 2.97 eV, respectively,[33] higher than that of 4CzIPN with a T_1 level = 2.50 eV—guarantees efficient exciton confinement to 4CzIPN and prohibits backward energy transfer from 4CzIPN to the host materials.

Orientation of the transition dipole moment of 4CzIPN in the mCP:B3PYMPM:(5 wt% 4CzIPN) film was measured using the angle-dependent p-polarized PL spectrum of the mCP:B3PYMPM:(5 wt% 4CzIPN) film on a fused silica substrate to simulate the outcoupling efficiency and optimum device structure.[5,32,36-38] The angle-dependent PL intensity was consistent with the horizontal transition dipole ratio (Θ) of 0.73 for 4CzIPN as shown in Figure 2.2a, where Θ is defined as the ratio of the horizontal portion of the dipoles to the total dipoles. Geometry optimization in the ground state and the transition dipole moment of the 4CzIPN molecule were further calculated using density functional theory (DFT) and time-dependent DFT to elucidate the orientation of the molecule. The calculation showed that the molecule has a flat planar structure along the x and y direction as shown in Figure 2.2b. This shape of the molecule typically enables stacking parallel to the substrate. In addition, the transition dipole moment of 4CzIPN is parallel to the x and y directions, leading to the strong preferred orientation parallel to the substrate. Based on the measured values of Θ = 0.73 and PLQY = 0.97 for 4CzIPN, optical simulation was performed under the assumption of negligible electrical loss to predict the maximum achievable EQE of the fluorescent OLEDs as a function of the thickness of the hole-transporting layer (HTL) and electron-transporting layer (ETL).[5] Both singlet and triplet excitons are also assumed to be harvested as light. The device structure used in the simulation was ITO (indium tin oxide, 70 nm)/mCP (X nm)/mCP:B3PYMPM:(5 wt% 4CzIPN) (30 nm)/B3PYMPM (Y nm)/Al (100 nm), as shown in Figure 2.2c. Figure 2.2d shows that a 29.3% EQE is achievable in the fluorescent OLED with 4CzIPN in the case of X = 65 nm and Y = 50 nm. The star in the EQE contour plot represents the highest experimental data actually achieved in this study.

The structure of the fabricated device was slightly modified from the simulated one by

inserting a hole-injection layer (HIL; *p*-doped mCP) and an electron-injection layer (EIL; *n*-doped B3PYMPM) to demonstrate the efficient charge injection.[40-44] The device structure (Figure 2.2c) is as follows: ITO (70 nm)/(4 wt% ReO_3):mCP (A nm)/mCP (15 nm)/mCP:B3PyMPM:(5 wt% 4CzIPN) (30 nm)/B3PYMPM (20 nm)/(4 wt% Rb_2CO_3):B3PYMPM (B nm)/Al (100 nm). The values used for the thicknesses of the HTL and ETL in the simulation (X and Y nm) correspond to the sum of the thickness of the *p*- or *n*-doped layers (A or B nm) and the intrinsic charge transporting layers (15 nm); this can be explained as follows: A nm + 15 nm = X nm for HTL and B nm + 15 nm = Y nm for ETL.

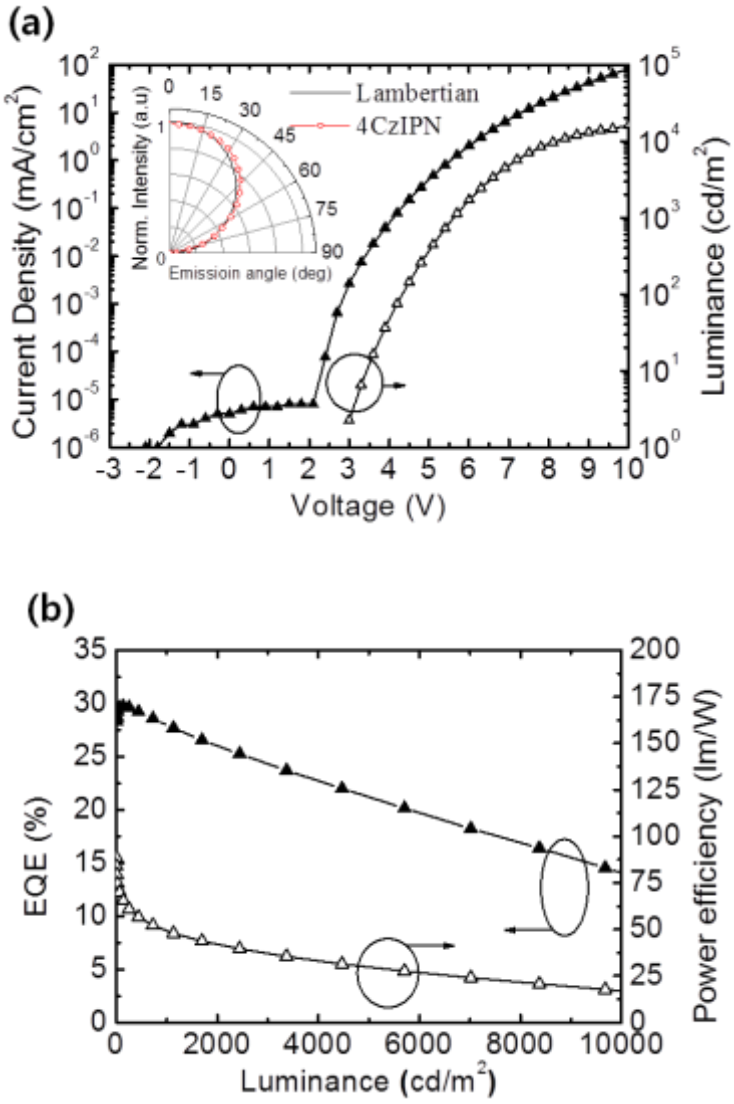

Figure 2.3 (a) Current density–voltage–luminance characteristics of the OLED. Inset: Angular distribution of the EL intensity of the OLED. The solid line represents the Lambertian distribution. (b) EQE and power efficiency of the optimized OLED with the thicknesses of HTL and ETL of 65 and 50 nm, respectively.

Table 2.1 The voltage, current efficiency, EQE and power efficiency of the OLED.

Voltage [V]			Current Efficiency [cd/A]			EQE [%]			Power Efficiency [lm/W]		
Turn on	1,000 cd/m^2	10,000 cd/m^2	Max.	1,000 cd/m^2	10,000 cd/m^2	Max.	1,000 cd/m^2	10,000 cd/m^2	Max.	1,000 cd/m^2	10,000 cd/m^2
3.0	5.6	8.1	94.5	88	46	29.6	27.8	14.5	88.6	49	17.7

The highest occupied molecular orbital (HOMO) level of 4CzIPN was defined as 5.7 eV based on the cyclic voltammetry (CV) measurements, and the lowest unoccupied molecular orbital (LUMO) was 3.12 eV.

Figure 2.3a and b shows the current density−voltage−luminance (J−V−L) characteristics and the calibrated efficiencies of the optimized fluorescent OLED, respectively. The factor used for the calibration of efficiency was 1.02, which was obtained from a pattern that is broader than the Lambertian curve on the angular distribution of the electroluminescence (EL) intensity of the OLED as shown in the inset of Figure 2.3a. The turn-on voltage of the OLED was 3.0 V, and a luminance of 1000 cd/m^2 was obtained at 5.6 V. The device surprisingly exhibited a high maximum EQE of 29.6% and a maximum current efficiency of 94.5 cd/A, which is consistent with the simulation results. The efficiencies are by far the highest values achieved for fluorescent OLEDs, and they are very close to the highest efficiencies of PhOLEDs reported up to now. However, the efficiency roll-off is large with EQE values of 27.8% at 1000 cd/m^2 and 14.5% at 10 000 cd/m^2, probably due to large triplet–triplet annihilation coming from the long triplet exciton lifetime of 4CzIPN. The voltage, current efficiency, EQE, and power efficiency of the OLED at different luminance values are sorted in Table 1. The origin of the large efficiency roll-off is currently under investigation and will be reported separately.

To validate the device simulation results shown in Figure 2.2c, seven different fluorescent OLEDs with different HTL and ETL thicknesses (X,Y) were fabricated, and the device performance values are provided in Figure 2.4. Figure 2.5a and b compare the experimentally obtained EQEs with the simulation results at fixed thicknesses of HTL and ETL, respectively. As expected, the efficiencies are more sensitive to the thickness variation of the ETL than that of the HTL because of the interference effect of the reflected light from the cathode. Both figures show that the achieved maximum EQEs of the OLEDs with different ETL and HTL thicknesses agree very well with predicted theoretical EQEs within an uncertainty range of ±2% for Θ and ±3% for PLQY, where the electrical loss could be assumed to be negligible in the devices. Hence, it is very

clear that the EQE that is close to the theoretical limit has been achieved in the fluorescent OLEDs harvesting all the singlet and triplet excitons without electrical loss. Efficiency roll-offs of the OLEDs in this study was the smallest among the reported OLEDs of 4CzIPN, from low exciton density owing to large recombination zone of exciplex. (Figure 2.6)

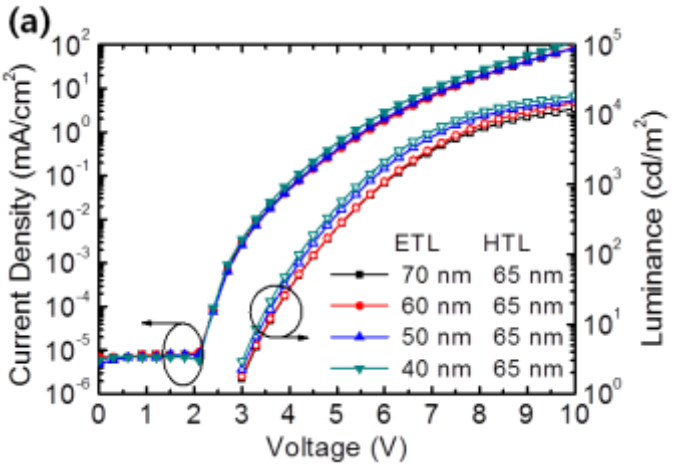
(a)
Current Density (mA/cm^2)
Luminance (cd/m^2)
Voltage (V)
ETL HTL
70 nm 65 nm
60 nm 65 nm
50 nm 65 nm
40 nm 65 nm

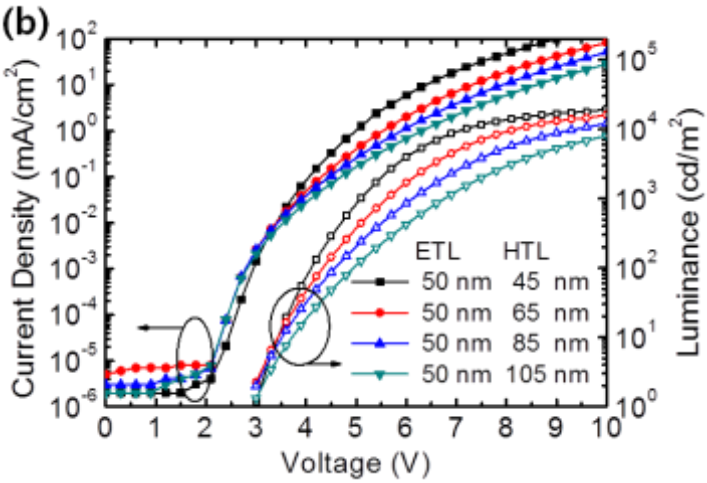
(b)
Current Density (mA/cm^2)
Luminance (cd/m^2)
Voltage (V)
ETL HTL
50 nm 45 nm
50 nm 65 nm
50 nm 85 nm
50 nm 105 nm

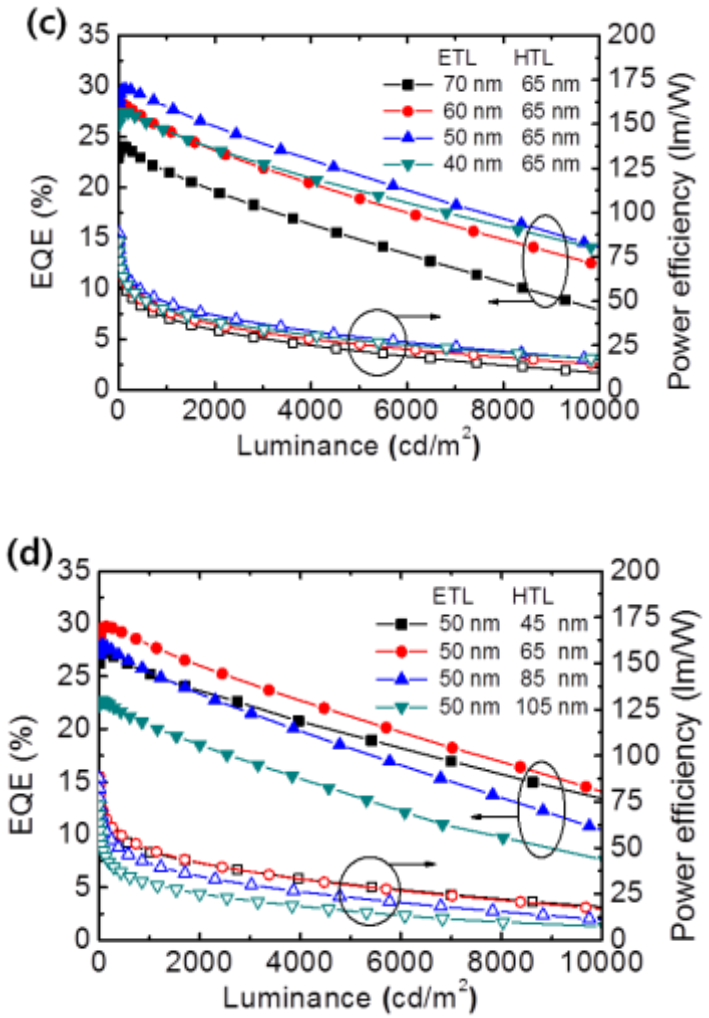

Figure 2.4. Current density–voltage–luminance characteristics of OLEDs (a) according to the thickness of ETL with the fixed thickness of HTL at 65nm and (b) according to the thickness of HTL with the fixed thickness of ETL at 50nm. EQE and power efficiency of the OLEDs (c) according to the thickness of ETL with the fixed thickness of HTL at 65nm and (d) according to the thickness of HTL with the fixed thickness of ETL at 50nm.

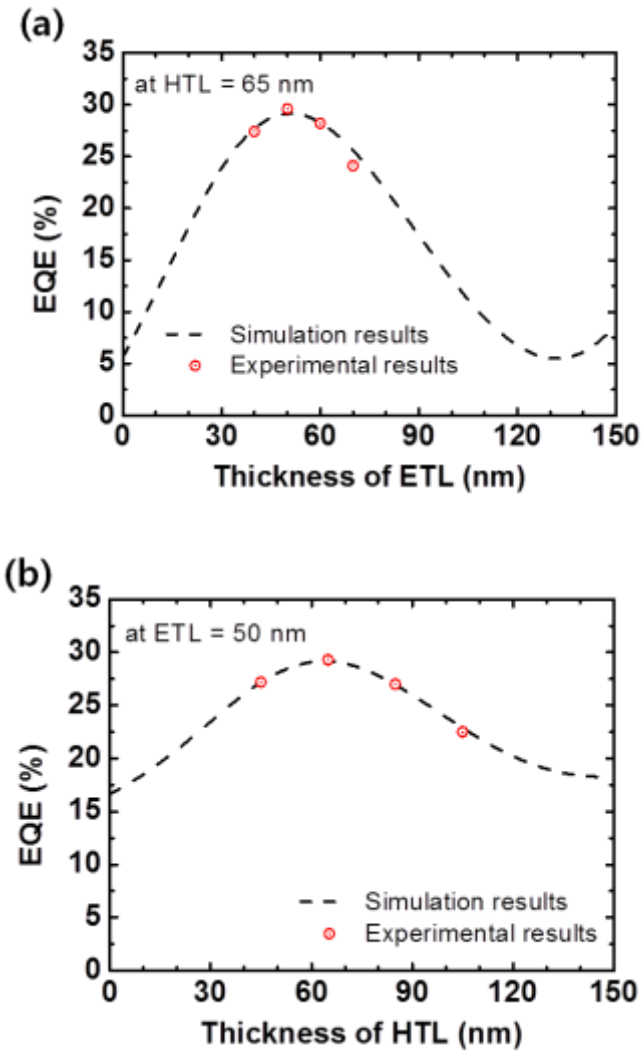

Figure 2.5 Comparison of the experimental (circle) and simulated (dashed line) EQEs (a) as a function of the thickness of ETL with the fixed thickness of HTL at 65 nm, and (b) as a function of the thickness of HTL with the fixed thickness of ETL at 50 nm.

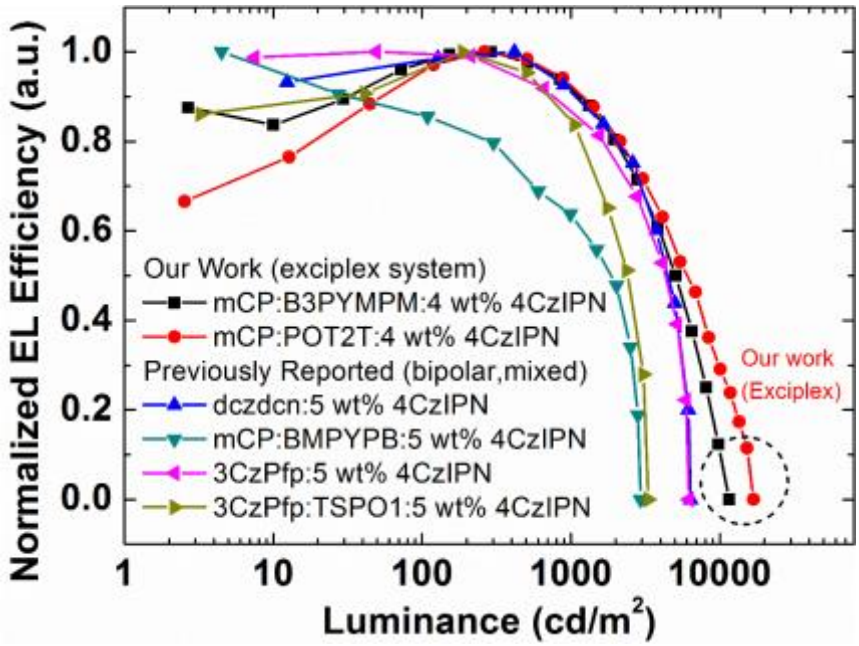

Figure 2.6 Efficiency roll-offs of the OLEDs in this work compared to the other reported OLEDs of 4CzIPN.[60-62]

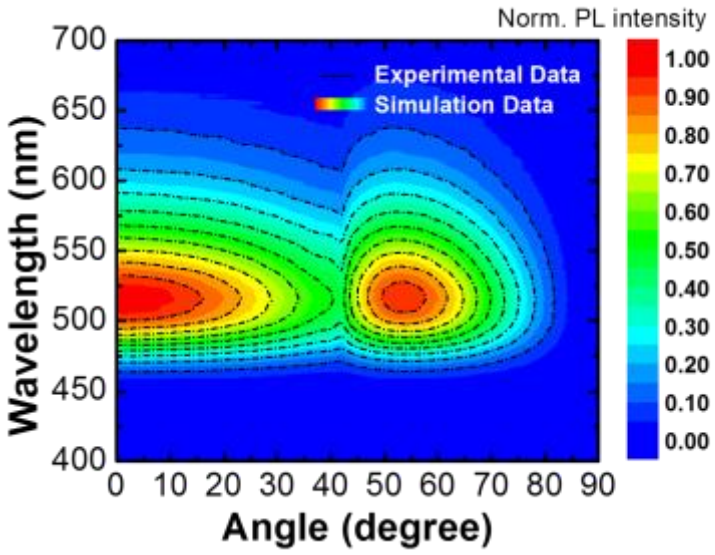

Figure 2.7 Comparison of the experimental (dashed line) and the simulated (colored contour) angle dependent p-polarized PL spectrum of the mCP:B3PYMPM:5 wt% 4CzIPN film.

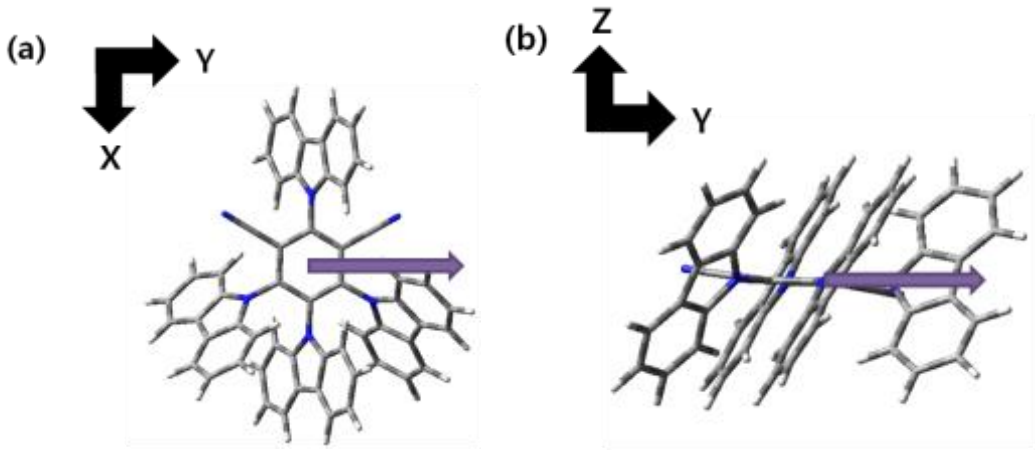

Figure 2.8 Optimized geometry and direction of transition dipole moment from S_1 to S_0 of 4CzIPN along (a) X, Y direction (b) Y, Z direction.

2.4 Conclusion

In summary, we have demonstrated a green fluorescent OLED with a maximum EQE of ~30%, which corresponds to almost 100% IQE, using 4CzIPN as the emitter in an exciplex-forming cohost system composed of mCP and B3PYMPM. The EQE is very close to the highest values for PhOLEDs, indicating that the fluorescent OLED harvested not only all the singlet excitons but also all the triplet excitons via RISC without electrical loss. The results clearly demonstrate that fluorescent OLEDs can perform as well as PhOLEDs.

Chapter 3. A highly efficient sky-blue fluorescent organic light emitting diode based on mixed co-host system for thermally activated delayed fluorescence emitter (2CzPN)

3.1 Introduction

Thermally activated delayed fluorescence (TADF) draws more and more attention because of its capacity to harvest triplet excitons to light in organic light emitting diodes (OLEDs). Blue emitting TADF materials and devices are especially attractive because low efficiency fluorescent molecules are in use in commercial products. Many efficient blue fluorescent OLEDs based on TADF materials have been reported including the report with the high external quantum efficiency (EQE) of 20.6%.[3,25,46-53] However, it is under question if the potential of the blue TADF emitters have been fully materialized in terms of efficiency. For example, 4,5-di (9H-carbazol-9-yl) phthalonitrile (2CzPN) which is known as an efficient TADF material emitting sky-blue showed the EQE of 13.6% although 2CzPN has a high photoluminescence quantum yield (PLQY) over 85%. The EQE of the device must be higher than the reported value if the triplets in OLEDs are sufficiently converted to singlet excitons.

In addition to the development of the TADF materials with good color purity, good stability, and high photoluminescence quantum yield, selection of a proper host and charge transporting materials along with the optimization of device structures are required to fully capitalize the potential of the materials by achieving good electrical balance and maximizing outcoupling efficiency. Double emitting layers, bipolar hosts, mixed hosts, and exciplex forming hosts instead of hole or electron transporting single hosts have been developed to realize good charge balance without electrical loss in conventional fluorescent and phosphorescent OLEDs.[28,54-58] However, most of blue TADF OLEDs adopted single hosts probably because of the difficulties in selecting host materials satisfying the requirements of high triplet levels, the low energy barrier for charge injection from electron and hole transporting layers and balanced electron and hole

mobilities.[3,25,46-50]

Through ambipolar transport of a mixed host in emitting layer (EML), charge balance can be improved in OLEDs. In this study, we have developed a mixed host consisting of a hole transporting material and an electron transporting materials for blue TADF OLEDs and demonstrated a highly efficient blue fluorescent OLED with 21.8% of EQE using 2CzPN as the TADF dopant in a mixed host. It is one of the most efficient blue fluorescent OLEDs. Additionally, theoretical calculation revealed that the EQE of 21.8% is indeed the maximum achievable efficiency using 2CzPN as the blue dopant, indicating that the mixed host gives little electrical loss and efficient triplet harvesting to realize efficient blue OLEDs in general. Origin of efficiency roll-off in 2CzPN based TADF OLEDs will be discussed by comparing the characteristics between the OLEDs of the different hosts.

3.2 Experimental

The OLEDs were fabricated on clean glass substrates pre-patterned with 70-㎚-thick ITO under a pressure of 5×10^{-7} Torr by thermal evaporation without breaking the vacuum. Before the deposition of organic layers, the ITO substrates were pre-cleaned with isopropyl alcohol and acetone, and then exposed to UV–ozone for 10 minutes. Organic layers were deposited at a rate of 1 Å/s, and the deposition rate of co-deposited layers was 1 Å/s in total.

Current density, luminance, and EL spectra were measured using a programmable source meter (Keithley 2400) and a spectrophotometer (Spectrascan CS100, Photo Research). The angular distribution of the EL was measured with a programmable source meter (Keithley 2400), goniometer, and fiber optic spectrometer (Ocean Optics S2000). The EQE and the power efficiency of the OLEDs were calculated from current density−voltage−luminance characteristics, EL spectra, and the angular distribution of the EL intensity.

Orientation of the transition dipole moments was measured using a continuous wave diode laser (405 nm, Edmund optics Inc.). The incident angle of the excitation light was fixed at 45° from the plane normal direction of the substrate, and the p-polarized emitted light was detected at 470 nm, which is close to the peak wavelength of the PL spectrum of the fluorescent dye.

Cyclic voltammetry was performed on a VSP versatile modular potentiostat, and data were analyzed using EC-LAB. A platinum wire was used as the counter-electrode, and a platinum disk was used as the working electrode.

PL spectra of the organic materials were measured using samples thermally deposited on fused silica under a vacuum of 5×10^{-7} Torr. The samples were excited with a He/Cd laser (325 nm) to detect PL using a photomultiplier tube attached to a monochromator.

Transient PL was measured by using a pulsed N_2 laser (KEN-2X, USHO) as the excitation light source and a streak camera (C10627, Hamamatsu) as the optical detection system.

3.3 Result and discussion

1,3-Bis(N-carbazolyl)benzene (mCP) and 2,8- bis(diphenylphosphoryl)dibenzothiophene (PO15) were selected as the cohosts for EML with the molar ratio of 1:1 for 2CzPN considering their higher singlet and triplet energies than those of 2CzPN to prevent the triplet excited state of 2CzPN from quenching by triplet energy transfer to the host molecules.[33,59] The molecular structures of the materials are shown in Figure 3.1a. The absorption spectrum of 2CzPN and photoluminescence (PL) spectra of all the materials used in this work are shown in Figure 3.1b. The UV–vis absorption spectrum of 2CzPN was measured in methylene chloride (MC) using a UV–vis–NIR spectrophotometer (Agilent, Cary-5000). The photoluminescence spectra of the materials except 2CzPN were measured using 50 nm thick films deposited on precleaned fused silica substrates. Monochromatic light with the wavelength of 250 nm from a xenon lamp was used as the excitation source and a photomultiplier tube as the detector (Photon Technology International). Large overlap of the emission spectra of the mixed cohosts of mCP:PO15 with the absorption spectrum of 2CzPN and the almost identical PL spectrum of the 2CzPN doped (5 wt %) mixed host film with the PL of the 2CzPN indicate that the energy transfer from the hosts to the TADF dopant takes place in the doped EML. Neither mCP nor PO15 forms an exciplex with 2CzPN as manifested in Figure 3.2a and 3.2b.

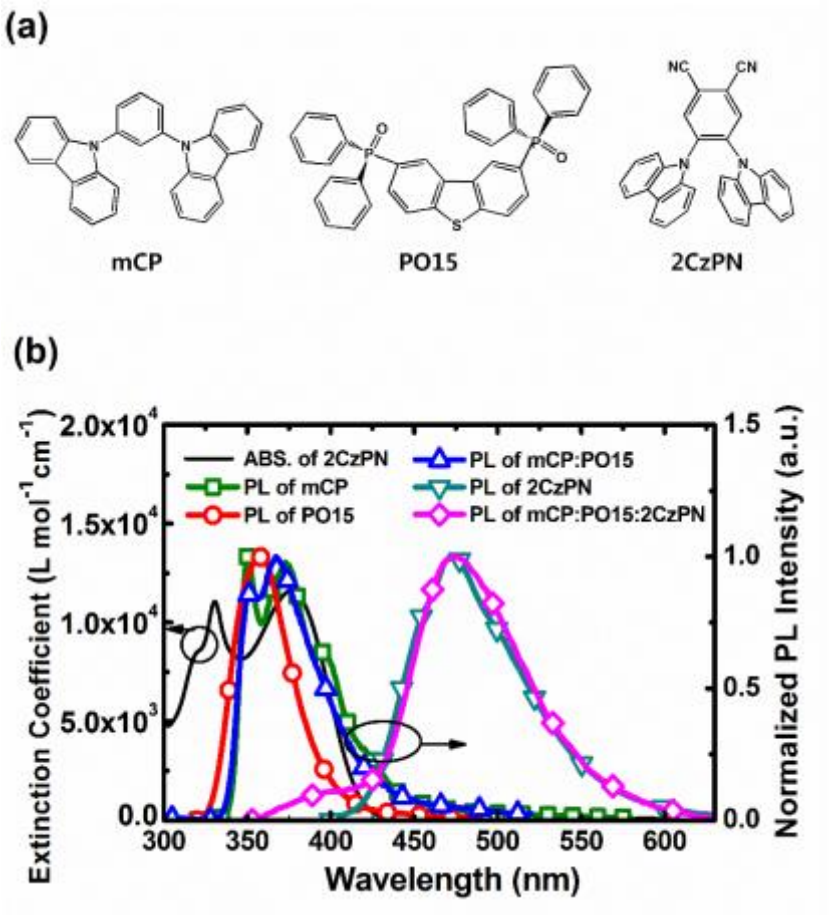

Figure 3.1 (a) Chemical structures of mCP, PO15 and 2CzPN. (b) The absorption and PL spectra of 2CzPN measured in methylene chloride and the PL spectra of mCP, PO15, mCP:PO15 and mCP:PO15:5 wt% 2CzPN were measured with 50 nm thick films on 1 mm thick fused silica.

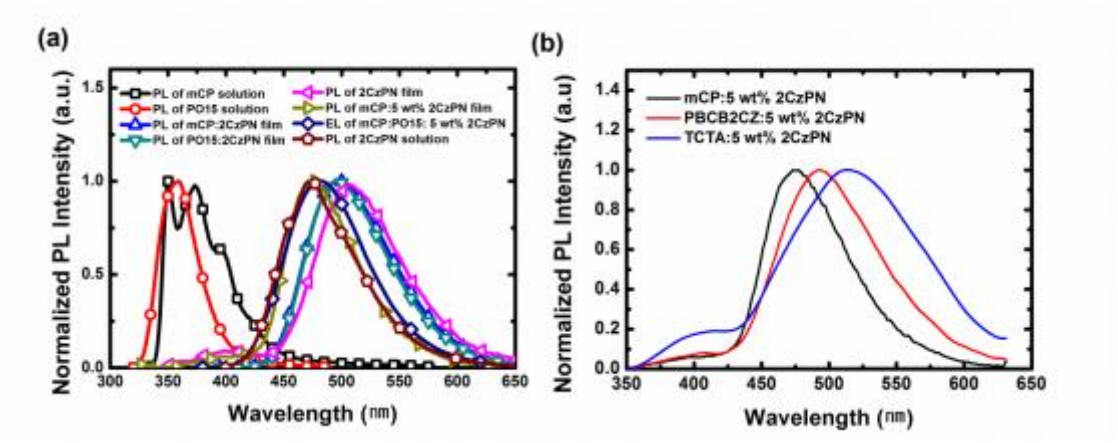

Figure 3.2 (a). The film PL spectra of mCP, PO15, 2CzPN, 50 wt% mCP: 50 wt% 2CzPN, 50 wt% PO15 : 50 wt% 2CzPN, and mCP:5 wt% 2CzPN, and the EL spectrum of the blue OLED. (b) PL spectra of mCP:5 wt% 2CzPN, PBCB2CZ:5 wt% 2CzPN and TCTA:5 wt% 2CzPN. The film PL spectra were measured using 50 nm thick films deposited on precleaned fused silica substrates. Monochromatic light with the wavelength of 250 nm~330 nm, considering 2nd harmonic, from a Xenon lamp was used as the excitation source and a photomultiplier tube as the detector. With the selection of different hosts for 2CzPN, the PL spectra were different from solvatochromic effect due to CT characteristics of the TADF material.

The PL spectra shift of 2CzPN in the different hosts must come from solvatochromic effect due to charge transfer (CT) nature of the TADF material of 2CzPN. The weak emission from the host near the wavelength of 425 nm indicates that the energy transfer from the host to 2CzPN is not 100% in the EML on photoexcitation, however under electrical excitation as shown later, the host emission disappeared in the EL spectrum due to direct charge trapping on the dopant in addition to energy tranfer.

The PLQY and the orientation of the transition dipole moment of 2CzPN molecules in the mCP:PO15:5 wt % 2CzPN film were measured using an integrating sphere and from the angle dependent PL spectra, respectively.[35-38] The PLQY of mCP:PO15:5 wt % 2CzPN was 84 ± 2% which is close to the reported one.[46] The horizontal emitting dipole ratio was 70% as shown in Figure 3.3a. The transient PL from the mCP:PO15:5 wt % 2CzPN showed that multiexponential decays fitted well with the prompt lifetime of 16 ns and four delayed lifetimes of 36 ns, 7 μs, 226 μs, and 897 μs (Figure 3.3b), which was measured using a streak camera (C4334, Hamamatsu Photonics) excited by a nitrogen gas laser at a wavelength of 337 nm with a pulse width of 500 ps (MNL200, Lasertechnik). The reason for the four components in the transient decay is not clear yet, and it is under investigation now. The portion of the prompt and the delayed emission intensity in PL calculated from the transient PL decay at room temperature (RT) was 0.62:0.38, resulting in the total, prompt, and delayed PLQYs of 84%, 52%, and 32%, respectively. Maximum achievable internal quantum efficiency (IQE) of OLEDs using the dye can be calculated by considering PLQYs and reverse intersystem crossing (RISC) efficiency (80%).[46] Maximum achievable IQE of the OLEDs was estimated to be 74%.

The structure of the OLED based on the emitting layer was optimized theoretically to maximize the outcoupling efficiency using the classical dipole model.[5] The device structure shown in Figure 3.4a was used for the simulation with the experimentally determined PLQY and horizontal portion of transition dipole moment of the 2CzPN in the emitting layer. mCP and PO15 were used not only as the cohosts but also as the hole transporting layer (HTL) and electron

transporting layer (ETL) in the device, respectively, to remove the charge injection barriers from the charge transporting layers to the EML. The *p*-doped HTL (4 wt % ReO3:mCP layer) and the *n*-doped ETL (4 wt % Rb2CO3:PO15 layer) were inserted as the hole and electron injection layers in the device to enhance charge injection from the electrodes to the HTL and ETL, respectively.[39-44] The thickness of the *p*-HTL and *n*-ETL were systematically varied to find the optimum thicknesses to calculate the EQEs with the fixed thickness of 15 nm for the HTL, ETL and EML. Maximum outcoupling efficiency of 29.4% was predicted when the thicknesses of the *p*-HTL and *n*-ETL were 45 and 50 nm, respectively (Figure 3.4b). Combined with the estimated IQE of 74%, the maximum achievable EQE was predicted to be 21.8% for this OLED under assumption of little electrical loss (charge balance factor =1).[5]

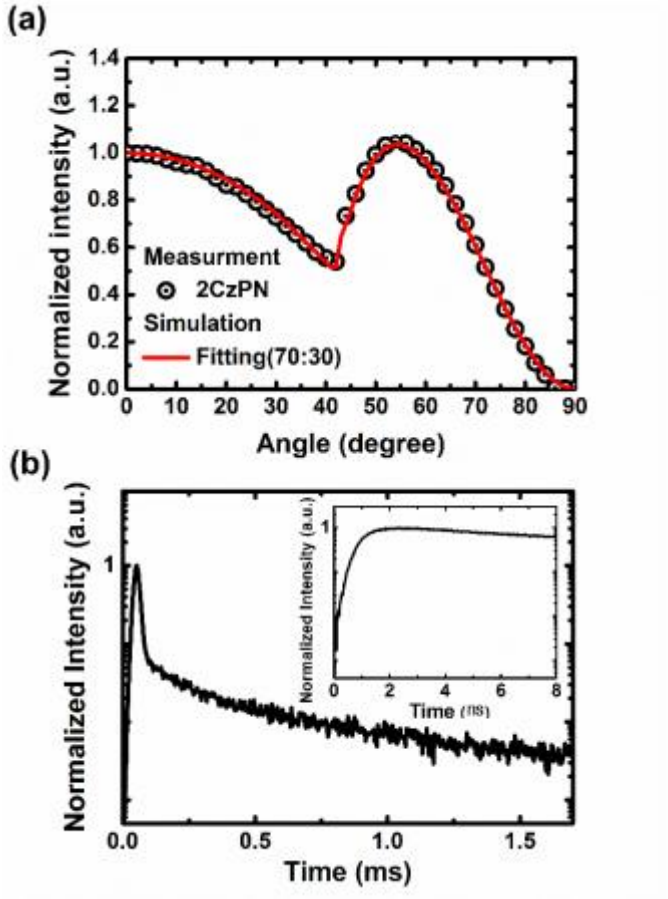

Figure 3.3 (a) Angle-dependent PL intensity of the *p*-polarized light from a 30-nm-thick film composed of mCP:PO15:5 wt% 2CzPN. Solid line represents the theoretical fit to the experimental data with the horizontal transition dipole ratio of 0.70. A continuous wave diode laser (405 nm, Edmund optics Inc.) was used as the excitation source and the incident angle of the excitation light was fixed at 45° from the plane normal direction of substrate and the *p*-polarized emitted light was detected at 480 nm. (b) Transient PL decays of mCP:PO15:5 wt% 2CzPN at room temperature. Inset: prompt fluorescence measured in the range of 0 to 10 ns after excitation.

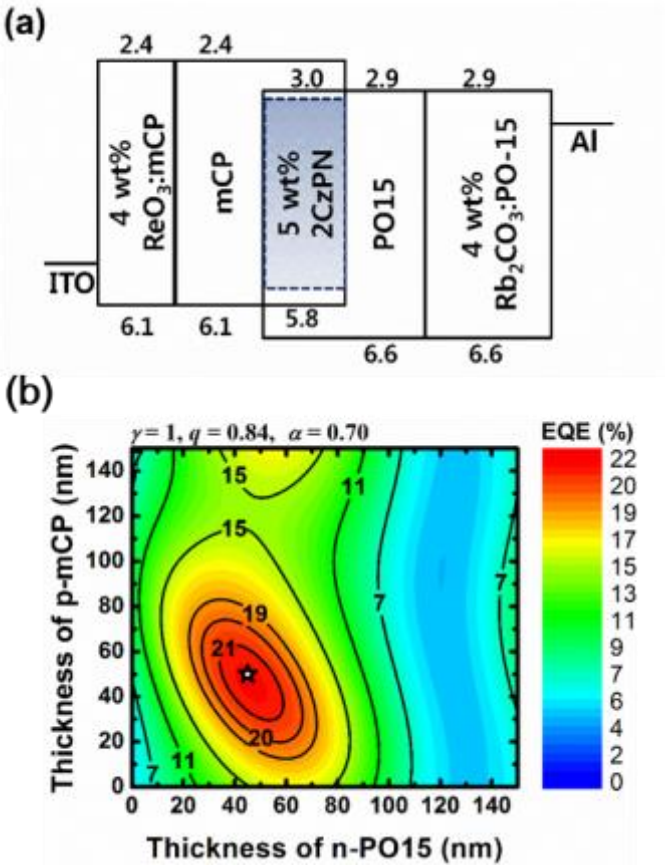

Figure 3.4 (a) Schematic diagram of the device structure and energy levels (eV) of the device. (b) Contour plot of the predicted maximum EQE values as functions of the thickness of the p-HTL and n-ETL for blue fluorescent OLEDs under the assumption of negligible electrical loss and the assumption that both singlet and triplet excitons are harvested as light in the OLEDs. The star represents the highest EQE of 21.8% achieved in this study where the thicknesses of the HTL and ETL are 45 and 50 nm, respectively.

The current density–voltage–luminance characteristics of the OLED are shown in Figure 3.5a. The turn-on voltage of the OLED was 3.0 V, which is comparable to those of previously reported efficient blue fluorescent OLEDs and the driving voltage at 1000 cd/m2 was 6.4 V.[3,25,46-50] The device emits sky blue fluorescence with the Commission Internationale de L'Eclairage (CIE) coordinates of (0.17, 0.27) and with the peak wavelength of 480 nm which was 7 nm red-shifted from the PL spectrum due to the cavity effect of the device (inset of Figure 3.5b). The device exhibited the EQE of 21.8% (Figure 3.5b), which is much higher than the previously reported 13.6% obtained from the device using 2CzPN doped in a single host.[46] Furthermore, the OLED using the mixed cohost of mCP:PO15 demonstrated higher EL efficiency than the OLEDs of single hosts of mCP and PO15 as shown in Figure 3.5c.

Since the PLQYs and horizontal dipole ratios of 2CzPN in the single host of mCP and the mixed cohosts (Figure 3.6) are almost the same, EL efficiency of the blue fluorescent OLED was boosted by improved electron and hole balance achieved by adopting the mixed cohosts with optimized device structure. The experimentally obtained EQE was identical to the theoretically calculated maximum achievable EQE, indicating that this fluorescent OLED based on the mixed cohosts showed little electrical loss.

As shown in Figure 3.5c, the comparison of roll-offs of this work to the previously reported OLEDs shows that the roll-offs of the OLEDs using 2CzPN are rather large. Large efficiency roll-offs in the OLED with the mixed host possessing excellent charge balance indicates that the roll-offs originate from quenching of excitons such as singlet–triplet annihilation (STA) and triplet–triplet annihilation (TTA) due to the slow RISC rate of 2CzPN rather than electron–hole imbalance. Therefore, a TADF material with high singlet radiative rate and high RISC rate to lower triplet density should be synthesized to improve the efficiency roll-offs in blue TADF OLEDs.

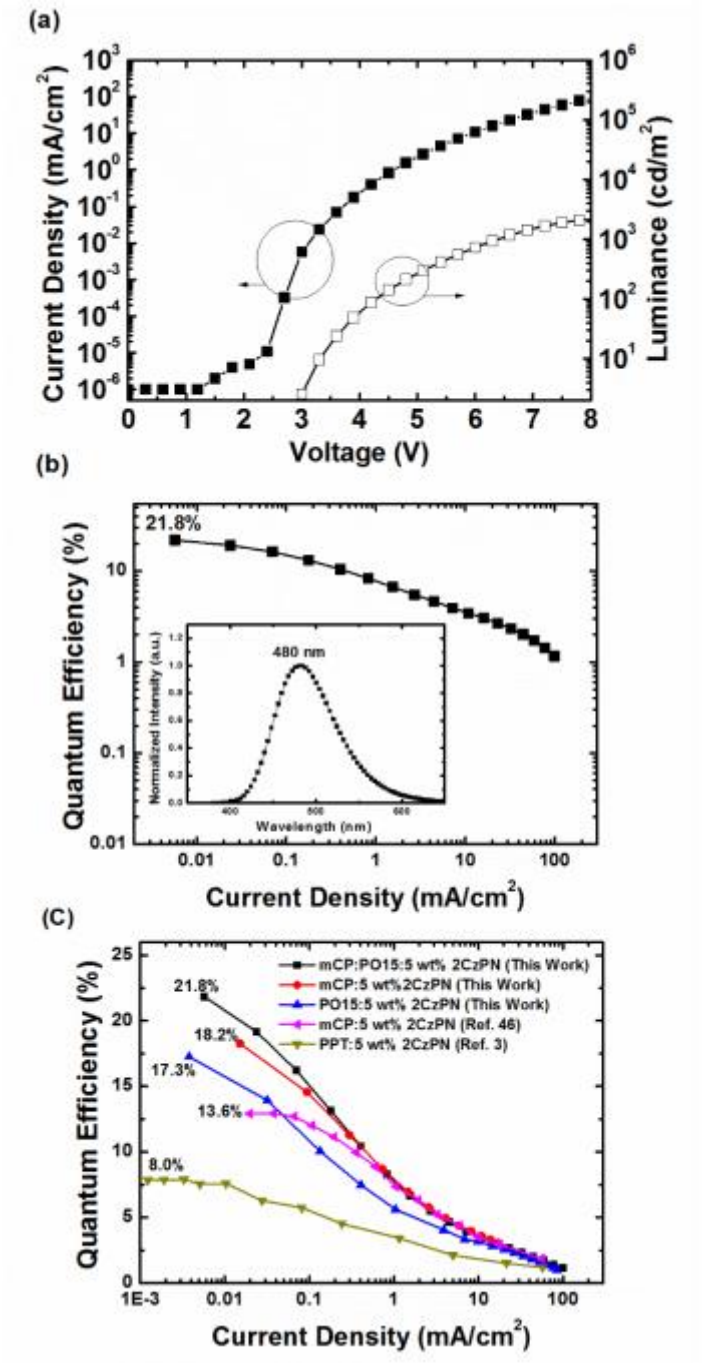

Figure 3.5 (a) Current density-voltage-luminance characteristics and (b) EQE of the blue fluorescent OLED. The reproducibility of the OLED is in the range of ±0.5 % EQE. Inset: EL spectrum of the OLED. (C) Comparison of the EQEs of the OLEDs of mCP:PO15:5 wt% 2CzPN (This Work), mCP:5 wt% 2CzPN (This Work) and PO15:5 wt% 2CzPN (This Work). The EQEs of previously reported OLEDs of mCP:5 wt% 2CzPN and PPT:5 wt% 2CzPN are added for

comparison. The device structures for the EMLs evaluated in this work are identical to the one addressed in the manuscript, except the EMLs.[3,46]

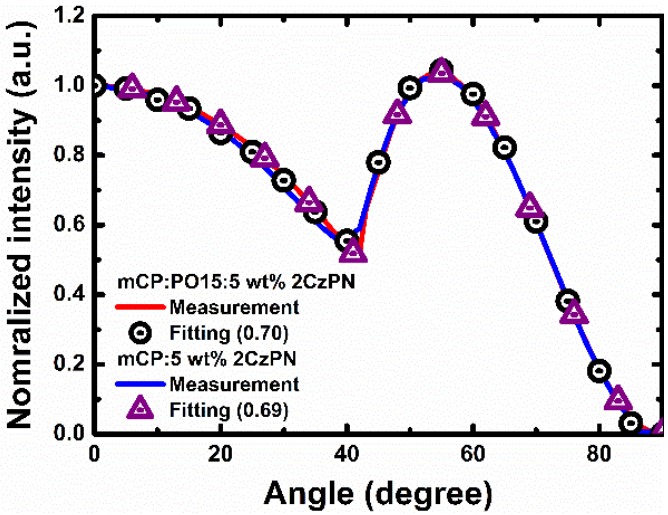

Figure 3.6 Angle-dependent PL intensities of the p-polarized light from a 30-nm-thick films of mCP:PO15:5 wt% 2CzPN and mCP:5 wt% 2CzPN. Solid line represents the theoretical fit to the experimental data with the horizontal transition dipole ratio of 0.70 and 0.69 for mCP:PO15:5 wt% 2CzPN and mCP:5 wt% 2CzPN, respectively. A continuous wave diode laser (405 nm, Edmund optics Inc.) was used as the excitation source and the incident angle of the excitation light was fixed at 45º from the plane normal direction of substrate and the p-polarized emitted light was detected at 480 nm.

Table 3.1 Voltage, current efficiency, current density, EQE, and power efficiency of the OLED.

	Turn on^{+}/Max.$^{\perp}$	1,000 cd/m^2	2,000 cd/m^2
Voltage [V]	3^{+}	6.4	7.6
Current Density [mA/cm^2]	5.7×10^{-3}$^{+}$	22	60
Current Efficiency [cd/A]	45.3$^{\perp}$	5.5	3
EQE [%]	21.8$^{\perp}$	2.8	1.6
Power Efficiency [lm/W]	47.4$^{\perp}$	3	1.4

3.4 Conclusion

In summary, we have demonstrated a highly efficient blue fluorescent OLED with the EQE of 21.8% using the mixed cohosts of mCP:PO15 doped with 2CzPN. Theoretical calculation showed that the blue fluorescent OLED with the mixed host used in this work pushed the device performance toward the theoretical limit by fullly utilizing the ability of the dopant. Efficiency roll-off is very large even in the OLED with excellent charge balance, indicating that the roll-off originates from the exciton quenching probably coming from low RISC of triplet exciton rather than charge imbalance. TADF materials with large RISC rates are required to reduce the efficiency roll-off.

Chapter 4. Thermally activated delayed fluorescence from azasiline based intramolecular charge-transfer emitter (DTPDDA) and a highly efficient blue light emitting diode

4.1 Introduction

Enhancing electroluminescence (EL) efficiency might be a never ending pursuit from displays to lightings where organic light emitting diodes (OLEDs) are being used. In the past years, phosphorescent OLEDs (PhOLEDs) based on heavy metal complexes have been considered as an only solution to realize high efficiencies by harvesting both singlet and triplet excitons as light.[5,12,28,31,33-34,63] However, recently reported OLEDs utilizing delayed fluorescence challenged the conventional idea of achieving high EL efficiencies and have demonstrated an equal performance to PhOLEDs by achieving 30% external quantum efficiency (EQE).[3,13,58,61] There are two different mechanisms that drive delayed fluorescence, which are triplet–triplet annihilation (TTA) and thermally activated delayed fluorescence (TADF).[64-65] Fluorescent materials showing TADF enables additional harvest of triplet excitons as well as singlet excitons to light via thermally activated reverse intersystem crossing (RISC) from triplet (T_1) to singlet (S_1) state due to small charge transfer singlet–triplet state splitting (ΔE_{ST}).

Replacing phosphorescent materials by efficient TADF materials will eventually lower cost with the potential of clearing stability issues. Especially, blue dyes among the three primary colors have been considered as the most crucial ones due to their important role in generating white light with good color purity. So far, blue fluorescent materials are being used for commercial OLEDs in spite of their low efficiency due to short device lifetime of phosphorescent blue OLEDs. Even with such importance, there are only a few reports on efficient blue TADF materials which meet both the high EL efficiency and color purity up to now. TADF materials are charge transfer (CT) type emitters which are composed of electron donating and accepting units to have small but a certain degree of overlap between the highest occupied molecular orbital

(HOMO) and the lowest unoccupied molecular orbital (LUMO) to minimize the singlet–triplet energy gap yet to still have large enough radiative transition rate. Carbazole and dimethyl dihydroacridine have been mainly used as the donor moieties and sulfone oxide and triazine as the acceptor unit in the blue TADF molecules. However, it seems quite challenging to search for an appropriate combination of donor and acceptor moieties to achieve good color purity and high EL efficiency for blue fluorescent OLEDs at the same time. Even a highly efficient blue fluorescent OLED of 20.6% was reported recently, yet the OLED displayed sky-blue light with the CIE coordinates of (0.19, 0.35).

The highest EQE ever reported in deep blue fluorescent OLEDs, in terms of CIE-y value below 0.2, was ～19.5%, which is still lower than the achieved EQE in this work.[25,47-49,66] In this article, we have utilized a new donor unit of the azasiline group to synthesize a deep blue TADF dye, 5-(4-(4,6-diphenyl-1,3,5-triazin-2-yl)phenyl)-10,10-diphenyl-5,10-dihydrodibenzo[b,e][1,4]azasiline (DTPDDA). An efficient blue fluorescent OLED with an unprecedented high EQE of 22.3% was fabricated by doping the TADF material in a mixed cohost system. The device emitted deep blue with the CIE coordinates of (0.149, 0.197). The comparison with the theoretical prediction of the EQE indicated that the RISC is efficient in the molecule to convert almost all the triplet excitons to the singlet excitons, and the device has little electrical loss.

4.2 Experimental

The material of DTPDDA was synthesized in the department of chemistry and research institute for green energy convergence technology (RIGET) of Gyeongsang National University supervised by professor Yun-Hi Kim.

Geometry optimization and energy level of HOMO and LUMO were calculated through DFT calculations with B3LYP level of theory, the 6-31G(d) basis set for all the atoms without solvent model and singlet and triplet energies, which were performed with TD-DFT calculations with Gaussian09.[45] Detailed information on the optimized molecular geometry is addressed in Table 4.2.

Organic films for the measurement of the PLQY and PL spectra were fabricated by thermal evaporation on precleaned quartz substrates at a base pressure of $<5 \times 10^{-7}$ Torr. The PLQY was measured by using an integrating sphere. A continuous-wave He/Cd laser (325 nm) was used as an excitation light source and a monochromator-attached photomultiplier tube (PMT) was used as an optical detection system. The PL spectra were also measured by PMT with a xenon lamp (260 nm) as an excitation light source.

Transient and time resolved PL spectra were measured using a streak camera (C10627, Hamamatsu Photonics) excited by a nitrogen gas laser with a pulse width of 800 ps (KEN-2X, Usho). Orientation of transition dipole moments was measured using a continuous wave diode laser (405 nm, Edmund optics Inc.). The incident angle of the excitation light was fixed at 45° from the plane normal direction of substrate, and the p-polarized emitted light was detected at 465 nm that is close to the peak wavelength of the PL spectrum of the fluorescent dye.

The OLEDs were fabricated on clean glass substrates prepatterned with 70-nm-thick ITO under a pressure of 5×10^{-7} Torr by thermal evaporation without breaking the vacuum. Before the deposition of organic layers the ITO substrates were precleaned with isopropyl alcohol and acetone and then exposed to ultraviolet (UV) ozone for 10 min. Organic layers were deposited at

a rate of 1 Å/s, and the deposition rate of the codeposited layers was 1 Å/s in total. Current density, luminance, and EL spectra were measured using a programmable source meter (Keithley 2400) and a spectrophotometer (Spectrascan PR650, Photo Research). The angular distribution of the EL was measured with a programmable source meter (Keithley 2400), goniometer, and fiber optic spectrometer (Ocean Optics S2000). The EQE and the power efficiency of the OLEDs were calculated from J–V–L characteristics, EL spectra, and the angular distribution of the EL intensity.

4.3 Result and discussion

Prior to synthesis of the blue fluorescent material with the chemical structure described in Figure 4.1a, the quantum chemical properties of the molecule have been investigated through the density functional theory (DFT) calculation. First, the geometry optimization (Figure 4.1b) and the energy levels of the compound and Kohn–Sham orbitals of the HOMO (Figure 4.1c) and the LUMO states (Figure 4.1d) were calculated through the DFT calculation. Then, singlet and triplet energies of DTPDDA were calculated with optimized geometry using the time-dependent(TD)-DFT. The details of the calculation method are explained in the Experimetal Section. The result showed that the HOMO and LUMO of DTPDDA are separated distinctively on two different units, the phenyl-dibenzo azasiline and the triphenyl triazine, respectively, by distorting 92–93° of the dihedral angle. The TD-DFT calculation predicted the ΔE_{ST} of 0.01 eV, indicating that the separation of Kohn–Sham orbitals of HOMO and LUMO lowered the exchange energy to enhance the RISC. However, the HOMO and LUMO levels were weakly overlapped in the phenyl unit, which is known to increase radiative transition rate.[3] As the HOMO of DTPDDA is distributed over the azasiline unit while the LUMO resides at the triphenyl triazine unit at the other side of DTPDDA molecule, the replacement of a carbon bridge with silicon in the phenyl-dibenzo azasiline resulted in deepening the HOMO level of DTPDDA, consequently enlarging the bandgap of DTPDDA, which is desired for blue emission. To further demonstrate the benefit of having an azasiline unit, HOMO and LUMO levels of DTPDDA and 2-phenoxazine-4,6-diphenyl-1,3,5-triazine (PXZ-TRZ) were compared through DFT calculation.[67] DTPDDA and PXZ-TRZ have the same acceptor unit as diphenyl-triazine but different donor units. DTPDDA with an azasiline unit has 0.5 eV lower HOMO level than PXZ-TRZ with a phenoxazine unit owing to a silicon bridge in the moiety (Table 4.1). Overall, from the DFT calculation, DTPDDA was expected to be an efficient CT type emitter for blue fluorescent OLEDs.

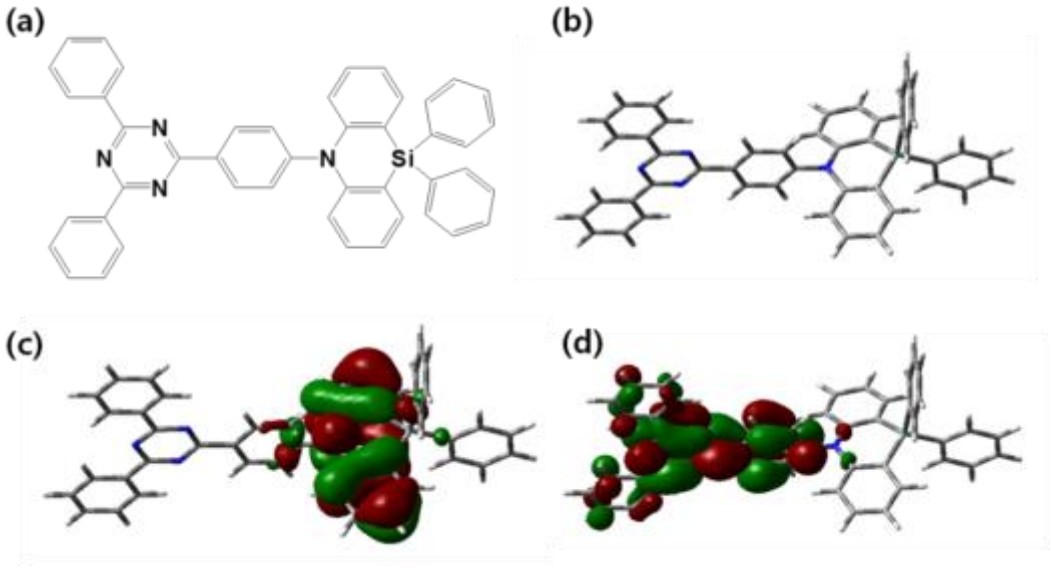

Figure 4.1 (a) Chemical structure of DTPDDA. DFT calculation data: (b) Molecular structure of DTPDDA. (c) HOMO level at the phenyl-dibenzo azasiline unit. (d) LUMO level at the triphenyl triazine unit.

Table 4.1 Comparison of LUMO and HOMO levels of DTPDDA and PXZ-TRZ through DFT calculations.

Emitter	Acceptor Unit	LUMO (eV)	Donor Unit	HOMO (eV)
DTPDDA	Triazine	1.98	Azasiline	5.15
PXZ-TRZ	Triazine	2.05	Phenoxazine	4.65

The mixed cohost of N,N′-dicarbazolyl-3,5-benzene (mCP) and diphenyl-4-triphenylsilylphenyl-phosphine oxide (TSPO1) with molar ratio of 1:1 was selected as an emitting layer (EML) for DTPDDA. Figure 4.2b shows the photoluminescence (PL) spectra of the materials used in this work. The resemblance of the spectrum of the mCP:TSPO1 film to that of the mCP film can be understood from the mixed CT and locally excited (LE) states of exciplexes between mCP and TSPO1.[68] The PL spectra of the DTPDDA doped films of mCP:DTPDDA, TSPO1:DTPDDA, and mCP:TSPO1:16 wt % DTPDDA showed the emission solely from DTPDDA without the emission from the hosts, indicating that energy transfer from the host molecules to the dopant is efficient in this system. The photoluminescent quantum yield (PLQY) of the mCP:TSPO1:16 wt % DTPDDA film was 74 ± 2%.

Experimentally achieved ΔE_{ST} of DTPDDA was 0.14 eV with S_1 and T_1 levels of 2.79 and 2.65 eV measured from the prompt and delayed PL spectra (Figure 4.3a) at 35 K, respectively. However, from the TD-DFT calculation, S_1 and T_1 levels were estimated to be 2.65 and 2.64, respectively, resulting in ΔE_{ST} of 0.01 eV. The gap between the achieved and calculated ΔE_{ST} can be caused by the selection of the DFT calculation scheme.[69-70] The transient PL decays of the film measured at the wavelength of 450 nm showed larger delayed emission and faster decay rate at room temperature (RT) than 35 K (Figure 4.3b), indicating that the delayed emission is coming from a thermally activiated process consistent with the nature of the TADF material.

The transient PL decays showed multiexponential decays fitted with the prompt lifetime of 11.8 ns and three delayed lifetimes of 100 ns, 2.3 μs, and 25.4 μs. The ratio of the prompt to delayed emission intensity in PL calculated from the decay pattern at RT is 0.13:0.87. Emission dipoles of DTPDDA in the mCP:TSPO1:16 wt % DTPDDA film are randomly oriented with the horizontal transition dipole ratio (Θ) of 0.66 characterized by theoretical fitting of the angle dependent p-polarized PL spectrum shown in Figure 4.7.[5,32,36-38]

TADF OLEDs were fabricated using mCP:TSPO1:16 wt % DPTDDA as the emitting layer. The device structure was ITO (70 nm)/4 wt % ReO_3:mCP (y nm)/mCP (15 nm)/mCP:TSPO1:16

wt % DPTDDA (15 nm) (0.42:0.42:0.16 in wt %)/TSPO1 (15 nm)/4 wt % Rb_2CO_3:TSPO1 (x nm)/Al (100 nm) shown in Figure 4.4a. The hole injection layer (p-doped mCP, HIL) and electron injection layer (n-doped TSPO1, EIL) were inserted in the device structure to enhance charge injection but were assumed to have the same refractive indices as the undoped layers.[39-44]

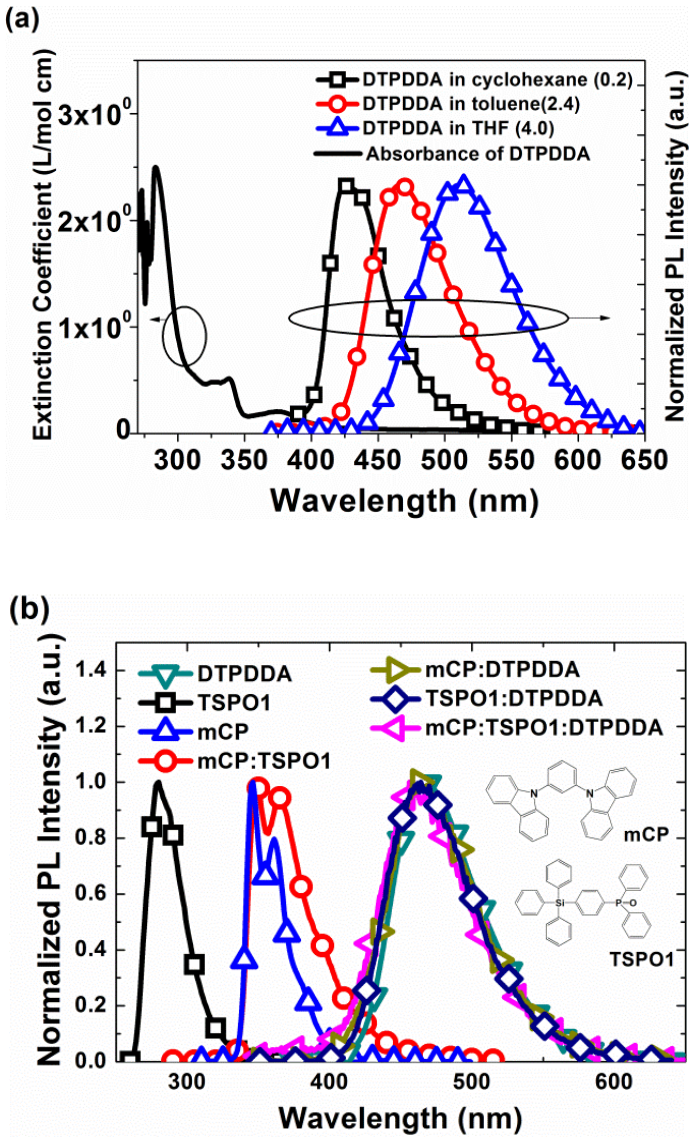

Figure 4.2 (a) The absorption spectrum of DTPDDA measured in toluene and PL spectra of DTPDDA in various solvents. Numbers in the brackets are the dielectric constants of the solvents. (b) The PL spectra of DTPDDA and TSPO1 measured in toluene and methylene chloride, espectively. The rest of the PL spectra of mCP, mCP:TSPO1, mCP:DTPDDA, TSPO1:DTPDDA and mCP:TSPO1:16 wt% DTPDDA were measured with 50 nm thick films on 1 mm thick fused silicas. Inset: the chemical structures of two hosts used for EML, mCP and TSPO1. mCP:DTPDDA, TSPO1:DTPDDA and mCP:TSPO1:16 wt% DTPDDA showed the emission

solely from DTPDDA without the emission from the hosts, indicating that energy transfer from the host molecules to the dopant is efficient in this system. The photoluminescent quantum yield (PLQY) of the mCP:TSPO1:16 wt% DTPDDA film was 74 ± 2%.

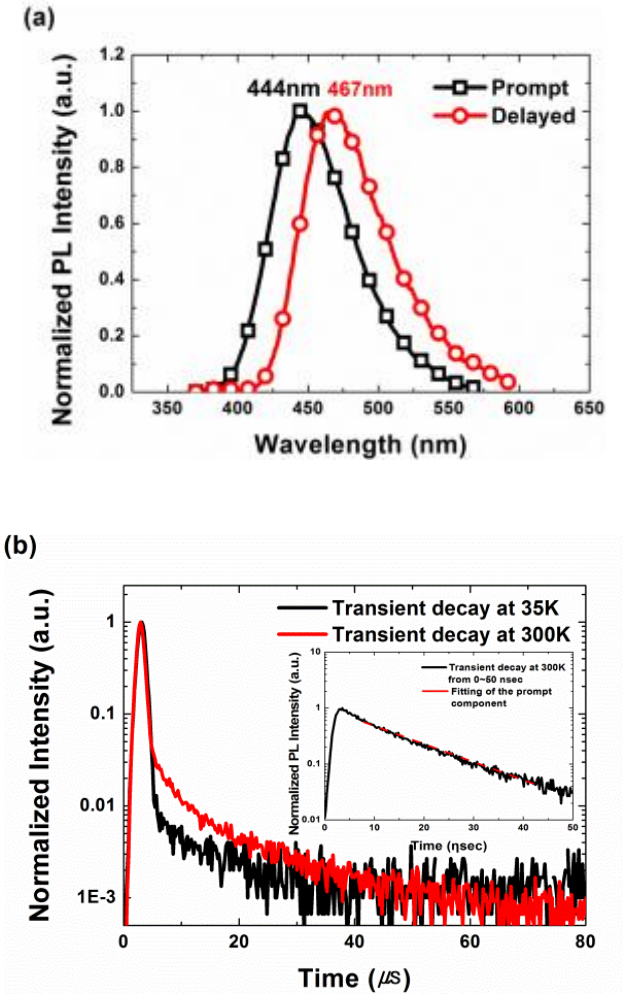

Figure 4.3 (a) Prompt and delayed PL spectra of mCP:TSPO1: 16 wt% DTPDDA at 35 K. Prompt and delayed components were collected at 20 ns and 300 μs, respectively. (b) Transient PL decays of mCP:TSPO1:16 wt% DTPDDA film measured at 450 nm at temperature of 300 K and 35 K. Inset: Transient PL within the range of 0 to 50 ns after excitation. Red dotted line is the single exponential fitting with decay time of 11.8 ns for the prompt fluorescence.

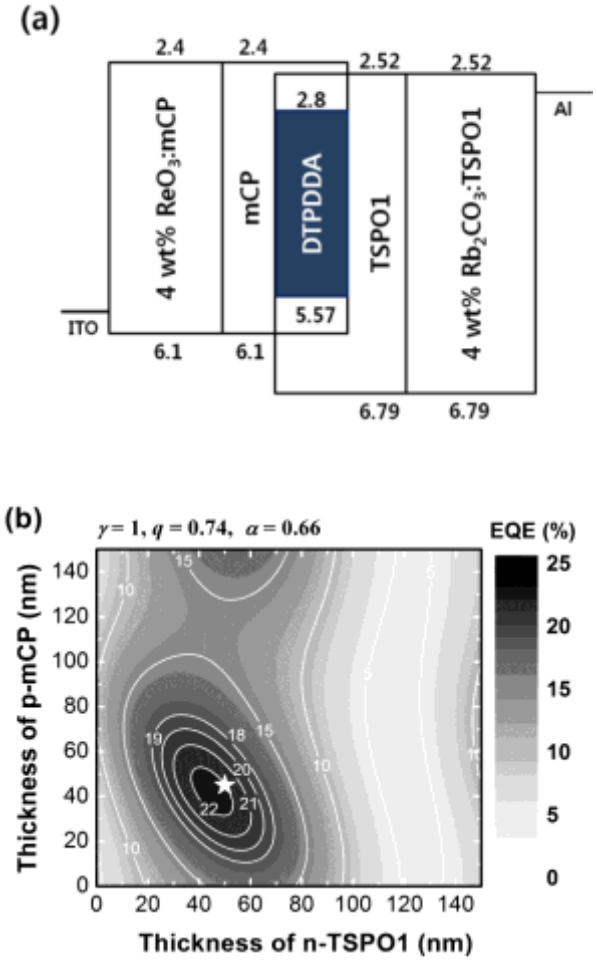

Figure 4.4 (a) Schematic diagram of the device structure and energy levels (eV) of the device. (b) Contour plot of the predicted maximum EQEs as function of the thickness of HIL and EIL for blue fluorescent OLEDs. A star indicates the achieved EQE in this work.

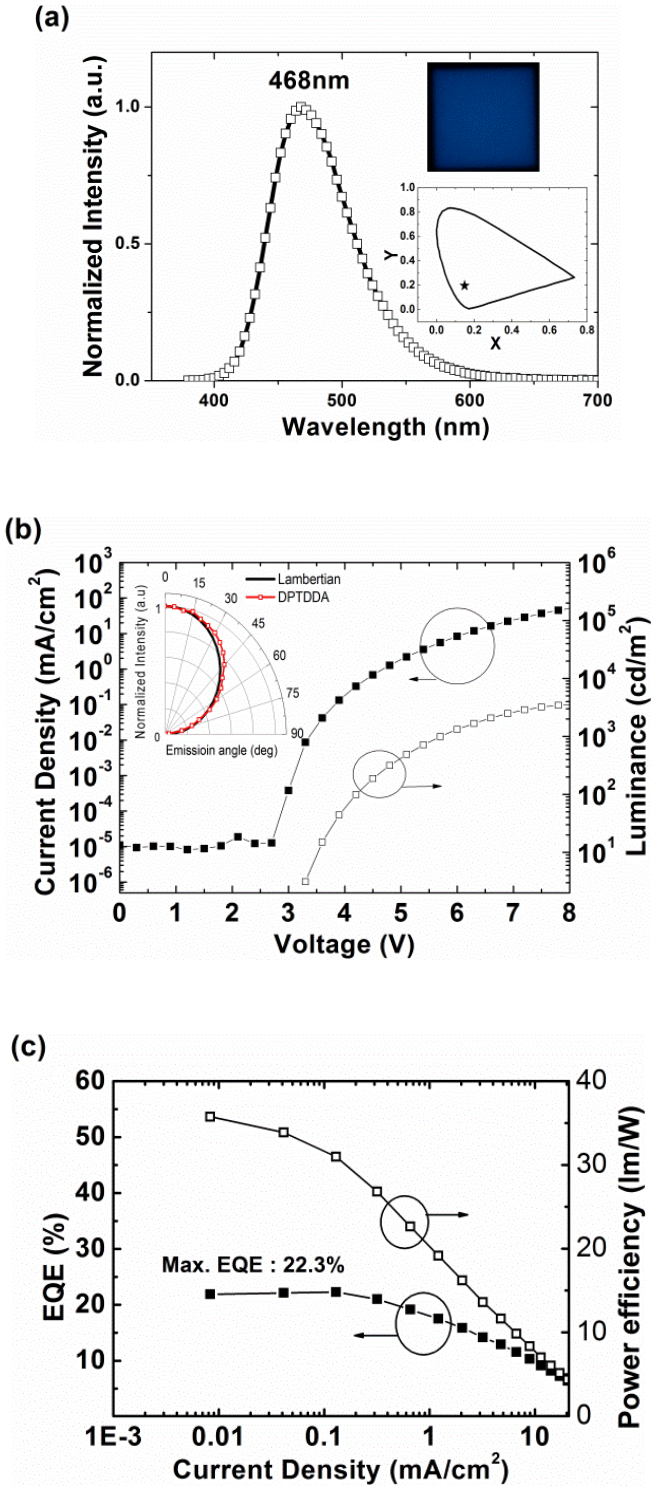

Figure 4.5 (a) EL spectrum of the blue fluorescent OLED Inset : (top) the image of blue emission from the OLED. (bottom) A star denotes the CIE coordinate of the EL spectrum at (0.149, 0.197). (b) Current density-voltage-luminance characteristics of the OLED. Inset: Angular distribution of

the EL intensity of the OLED. The solid line represents the Lambertian distribution. (c) EQE and power efficiency of the blue fluorescent OLED to current densities.

Optical simulation was performed using the classical dipole model with the measured Θ = 0.66 and PLQY = 0.74 of DTPDDA to predict the maximum achievable EQE of the blue fluorescent OLEDs as functions of the thickness of the HIL and EIL under the assumption of no electrical loss, and all the triplet excitons are converted to the singlet excitons at RT in the device. Details of the simulation procedure were described before.[5]

The simulation results displayed in Figure 4.4b indicate that maximum EQE of 22% is achievable in the blue fluorescent OLEDs when the thicknesses of the hole and electron injection layers are 45 and 50 nm, respectively.

The fabricated OLED with the optimized structure emitted blue fluorescence which is 13 nm red-shifted from the PL spectrum due to the cavity effect as shown in Figure 4.5a. The CIE coordinates of the blue fluorescence from the device are (0.149, 0.197) (inset of Figure 4.5a). Figure 4.5b shows the current density–voltage–luminance (J–V–L) characterstics and the power efficiency of optimized OLED, respectively. The factor of 1.07 was used for the calibration of efficiency obtained from the broader angular distribution of the EL intensity of the OLED than the Lambertian as shown in the inset of Figure 4.5b. The turn-on voltage of the OLED was 3.0 V, and the driving voltage was 5.7 V and 6.5 V at 1000 cd/m^2 and 2000 cd/m^2, respectively. The maximum power efficiency of the OLED was 30.4 lm/W. In comparison with the previously reported efficient blue fluorescent OLED with 20.6% EQE, the device using DTPDDA demonstrated not only higher EL efficiency but also deeper blue emission with lower turn-on voltage.[48]

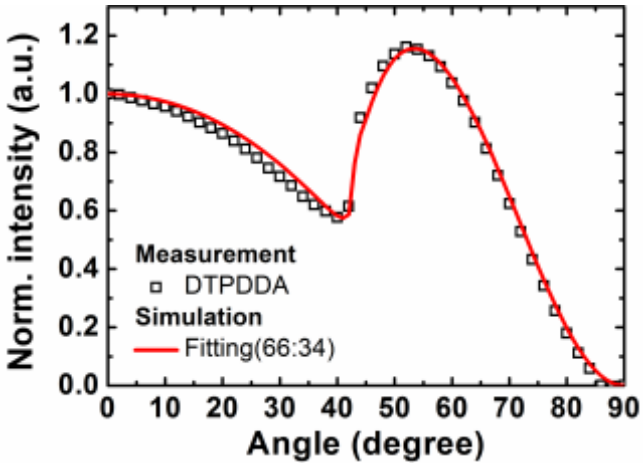

Figure 4.6 Angle-dependent PL intensities of the p-polarized light from 30-nm-thick films composed of mCP:TSPO1:16 wt% DTPDDA at 465nm. Solid lines represent theoretical fits to the experimental data.

Table 4.2 X, Y, Z-Coordinates of DTPDDA with DFT calculation.

	X (nm)	Y (nm)	Z (nm)
Si	4.825756	-0.01983	-0.0013
N1	1.754779	-0.66961	0.028825
N2	-4.69321	-1.22667	0.007917
N3	-6.61562	0.161542	-0.00242
N4	-4.45263	1.13321	0.006289
C1	-2.47389	-0.26076	0.015871
C2	-1.6425	0.86879	-0.01837
C3	-0.25753	0.726543	-0.01506
C4	0.319174	-0.54623	0.024926
C5	-0.50504	-1.67801	0.061544
C6	-1.8893	-1.53659	0.055481
C7	2.393784	-0.83807	-1.23168
C8	3.789756	-0.66045	-1.40853
C9	3.788667	-0.5208	1.460791
C10	2.394405	-0.72327	1.299214
C11	4.347256	-0.6482	2.745286
C12	3.575564	-0.92082	3.869721
C13	2.19826	-1.07483	3.705652
C14	1.614299	-0.98427	2.44724
C15	1.61269	-1.19186	-2.35393
C16	2.197475	-1.40052	-3.5978

C17	3.576476	-1.27577	-3.77182
C18	4.348844	-0.90855	-2.67515
C19	5.006624	1.86505	-0.09398
C20	6.53953	-0.81447	0.035805
C21	5.105754	2.526136	-1.33239
C22	5.265423	3.910982	-1.40459
C23	5.325413	4.669324	-0.23389
C24	5.220937	4.036566	1.006045
C25	5.061024	2.651227	1.071943
C26	6.664108	-2.21771	0.052458
C27	7.915007	-2.83301	0.085506
C28	9.075495	-2.05491	0.102983
C29	8.976678	-0.66352	0.086627
C30	7.720823	-0.05225	0.052934
C31	-3.95051	-0.11008	0.00986
C32	-6.02327	-1.04238	0.000221
C33	-5.79251	1.221333	0.001583
C34	-6.89127	-2.24441	-0.00673
C35	-6.4	2.573725	0.001358
C36	-6.3256	-3.52925	-0.01644
C37	-7.14251	-4.65695	-0.02431
C38	-8.53249	-4.51652	-0.02222
C39	-9.10257	-3.24101	-0.01235

C40	-8.28881	-2.11105	-0.00486
C41	-7.79564	2.724999	-0.01458
C42	-8.36489	3.99583	-0.01436
C43	-7.54943	5.130158	0.002211
C44	-6.15978	4.987346	0.018407
C45	-5.58691	3.71808	0.017804
H1	-2.0952	1.853069	-0.049
H2	0.389311	1.59826	-0.04327
H3	-0.05118	-2.66417	0.093567
H4	-2.53306	-2.40812	0.082258
H5	5.422454	-0.52316	2.857595
H6	4.032974	-1.00588	4.851228
H7	1.56373	-1.28204	4.563779
H8	0.545211	-1.12837	2.361004
H9	0.542077	-1.31666	-2.25817
H10	1.56194	-1.67691	-4.43545
H11	4.034531	-1.45355	-4.74054
H12	5.425086	-0.80267	-2.79655
H13	5.045257	1.954086	-2.25559
H14	5.337835	4.39836	-2.37382
H15	5.446978	5.748331	-0.28789
H16	5.258494	4.621849	1.921596
H17	4.965486	2.177973	2.046666

H18	5.770768	-2.83855	0.037981
H19	7.986263	-3.91782	0.097339
H20	10.05172	-2.53273	0.128722
H21	9.87614	-0.05288	0.099349
H22	7.659853	1.032924	0.038835
H23	-5.24603	-3.62648	-0.01843
H24	-6.69509	-5.64714	-0.03231
H25	-9.16895	-5.39751	-0.02837
H26	-10.1832	-3.12746	-0.01062
H27	-8.7198	-1.11654	0.002623
H28	-8.41851	1.83797	-0.02722
H29	-9.44619	4.102471	-0.02703
H30	-7.99507	6.121448	0.002635
H31	-5.52185	5.866892	0.031646
H32	-4.50996	3.595813	0.030625

Table 4.3 The voltage, current efficiency, EQE, and power efficiency of the OLED.

Voltage [V]			Current Efficiency [cd/A]			EQE [%]			Power Efficiency [lm/W]		
Turn on	1,000 cd/m^2	2,000 cd/m^2	Max.	1,000 cd/m^2	2,000 cd/m^2	Max.	1,000 cd/m^2	2,000 cd/m^2	Max.	1,000 cd/m^2	2,000 cd/m^2
3.0	5.7	6.5	35.6	17.9	13	22.3	10.6	8	30.4	9.8	5.7

4.4 Conclusion

In this article, the azasiline unit was introduced for the first time as the donor moiety to synthesize a new deep blue TADF dye, 5-(4-(4,6-diphenyl-1,3,5-triazin-2-yl)phenyl)-10,10-diphenyl-5,10-dihydrodibenzo[b,e][1,4]azasiline (DTPDDA). The azasiline unit was separated spatially from the acceptor of triazine owing to the large dihedral angle formed at the nitrogen–carbon bridge. Replacing the carbon connection by a silicon connection widens the bandgap suitable for blue emission. An efficient blue fluorescent OLED with the CIE coordinates of (0.149, 0.197) was fabricated with an unprecedented high EQE of 22.3% and low efficiency roll-off by doping DTPDDA in a mixed cohost system of mCP:TSPO1. Theoretical prediction assuming the fraction of radiative exciton as unity agrees well with EQE indicating efficient harvest of triplets occurring in DTPDDA through RISC.

Chapter 5. Azasiline-based thermally activated delayed fluorescence emitters for blue organic light emitting diodes

5.1 Introduction

100% internal quantum efficiency in fluorescent organic light emitting diodes (FOLEDs) became an achievable goal upon implementing efficient thermally activated delayed fluorescence (TADF) materials which enable reverse intersystem crossing (RISC).[3,58,62,71-72] In particular, highly efficient TADF blue emitters such as benzophenone- and diphenylsulfone-based blue TADF emitters have been reported in order to replace blue FOLEDs currently being used commercially despite their low efficiency.[9,25,48,51-53,66,73-79] Recently, a highly efficient blue FOLED containing the TADF emitter 5-(4-(4,6-diphenyl-1,3,5-triazin-2-yl)phenyl)-10,10-diphenyl-5,10-dihydrodibenzo[b,e][1,4]azasiline (DTPDDA), which consists of the unique azasiline unit as a donor and a triazine unit as an acceptor, has been reported.[51] Replacing the carbon bridge with silicone in phenyl-dibenzo azasiline lowers the highest occupied molecular orbital (HOMO) of the material, enlarging the bandgap such that it is suitable for deep blue emission with a Commission Internationale de l'Eclairage (CIE) Y-value below 0.2. Also, a notable 22.3% external quantum efficiency (EQE) was reported by utilizing DTPDDA in a blue fluorescent OLED. Therefore, it is necessary to further investigate the ability of the azasiline unit in blue fluorescent emitters.

Herein, we report three systematically different blue TADF emitters based on the azasiline donor unit with different acceptors. An addition of a phenyl ring to the donor–connector–acceptor (D–C–A) type DTPDDA resulted in an increased spatial separation of the donor and acceptor and a horizontal dipole ratio of 5-(4′-(4,6-diphenyl-1,3,5-triazin-2-yl)-[1,1′-biphenyl]-4-yl)-10,10-diphenyl-5,10-dihydrodibenzo[b,e][1,4]azasiline (DTPPDDA). Blue OLEDs adopting DTPPDDA demonstrated an EL efficiency of 4.7% with deep blue emission at CIE coordinates of (0.151, 0.087), approaching the National Television Standards Committee (NTSC) standard of

(0.14, 0.08). Carbonyl and sulfone units were compared in the donor–acceptor–donor (D–A–D) type materials of bis(4-(10,10-diphenyldibenzo[b,e][1,4]azasilin-5(10H)-yl)phenyl)methanone (BDAPM) and 5,5′-(sulfonylbis(4,1-phenylene))bis(10,10-diphenyl-5,10-dihydrodibenzo[b,e][1,4]azasiline) (SPDDA), in which the acceptor units influence the twist of the chemical structure. With a planar molecular structured acceptor because of sp^2 hybridization, the blue OLED using BDAPM demonstrated a higher EL efficiency of 11.4% than that of the SPDDA device, emitting sky blue emission at CIE coordinates of (0.174, 0.310). The twisted molecular structure of SPDDA led the device performance to 2.3% maximum EL efficiency, however with deep blue emission at CIE coordinates of (0.154, 0.107). The achieved EQEs from the OLED devices using all three TADF emitters were in good agreement with the predicted values, indicating that the potential of blue TADF emitters has been fully utilized in the optimized device structure.

5.2 Experimental

The material of DTPPDDA, BDAPM and SPDDA were synthesized in the department of chemistry and research institute for green energy convergence technology (RIGET) of Gyeongsang National university supervised by professor Yun-Hi Kim.

Geometry optimization and energy level of HOMO and LUMO were calculated through DFT calculations with B3LYP level of theory, the 6-31G(d) basis set for all the atoms without solvent model and singlet and triplet energies, which were performed with TD-DFT calculations with Gaussian09.[45] Detailed information on the optimized molecular geometry is addressed in Table 5.3, 5.4 and 5.5.

UV–vis absorption spectra and photoluminescence (PL) spectra were measured with a Shimadzu UV-1650PC spectrophotometer and LS-50B luminescence spectrophotometer, respectively.

Organic films for the measurement of the PLQY and PL spectra were fabricated by thermal evaporation on precleaned quartz substrates at a base pressure of $<5 \times 10^{-7}$ Torr. The PLQY was measured by using an integrating sphere. A continuous-wave He/Cd laser (325 nm) was used as an excitation light source and a monochromator-attached photomultiplier tube (PMT) was used as an optical detection system. The PL spectra were also measured by PMT with a xenon lamp (260 nm) as an excitation light source.

Transient and time resolved PL spectra were measured using a streak camera (C10627, Hamamatsu Photonics) excited by a nitrogen gas laser with a pulse width of 800 ps (KEN-2X, Usho).

Orientation of transition dipole moments was measured using a continuous wave diode laser (405 nm, Edmund optics Inc.). The incident angle of the excitation light was fixed at 45°

from the plane normal direction of substrate, and the p-polarized emitted light was detected at 465 nm that is close to the peak wavelength of the PL spectrum of the fluorescent dye.

The OLEDs were fabricated on clean glass substrates prepatterned with 70-nm-thick ITO under a pressure of 5×10^{-7} Torr by thermal evaporation without breaking the vacuum. Before the deposition of organic layers the ITO substrates were precleaned with isopropyl alcohol and acetone and then exposed to ultraviolet (UV) ozone for 10 min. Organic layers were deposited at a rate of 1 Å/s, and the deposition rate of the codeposited layers was 1 Å/s in total. Current density, luminance, and EL spectra were measured using a programmable source meter (Keithley 2400) and a spectrophotometer (Spectrascan PR650, Photo Research). The angular distribution of the EL was measured with a programmable source meter (Keithley 2400), goniometer, and fiber optic spectrometer (Ocean Optics S2000). The EQE and the power efficiency of the OLEDs were calculated from J–V–L characteristics, EL spectra, and the angular distribution of the EL intensity.

5.3 Result and discussion

Prior to synthesis of the blue fluorescent material, the quantum chemical properties of the molecule were investigated through density functional theory (DFT) calculations. First, geometry optimization (Figure 5.1), the energy levels of the compound and the Kohn–Sham orbitals of the HOMO and the lowest unoccupied molecular orbital (LUMO) states were calculated through DFT calculations by implementing the B3LYP level of theory, the 6-31G(d) basis set for all atoms without a solvent model and singlet and triplet energies, which were performed with TD-DFT calculations with Gaussian09.[45] Detailed information on the optimized molecular geometry is addressed in Tables 5.2–5.4. The results show that the HOMO and LUMO of DTPPDDA are separated distinctly on the two different units, the phenyldibenzo azasiline and the triphenyl triazine, respectively. The TD-DFT calculations predicted a splitting of singlet and triplet energies (ΔE_{ST}) of 0.01 eV, indicating that addition of the phenyl ring in the D–C–A type molecule increased the separation of the Kohn–Sham orbitals, and the bandgap of the HOMO and LUMO as well, such that it is suitable for deep blue emission. In the cases of BDAPM and SPDDA, BDAPM shows a more planar structure while SPDDA has a noticeable twisted structure. Alarger twist is known to be beneficial for spatial separation of the HOMO and LUMO, leading to a larger band gap than that of BDAPM. However, with a highly twisted molecular structure, SPDDA shows symmetric distribution of the Kohn–Sham orbitals in the LUMO. The TD-DFT calculations predicted the ΔE_{ST} of BDAPM and SPDDA to be 0.01 and 0.02 eV, respectively, also indicating a large spatial separation of the donors and acceptors in the D–A–D type molecules. Therefore, the calculation predicted the charge transfer (CT) character of the designed emitters in this work.

Organic films for measurement of the Photoluminescence Quantum Yields (PLQYs) were fabricated using thermal evaporation on precleaned quartz substrates at a base pressure of $<5 \times 10^{-7}$ Torr. The PLQY was measured using an integrating sphere. A continuous-wave He/Cd laser (325 nm) was used as an excitation light source and a monochromator-attached photomultiplier

tube (PMT) was used as an optical detection system. The mixed cohost of N,N′-dicarbazolyl-3,5-benzene (mCP) and diphenyl-4-triphenylsilylphenyl-phosphine oxide (TSPO1), with a molar ratio of 1:1, was selected as an emitting layer (EML) for the emitters. The doping ratios of the materials were determined as 8, 16 and 2 wt% for DTPPDDA, BDAPM and SPDDA, respectively, considering the electroluminescence (EL) efficiencies of the OLEDs. The PLQYs of the emitters doped into mCP:TSPO1 were 38%, 70% and 20% for DTPPDDA, BDAPM and SPDDA, respectively. The low PLQYs of DTPPDDA and SPDDA were largely due to a reduced radiative transition rate coming from the large spatial separation of the donor and acceptor units from the long phenyl bridges and highly twisted structure of DTPPDDA and SPDDA, respectively. However, such large spatial separation of the HOMO and LUMO enabled deep blue emission. The orientation of the transition dipole moments was measured using a continuous wave diode laser (405 nm, Edmund optics Inc.). The incident angle of the excitation light was fixed at 45° from the plane normal direction of the substrate and the p-polarized emitted light was detected at different wavelengths considering each material's peak wavelength.[5,32,36-38] The horizontal transition dipole ratios of the materials doped in mCP: TSPO1 were 0.73, 0.77 and 0.76 for DTPPDDA, BDAPM and SPDDA, respectively. Adding a phenyl bridge increased the orientation of the transition dipole moment to 0.73 from 0.66 for DTPDDA.[25]

Figure 5.2 shows the photoluminescence (PL) spectra of the materials used in this work. The shifts in the PL spectra observed in the film samples of mCP: TSPO1: 8 wt% DTPPDDA and mCP: TSPO1: 2 wt% SPDDA compared to those of the solutions is attributed to solvatochromism.

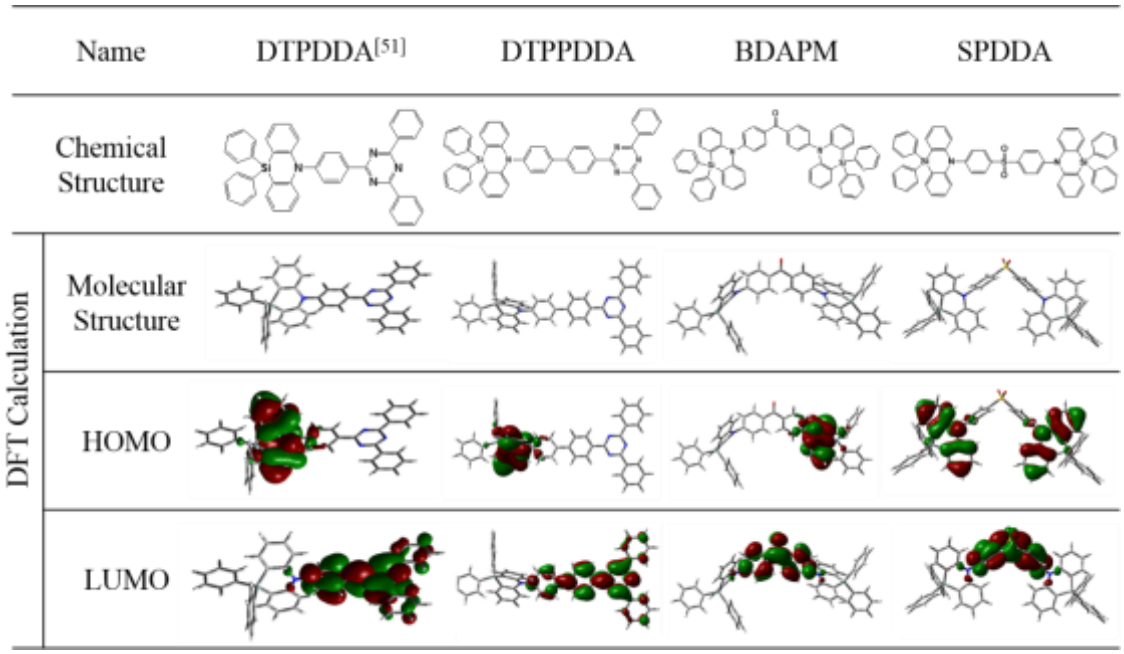

Figure 5.1 Chemical structure, molecular structure, HOMO and LUMO of the emitters.

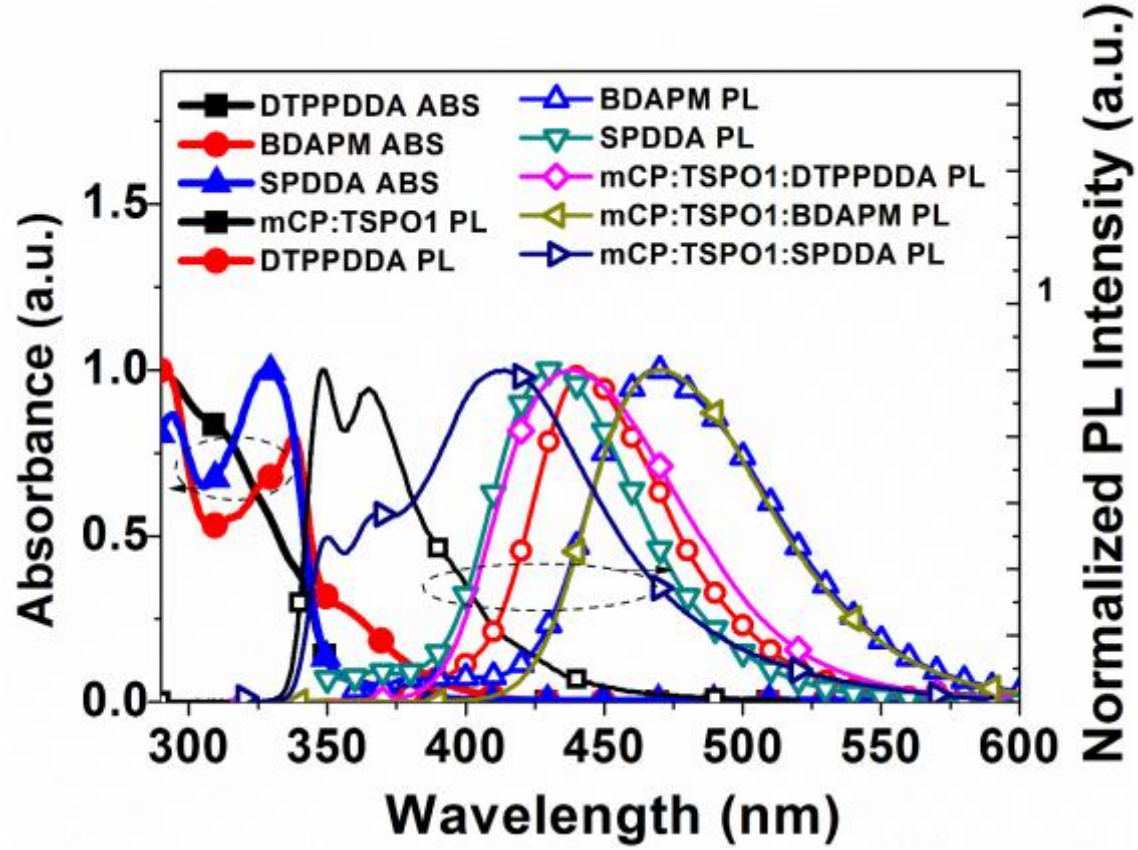

Figure 5.2 PL spectra of the host of mCP:TSPO1 and the emitters. Absorption and PL spectra of DTPPDDA, BDAPM and SPDDA were measured in toluene. PL spectra of mCP:TSPO1 and mCP:TSPO1:X wt% emitter were measured with 50 nm thick films on 1 mm thick fused silicas. Doping ratios were 8, 16 and 2 wt% for DTPPDDA, BDAPM and SPDDA, respectively.

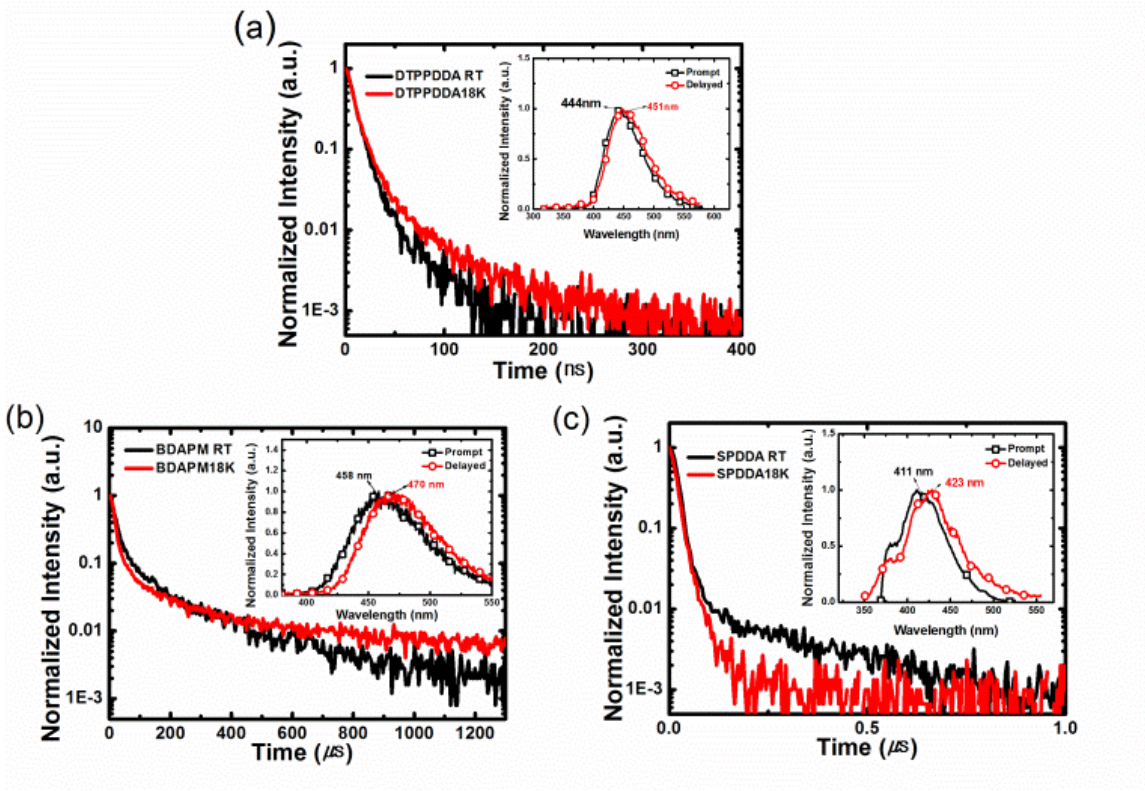

Figure 5.3 Transient PL decays of (a) mCP:TSPO1: 8 wt% DTPPDDA, (b) mCP:TSPO1: 16 wt% BDAPM and (c) mCP:TSPO1: 2 wt% SPDDA films measured at the peak wavelengths of each materials at temperature of 300 K and 18 K. Insets : Prompt and delayed PL spectra measured at 18K for the estimation of S_1 and T_1.

In Figure 5.3, the transient PL decays were compared at room temperature (RT) and 18 K. Also, prompt and delayed PL spectra of the samples were compared at 18 K in the insets. Transient and time resolved PL spectra were measured using a streak camera (C10627, Hamamatsu Photonics) excited by a nitrogen gas laser with a pulse width of 800 ps (KEN-2X, Usho). Samples were prepared as 50 nm films on a quartz substrate. mCP:TSPO1: 8 wt% DTPPDDA and mCP: TSPO1: 2 wt% SPDDA showed double exponential decays, however the decay times of the prompt (τ_p) and delayed (τ_d) emission of both mCP: TSPO1: 8 wt% DTPPDDA (τ_p = 6 ns, τ_d = 20 ns) and mCP: TSPO1: 2 wt% SPDDA (τ_p = 4 ns, τ_d = 16 ns) were small, even with the estimated small singlet–triplet splittings of 0.04 eV and 0.07 eV from the insets of Figure 3a and 3c, respectively, which indicates that non-radiative decay rates from T_1 are higher than the RISC rates for both emitters.[67,80-81] Further, the delayed emission was increased in the case of mCP:TSPO1:8 wt% DTPPDDA as the temperature decreased from suppressing the non-radiative decay of the triplet channel. The transient decay of mCP:TSPO1:16 wt% BDAPM was fitted well with 3 exponential components (τ_p = 134 ns, τ_{d1} = 5.2 μs, τ_{d2} = 42.96 μs). From the prompt and delayed PL spectra (inset of Figure 5.3b) at 18 K, the experimentally achieved ΔE_{ST} of mCP:TSPO1:16 wt% BDAPM was 0.06 eV for BDAPM. From the experiments, the estimated values of ΔE_{ST} were higher with SPDDA (0.07 eV) than with DTPPDDA (0.04 eV) and BDAPM (0.06 eV), which is similar to the predicted ΔE_{ST} value of SPDDA (0.02 eV) being higher than those of DTPPDDA (0.01 eV) and BDAPM (0.01 eV). However the gap between the achieved and predicted values can be caused by the selection of the DFT calculation scheme and also the difference in geometries of the molecules in solid-state films and gas-phase structures.[69-70]

In the case of the time resolved PL spectra of mCP:TSPO1:2 wt% SPDDA (inset of Figure 5.3c), the emission at 370 nm could be assigned to the host mCP:TSPO1 considering the peak wavelength of the PL spectra which was reduced in the delayed emission, indicating that energy transfer from the host to the emitter is slow in this system due to the high singlet energy state (3.0 eV) of SPDDA.

Blue TADF OLEDs were fabricated as shown in Figure 5.4a. The optimized device structure was ITO (70 nm)/4 wt% ReO_3:mCP (45 nm)/mCP (15 nm)/mCP:TSPO1:X wt% emitter (15 nm)/TSPO1 (15 nm)/4 wt% Rb_2CO_3:TSPO1 (50 nm)/Al (100 nm). The hole injection layer (*p*-doped mCP, HIL) and electron injection layer (*n*-doped TSPO1, EIL) were inserted in the device structure to enhance charge injection, but were assumed to have the same refractive indices as the un-doped layers.[39-44] Under electrical excitation, the fabricated OLEDs with the optimized structure emitted blue fluorescence at 440, 484 and 440 nm for the devices containing DTPPDDA, BDAPM and SPDDA, respectively, different from the PL spectra due to the cavity effect of the device as shown in Figure 5.4b. In case of the OLED containing SPDDA, the host emission from mCP:TSPO1 that appeared in the PL spectrum (Figure 5.2d) disappeared in the EL spectrum, showing that charge trapping to the emitter was dominant in the device. Deep blue fluorescence was realized in the OLEDs containing DTPPDDA and SPDDA with CIE Y-values of 0.087 and 0.107, respectively. The CIE value of the device containing DTPPDDA was (0.151, 0.087), close to the NTSC standard of (0.140, 0.080), showing that the blue fluorescent OLED containing DTPPDDA achieved color purity up to the commercial standard for blue emission.

The OLED containing BDAPM exhibited sky blue emission with a CIE Y-value of 0.310. Figure 5.4c shows the J–V–L graph for the OLEDs where the turn-on voltages are 3.3, 3.6 and 3.6 volts for the devices containing DTPPDDA, BDAPM and SPDDA, respectively, lower than the previously reported blue fluorescent OLED devices containing a mixed cohost system. [9,25,48,51-53,66,73-79] As shown in Figure 5.4d, the maximum EL efficiencies were 4.7, 11.4 and 2.3% for the OLED devices containing DTPPDDA, BDAPM and SPDDA, respectively. In terms of efficiency roll-off, triplet–triplet annihilation (TTA) and triplet–polaron quenching (TPQ) can be major causes, however by further developing TADF emitters with high RISC rates, efficiency roll-off can be improved.[82] EQEs, turn-on voltages, maximum luminances and CIE values are listed in Table 5.1.

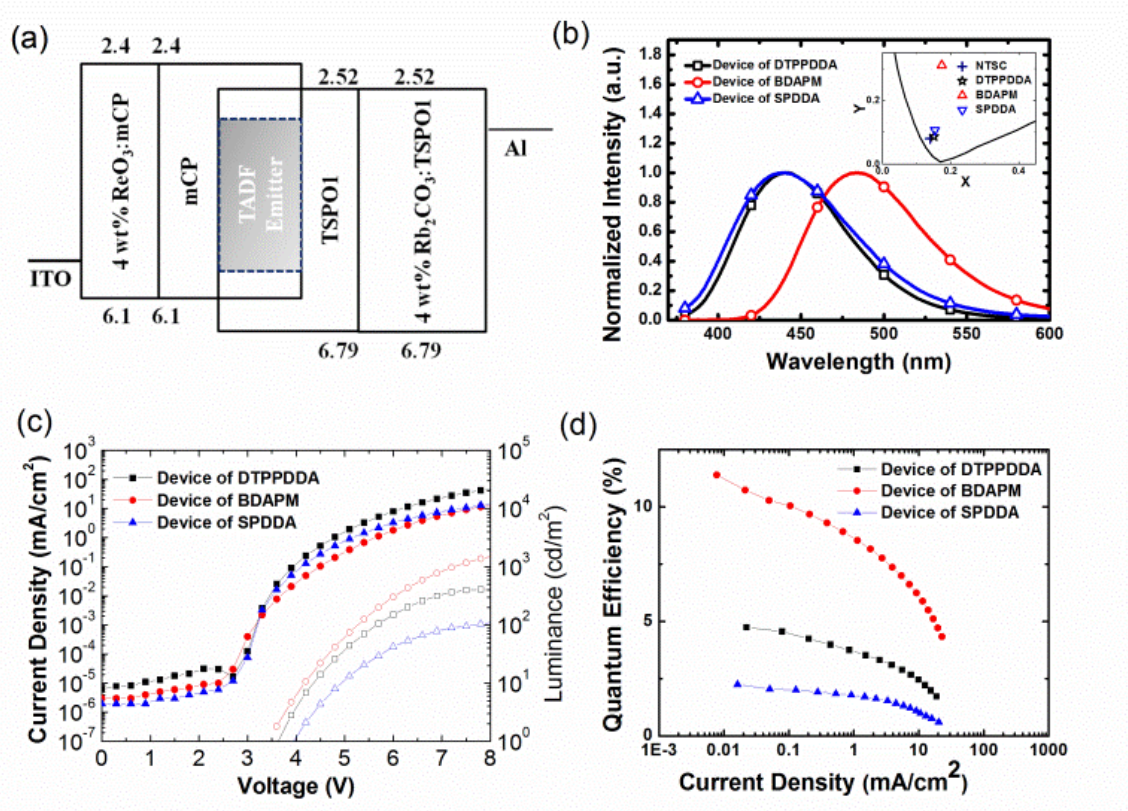

Figure 5.4 (a) Schematic diagram of the device structure and energy levels (eV) of the device. (b) EL spectra of the blue fluorescent OLEDs Inset:CIE coordinates of the OLEDs in this work compared to that of NTSC. (c) Current density-voltage-luminance characteristics of the OLEDs. (d) EQEs of the blue fluorescent OLEDs to current densities.

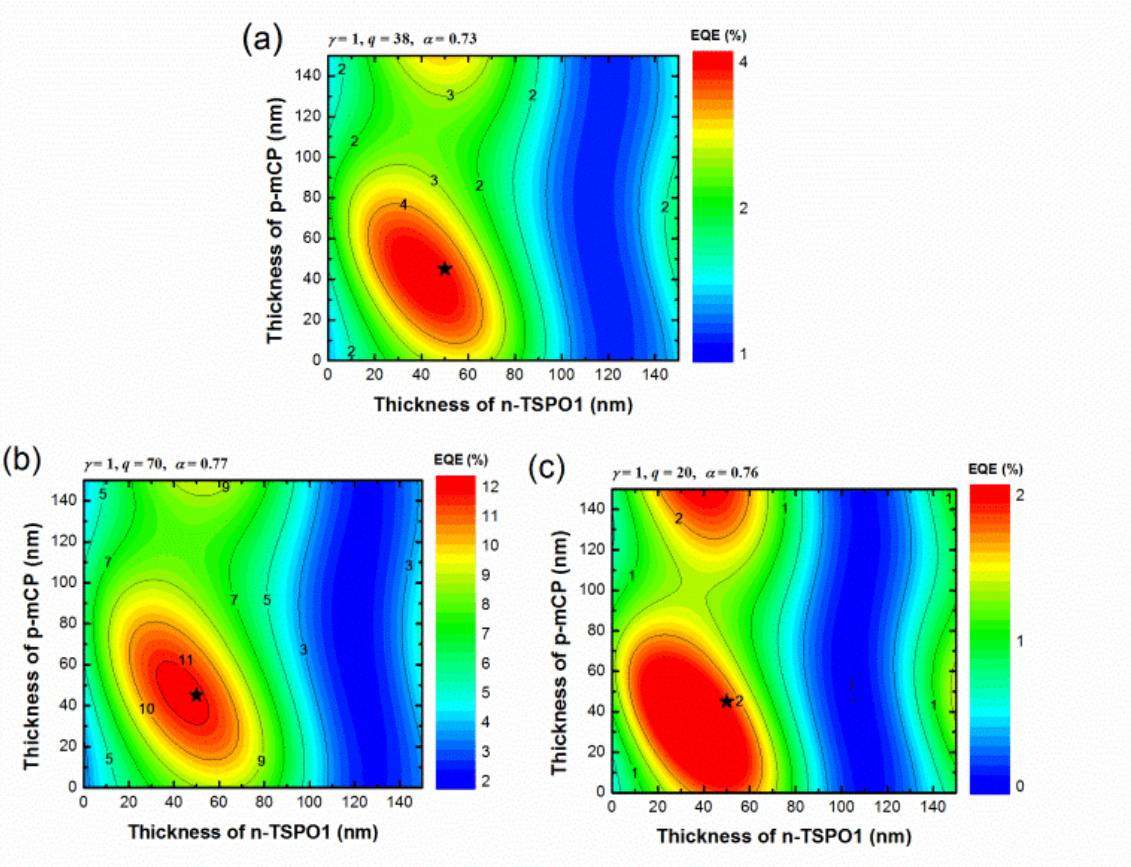

Figure 5.5 Contour plot of the predicted maximum EQEs as a function of the thickness of HIL and EIL for OLED device of (a)DTPPDDA (b)BDAPM and (c)SPDDA. Stars indicate the achieved EQE in this work.

Table 5.1 Device performances. $\eta_{S/T}$ indicates singlet-triplet factor**.**

Name	Max. EQE(%)		$\eta_{S/T}$	Turn-on	Max. Luminance	EQE(%)	CIE(x,y)
	Achieved	Theoretical		(volts)	(cd/m^2)	@100cd/m^2	
DTPPDDA	4.7	4.4	0.32	3.3	281	2.2	(0.151, 0.087)
BDAPM	11.4	11.9	0.48	3.6	2021	9	(0.174, 0.310)
SPDDA	2.3	2.3	0.34	3.6	117	0.9	(0.154,. 0.107)

Table 5.2 DFT Geometry of DTPPDDA.

Si	-6.73461	0.052267	-0.05573
N1	7.021699	-1.16331	-0.03585
N2	8.99982	0.144036	-0.06995
N3	6.881423	1.203462	0.050663
N4	-3.71138	-0.62441	0.392394
C1	0.544733	-0.3747	0.248398
C2	-0.08906	-1.42846	0.930666
C3	-1.47785	-1.5189	0.983724
C4	-2.27265	-0.55332	0.355547
C5	-1.65654	0.499668	-0.32508
C6	-0.26709	0.586172	-0.37795
C7	2.024252	-0.28231	0.192012
C8	2.81947	-1.43828	0.095907
C9	4.205545	-1.35521	0.044829
C10	4.848021	-0.10822	0.086012
C11	4.062249	1.050626	0.180416
C12	2.676333	0.963125	0.233557
C13	6.325782	-0.01788	0.030737
C14	8.356627	-1.03366	-0.08373
C15	8.222158	1.235691	-0.00216
C16	9.172433	-2.27013	-0.15519

C17	8.886547	2.561546	0.014996
C18	8.553338	-3.53003	-0.16463
C19	9.320832	-4.69012	-0.23058
C20	10.71425	-4.60755	-0.2883
C21	11.33736	-3.35713	-0.2795
C22	10.57301	-2.19494	-0.21329
C23	10.2864	2.654765	-0.03382
C24	10.90891	3.900353	-0.01831
C25	10.14303	5.06704	0.045843
C26	8.749399	4.982023	0.094721
C27	8.123496	3.738102	0.079504
C28	-3.60851	0.274346	2.662249
C29	-4.21007	0.823153	3.789151
C30	-5.58157	1.079871	3.816425
C31	-6.32836	0.800197	2.676782
C32	-5.74999	0.271763	1.508827
C33	-4.36429	-0.03092	1.509269
C34	-4.34882	-1.38007	-0.63172
C35	-3.58084	-2.28933	-1.39164
C36	-4.16667	-3.06989	-2.38184
C37	-5.53431	-2.98475	-2.64653
C38	-6.29344	-2.0791	-1.91293
C39	-5.73073	-1.2527	-0.92398

C40	-6.76934	1.658002	-1.06255
C41	-8.50353	-0.51398	0.28739
C42	-6.83301	2.912479	-0.42769
C43	-6.88272	4.096858	-1.16468
C44	-6.86593	4.052547	-2.56005
C45	-6.79578	2.820132	-3.21194
C46	-6.746	1.638876	-2.46944
C47	-8.73877	-1.66685	1.062518
C48	-10.0345	-2.10844	1.328518
C49	-11.1301	-1.40419	0.822553
C50	-10.9216	-0.25988	0.052446
C51	-9.62147	0.178548	-0.21056
H1	0.512265	-2.171	1.44705
H2	-1.95519	-2.33377	1.520434
H3	-2.27522	1.242197	-0.82017
H4	0.19382	1.396136	-0.93557
H5	2.342412	-2.41208	0.033048
H6	4.807675	-2.25282	-0.03728
H7	4.554247	2.015657	0.221442
H8	2.089531	1.871422	0.335985
H9	7.471596	-3.58226	-0.11936
H10	8.832005	-5.66059	-0.23706
H11	11.31205	-5.5138	-0.33982

H12	12.42089	-3.28818	-0.3242
H13	11.0457	-1.21951	-0.20551
H14	10.87036	1.742934	-0.08351
H15	11.99314	3.962026	-0.05632
H16	10.63025	6.038524	0.057763
H17	8.149913	5.886973	0.144614
H18	7.042979	3.660021	0.116556
H19	-2.5454	0.073889	2.687211
H20	-3.59482	1.038382	4.659304
H21	-6.05333	1.495048	4.702404
H22	-7.39795	1.000388	2.681423
H23	-2.52047	-2.39811	-1.20459
H24	-3.54227	-3.76189	-2.94154
H25	-5.99377	-3.60504	-3.41073
H26	-7.36049	-1.99843	-2.11082
H27	-6.83232	2.968046	0.658709
H28	-6.92977	5.053653	-0.65035
H29	-6.90191	4.973847	-3.13612
H30	-6.77486	2.778597	-4.29824
H31	-6.67643	0.689005	-2.99488
H32	-7.89792	-2.22731	1.465824
H33	-10.1909	-3.00065	1.929782
H34	-12.1409	-1.74697	1.028952

H35	-11.77	0.292733	-0.34375
H36	-9.47577	1.073044	-0.81074

Table 5.3 DFT Geometry of BDAPM.

Si1	-7.7094	0.728404	-0.01854
Si2	7.769965	0.673088	0.014688
O	0.086623	-4.64758	-0.34654
N1	-5.36186	-1.3225	0.180392
N2	4.8221	-0.39333	0.294127
C1	-0.02875	-3.44379	-0.14744
C2	1.199502	-2.58885	-0.02914
C3	1.256531	-1.43409	0.767112
C4	2.445839	-0.71682	0.885738
C5	3.591191	-1.13491	0.199073
C6	3.543816	-2.29049	-0.58811
C7	2.361856	-3.01742	-0.68898
C8	-2.98762	-1.02512	-0.31885
C9	-1.68208	-1.51066	-0.38593
C10	-1.39655	-2.83693	-0.02887
C11	-2.44954	-3.6714	0.380665
C12	-3.74931	-3.18402	0.46226
C13	-4.02541	-1.85406	0.113754
C14	-5.09966	-1.14918	2.604397
C15	-5.50476	-0.67468	3.847165
C16	-6.6138	0.163776	3.96678

C17	-7.28926	0.536407	2.809035
C18	-6.89099	0.100321	1.532958
C19	-5.79173	-0.78876	1.428433
C20	-6.17039	-1.45402	-0.985
C21	-5.81923	-2.41633	-1.95564
C22	-6.59408	-2.59775	-3.09585
C23	-7.7476	-1.84071	-3.30538
C24	-8.09131	-0.8815	-2.35819
C25	-7.31593	-0.64931	-1.20814
C26	-6.91588	2.353876	-0.5838
C27	-9.56813	0.971582	0.204216
C28	-6.4713	3.308677	0.349826
C29	-5.91066	4.519078	-0.06141
C30	-5.77755	4.800342	-1.42246
C31	-6.20403	3.865068	-2.36704
C32	-6.76427	2.656266	-1.9498
C33	-10.3722	-0.10151	0.6367
C34	-11.7482	0.04765	0.806602
C35	-12.3542	1.279438	0.546388
C36	-11.578	2.356425	0.1178
C37	-10.1998	2.201817	-0.05054
C38	5.203784	-1.54135	2.416557
C39	6.00356	-1.86767	3.505843

C40	7.309768	-1.38732	3.605089
C41	7.801032	-0.59563	2.572662
C42	7.032121	-0.26793	1.441176
C43	5.691014	-0.72393	1.372684
C44	4.989574	0.692612	-0.61143
C45	3.875223	1.145715	-1.35205
C46	3.981998	2.22386	-2.22333
C47	5.192984	2.897736	-2.38444
C48	6.298537	2.444545	-1.67276
C49	6.236637	1.339186	-0.80526
C50	8.713739	-0.48339	-1.15341
C51	8.919055	2.054268	0.59741
C52	9.420132	-1.59684	-0.66156
C53	10.13742	-2.43598	-1.51578
C54	10.16202	-2.18032	-2.88802
C55	9.463131	-1.08578	-3.40012
C56	8.746576	-0.25067	-2.54102
C57	8.470277	2.987537	1.552512
C58	9.291446	4.025354	1.99183
C59	10.58634	4.154259	1.482827
C60	11.05263	3.241494	0.536538
C61	10.22608	2.202871	0.100691
H1	0.379318	-1.10641	1.315532

H2	2.495242	0.170409	1.509935
H3	4.439996	-2.60985	-1.11132
H4	2.317916	-3.92665	-1.27958
H5	-3.21314	-0.00227	-0.60454
H6	-0.89045	-0.85999	-0.74256
H7	-2.22668	-4.70429	0.627476
H8	-4.56152	-3.82661	0.789421
H9	-4.24662	-1.81365	2.555469
H10	-4.95047	-0.97963	4.73131
H11	-6.93824	0.522458	4.939345
H12	-8.15316	1.193429	2.886812
H13	-4.94316	-3.03719	-1.81843
H14	-6.29484	-3.35244	-3.81882
H15	-8.35999	-1.99263	-4.18951
H16	-8.98715	-0.28289	-2.51031
H17	-6.55289	3.101065	1.414515
H18	-5.57373	5.239916	0.67955
H19	-5.33902	5.741312	-1.7452
H20	-6.09672	4.074788	-3.42848
H21	-7.07796	1.933886	-2.70008
H22	-9.91679	-1.06764	0.843706
H23	-12.3482	-0.79486	1.141373
H24	-13.4269	1.397705	0.677975

H25	-12.044	3.317389	-0.08571
H26	-9.60874	3.050856	-0.38434
H27	4.191024	-1.92105	2.387949
H28	5.589235	-2.4964	4.289962
H29	7.929739	-1.63046	4.463128
H30	8.818958	-0.21599	2.635361
H31	2.912803	0.663304	-1.24431
H32	3.099133	2.544148	-2.77096
H33	5.272575	3.74986	-3.0532
H34	7.250837	2.957874	-1.79083
H35	9.401687	-1.82092	0.402632
H36	10.67293	-3.29136	-1.11122
H37	10.71805	-2.83405	-3.55535
H38	9.471219	-0.88539	-4.46873
H39	8.195499	0.587932	-2.96079
H40	7.465325	2.900622	1.96017
H41	8.923541	4.733357	2.730331
H42	11.22808	4.96272	1.824148
H43	12.05971	3.335876	0.137942
H44	10.60472	1.498008	-0.63512

Table 5.4 DFT Geometry of SPDDA.

S	0.000044	4.308424	-5.3E-05
Si1	7.262044	-1.0304	0.005511
Si2	-7.26207	-1.03038	-0.00545
O1	0.200832	5.022138	1.271021
O2	-0.20079	5.022166	-1.27111
N1	4.754059	0.685915	-0.7242
N2	-4.75398	0.685908	0.724012
C1	-1.41224	3.208855	0.222862
C2	-2.16962	2.834218	-0.88775
C3	-3.26955	1.996503	-0.70798
C4	-3.60824	1.542029	0.570535
C5	-2.84347	1.934632	1.677121
C6	-1.74239	2.771889	1.50753
C7	3.269756	1.996655	0.707788
C8	2.169831	2.834372	0.887583
C9	1.412378	3.208944	-0.22301
C10	1.74246	2.771919	-1.50767
C11	2.843534	1.934657	-1.67728
C12	3.608365	1.5421	-0.57072
C13	6.015966	2.644648	-1.46573
C14	7.212928	3.288703	-1.76015

C15	8.435451	2.635431	-1.5998
C16	8.430836	1.332406	-1.11269
C17	7.242552	0.659959	-0.77654
C18	6.004921	1.317802	-0.98582
C19	4.525481	-0.71997	-0.698
C20	3.219252	-1.20753	-0.91629
C21	2.957728	-2.5734	-0.92849
C22	3.982758	-3.50016	-0.73534
C23	5.269405	-3.02464	-0.50289
C24	5.566278	-1.65119	-0.45442
C25	7.443278	-0.89878	1.887016
C26	8.634356	-2.12486	-0.68939
C27	8.195952	0.134371	2.475707
C28	8.354187	0.21804	3.860272
C29	7.75655	-0.73201	4.690326
C30	6.99878	-1.76184	4.129416
C31	6.84417	-1.84052	2.744361
C32	8.692668	-2.39286	-2.07141
C33	9.697487	-3.1951	-2.61104
C34	10.67143	-3.7497	-1.77663
C35	10.63381	-3.49784	-0.40503
C36	9.624859	-2.6937	0.130633
C37	-3.21926	-1.20756	0.916266

C38	-2.95778	-2.57344	0.928594
C39	-3.98285	-3.50019	0.735568
C40	-5.26949	-3.02464	0.503092
C41	-5.56631	-1.65119	0.454487
C42	-4.52548	-0.71998	0.697962
C43	-6.00481	1.317892	0.985537
C44	-6.0158	2.644828	1.465213
C45	-7.21273	3.288978	1.759547
C46	-8.43528	2.635721	1.599349
C47	-8.43072	1.332611	1.112469
C48	-7.24247	0.66006	0.776411
C49	-8.63446	-2.12461	0.689666
C50	-7.44335	-0.89905	-1.88697
C51	-8.69336	-2.39154	2.071873
C52	-9.69817	-3.19368	2.611645
C53	-10.6715	-3.74927	1.777208
C54	-10.6333	-3.49848	0.405427
C55	-9.62438	-2.69443	-0.13039
C56	-6.84357	-1.84037	-2.74428
C57	-6.99825	-1.76185	-4.12934
C58	-7.75677	-0.73259	-4.69028
C59	-8.35509	0.217053	-3.86025
C60	-8.19679	0.133541	-2.47569

H1	-1.91317	3.214399	-1.87083
H2	-3.87964	1.69501	-1.55378
H3	-3.12435	1.587256	2.666736
H4	-1.15893	3.104064	2.359678
H5	3.8799	1.695196	1.55357
H6	1.913428	3.21461	1.870654
H7	1.158959	3.104047	-2.35981
H8	3.124343	1.587221	-2.6669
H9	5.088517	3.180494	-1.62153
H10	7.181235	4.309661	-2.13192
H11	9.369039	3.134334	-1.84314
H12	9.377194	0.81228	-0.97943
H13	2.399896	-0.52168	-1.0895
H14	1.939769	-2.91098	-1.1065
H15	3.780571	-4.56707	-0.75935
H16	6.077554	-3.73618	-0.34604
H17	8.65765	0.891755	1.846073
H18	8.939482	1.026843	4.290765
H19	7.876195	-0.66727	5.768891
H20	6.524599	-2.50093	4.770521
H21	6.238494	-2.64211	2.327112
H22	7.94232	-1.96928	-2.73573
H23	9.722178	-3.38828	-3.68059

H24	11.4557	-4.37534	-2.19539
H25	11.389	-3.92685	0.248865
H26	9.608198	-2.5068	1.201247
H27	-2.39987	-0.52173	1.089384
H28	-1.93983	-2.91104	1.106622
H29	-3.7807	-4.5671	0.759687
H30	-6.07767	-3.73617	0.346335
H31	-5.08833	3.180674	1.620892
H32	-7.18099	4.310005	2.131122
H33	-9.36884	3.134697	1.842633
H34	-9.37711	0.812492	0.979345
H35	-7.94349	-1.96715	2.736218
H36	-9.72332	-3.38602	3.681344
H37	-11.4558	-4.37484	2.196082
H38	-11.3881	-3.92825	-0.2485
H39	-9.6073	-2.50833	-1.20113
H40	-6.23731	-2.6415	-2.327
H41	-6.52354	-2.50062	-4.77042
H42	-7.87646	-0.66797	-5.76885
H43	-8.94097	1.025419	-4.29077
H44	-8.65903	0.890618	-1.84608

Table 5.5 Max. EQEs of OLED devices of the TADF emitters in various doping ratios of 2, 8 and 16 wt% in the host of mCP:TSPO1.

Doping Ratio	Max. EQEs of the OLED devices of		
	DTPPDDA	BDAPM	SPDDA
2 wt%	3.4%	3.8%	2.3%
8 wt%	4.7%	10.2%	1.7%
16 wt%	3.2%	11.4%	1.1%

Table 5.6 Singlet(S_1) & triplet(T_1) energy levels, Experimental and calculated singlet-triplet splittings($\triangle E_{ST}$) and prompt(τ_p) and delayed(τ_d) decay rates.

Name	S_1 (eV)	T_1 (eV)	ΔE_{ST} (eV) (Experimental)	ΔE_{ST} (eV) (Calculated)	Decay time	
					Prompt(τ_p)	Delayed(τ_d)
DTPPDDA	2.79	2.75	0.04	0.01	6 ns	20 ns
BDAPM	2.7	2.64	0.06	0.01	134 ns	5,2 μs, 42.96 μs
SPDDA	3.0	2.93	0.07	0.02	4 ns	16 ns

Table 5.7 Oscillator strength for the materials.

	DTPPDDA	**BDAPM**	**SPDDA**
Oscillator strength (f)	0.0012	0.0004	0.0011

In order to find out whether the fabricated OLEDs achieved the theoretical maximum EQEs, an optical simulation was performed using the classical dipole model based on the measured PLQYs and horizontal dipole ratios (Figure 5.5).[5]

The calculation showed that the values of 4.4, 11.9 and 2.3% for the achievable EL efficiencies are close to the actually achieved values of 4.7, 11.4 and 2.3%, indicating that the OLEDs fabricated in this study fully utilized the blue fluorescent emitters. As shown in Table 5.1, comparing the achieved and theoretical values, the singlet–triplet factors of the emitters were higher than 0.25, indicating that an additional harvest of triplets through RISC is occurring in the blue fluorescent emitters.

5.4 Conclusion

The donor unit of azasiline was utilized in blue fluorescent emitters in order to exploit the full potential of this unique moiety. The addition of a phenyl bridge to the D–C–A type material DTPDDA, DTPPDDA, demonstrated an increased horizontal dipole ratio of 0.73 compared to that of DTPDDA (0.66). From observation of the time resolved spectra, the large spatial separation of the donor and acceptor enabled a small singlet–triplet splitting of 0.04 eV, however in terms of CT character, DTPPDDA did not show a linear solvatochromic shift in response to increasing dielectric constants of the solvents, only responding to the specific solvent, chloroform. Also, the delayed emission of DTPPDDA was small, increasing at lower temperatures unlike the typical TADF phenomenon. The blue fluorescent OLED containing DTPPDDA achieved an EQE of 4.7% emitting deep blue fluorescence at CIE coordinates of (0.151, 0.087), approaching the NTSC value. Good agreement of the theoretical and achieved EQEs and minimal ΔE_{ST} values indicates that an additional harvest of triplets occurred via RISC.

Carbonyl and sulfone units were adopted as acceptors in BDAPM and SPDDA, respectively, where the carbonyl unit possessed a more planar molecular structure than the sulfone unit. DFT calculations showed that a highly twisted chemical structure resulted in a large orbital overlap in the acceptor unit of SPDDA. The PLQY was higher with BDAPM, showing larger delayed emission at room temperature. The experimentally achieved singlet–triplet splittings were 0.06 and 0.07 eV for BDAPM and SPDDA, respectively. However, the delayed emission of SPDDA was small. The OLED devices containing BDAPM and SPDDA emitted sky and deep blue fluorescence with 11.9% and 2.3% EQEs, respectively. The theoretical EQEs were close to the achieved EQEs, showing that RISC is happening in the OLEDs due to the small ΔE_{ST} values.

Overall, the azasiline moiety showed potential as a suitable donor unit for blue TADF emitters, hence the azasiline unit needs to be further investigated and utilized in blue TADF materials.

Chapter 6. Almost All the Triplets Harvested in Conventional Blue Fluorescent Organic Light Emitting Diode

6.1 Introduction

It is still under debate if fluorescent organic light emitting diodes (OLEDs) can entirely replace phosphorescent OLEDs for the ultimate commercial use. Despite the drawback of low electroluminescence (EL) efficiency of blue fluorescent OLED, it is being used in display industry for its higher stability than that of blue phosphorescent OLED. Therefore, numerous approaches have been made in order to enhance deficit EL efficiency of blue fluorescent OLEDs, such as recently reported fluorescent OLEDs with high EL efficiencies based on thermally activated delayed fluorescence (TADF) emitters.[3,51,58,62,71,72,77,83] However, emitting from TADF material often shows broad EL spectrum due to the charge transfer (CT) state of the material, and the stability of the TADF based OLEDs still need to be improved. As an alternative, conventional fluorophore can be used as an emitter, where assisted dopants either phosphorescent or TADF material is strategically implemented to enhance spin mixing of singlet and triplet excited states. Recently, the high EL efficiencies were reported from blue fluorescent OLEDs based on conventional blue fluorescent dye, taking advantage of TADF material as a sensitizer.[8,84] With small singlet-triplet splitting (ΔE_{ST}) of TADF material, reverse intersystem crossing (RISC) can occur effectively harvesting additional triplet excitons. Also, adopting heavy metal compound of platinum or iridium enhances spin mixing of singlet and triplet from heavy atom effect (HAE), consequently EL efficiency of OLED can be improved.[85-87] Even more, increased spin reversal of triplet to singlet was observed by taking advantage of CT state of host on the induction of HAE from iridium complex, eventually enhancing the singlet to triplet ratio ($\eta_{s/T}$).[88] However, compared to other primary colors, very few has been reported on blue fluorescent OLEDs in this regard, probably due to its difficulty in constituting host materials to satisfy high triplet level of blue emitter. Hence, it would be worth to discover the new concept for emitting layer (EML)

where HAE and sensitizing effects are combined to enhance spin mixing of singlet and triplet state, yet emitting from conventional fluorescent dye without sacrificing any virtue of blue fluorescent OLEDs. In this article, a new concept of EML boosting EL efficiency of blue fluorescent OLED was investigated, which the EML is consisted of host and two different assisted dopants of phosphorescent and TADF material. By doping TADF material and phosphorescent material into EML, efficiency of electroluminescence from conventional blue emitter was increased largely from both the HAE and sensitizing effect. Comparison of the theoretical and experimental data shows that almost all the triplets were harvested in the blue fluorescent OLED. $\eta_{s/T}$ was increased from typical singlet-exciton production factor of 0.25 to 0.94 when the both of phosphorescent and TADF materials were used as assisted dopants, with increased external quantum efficiency (EQE) of 5.6% to 12.3% in the conventional blue fluorescent OLED.

6.2 Experimental

The OLEDs were fabricated on clean glass substrates pre-patterned with 70-nm-thick ITO under a pressure of 5×10^{-7} Torr by thermal evaporation without breaking the vacuum. Before the deposition of organic layers, the ITO substrates were pre-cleaned with isopropyl alcohol and acetone, and then exposed to UV–ozone for 10 minutes. Organic layers were deposited at a rate of 1 Å/s, and the deposition rate of co-deposited layers was 1 Å/s in total.

Current density, luminance, and EL spectra were measured using a programmable source meter (Keithley 2400) and a spectrophotometer (Spectrascan CS100, Photo Research). The angular distribution of the EL was measured with a programmable source meter (Keithley 2400), goniometer, and fiber optic spectrometer (Ocean Optics S2000). The EQE and the power efficiency of the OLEDs were calculated from current density−voltage−luminance characteristics, EL spectra, and the angular distribution of the EL intensity.

Orientation of the transition dipole moments was measured using a continuous wave diode laser (405 nm, Edmund optics Inc.). The incident angle of the excitation light was fixed at 45° from the plane normal direction of the substrate, and the *p*-polarized emitted light was detected at 470 nm, which is close to the peak wavelength of the PL spectrum of the fluorescent dye.

Cyclic voltammetry was performed on a VSP versatile modular potentiostat, and data were analyzed using EC-LAB. A platinum wire was used as the counter-electrode, and a platinum disk was used as the working electrode.

PL spectra of the organic materials were measured using samples thermally deposited on fused silica under a vacuum of 5×10^{-7} Torr. The samples were excited with a He/Cd laser (325 nm) to detect PL using a photomultiplier tube attached to a monochromator.

Transient PL was measured by using a pulsed N_2 laser (KEN-2X, USHO) as the excitation light source and a streak camera (C10627, Hamamatsu) as the optical detection system.

6.3 Result and discussion

In order to enhance EL efficiency of blue fluorescent OLED using 2,5,8,11-tetra-tert-butylperylene (TBPe) as an emitter, TADF material of 5-(4'-(4,6-diphenyl-1,3,5-triazin-2-yl)-[1,1'-biphenyl]-4-yl)-10,10-diphenyl-5,10-dihydrodibenzo[b,e][1,4]azasiline (DTPPDDA) and phosphorescence material of bis-2-(2,4-difluoro-3-(perfluoropropyl)phenyl)-4-methylpyridine-Ir ^{III}-picolinate $(HFP)_2Ir(pic)$ were used as assisted dopants in the host of N,N′-dicarbazolyl-3,5-benzene (mCP). The absorption and photoluminescence (PL) spectra of all the materials used in this work are shown in Figure 6.1. The UV-vis absorption spectra of the materials were measured in methylen chloride (MC) using a UV-Vis-NIR spectrophotometer (Agilent, Cary-5000). The photoluminescence spectra of the materials were measured using 50 nm thick films deposited on precleaned fused silica substrates, except TBPe which was measured diluted in MC. Monochromatic light with the wavelength of 250 nm from a Xenon lamp was used as the excitation source and a photomultiplier tube as the detector (Photon Technology International). As shown in Figure 6.1, the peak positions of PL spectra of the constituents are rather tightly arranged to each other since selecting materials for host and assistant dopant in blue fluorescent OLED is especially complex to satisfy wide energy band gap of an emitter for blue emission. Ir complex of $(HFP)_2Ir(pic)$ and TADF material of DTPPDDA were used as assisted dopants for this work. DTPPDDA was chosen for its ΔE_{ST} of 0.01 eV, which is small enough that RISC of DTPPDDA can be enhanced by induced HAE from Ir complex of $(HFP)_2Ir(pic)$.[51] $(HFP)_2Ir(pic)$ has been reported as a deep blue phosphorescent emitter with high photoluminescence quantum yield (PLQY), which satisfies our needs in both high triplet energy and efficient Ir complex.[89] As shown in Figures 6.5, both the host and assisted dopants have higher singlet and triplet energy states than those of TBPe.

Investigating the contribution of the each assisted dopant, four different EML samples of 50 nm films of mCP:0.5 wt% TBPe, mCP:6 wt% DTPPDDA:0.5 wt% TBPe, mCP:8 wt% $(HFP)_2Ir(pic)$:0.5 wt% TBPe and mCP:8 wt% $(HFP)_2Ir(pic)$:6 wt% DTPPDDA:0.5 wt% TBPe

were prepared. Doping ratio of TBPe was determined to be 0.5 wt% to prevent undesired Dexter energy transfer (ET) from triplet states of the other constituents to that of TBPe. From the time resolved PL spectra of the samples as shown in Figure 6.2a, all the spectra of all the samples were similar to that of mCP:0.5 wt% TBPe, indicating that energy transfer to the emitter of TBPe could be efficient in all the different EML systems in this work. The transient PL decays of all the systems are described in Figure 6.2b. The prompt transient decay rates (τ_p) were similar in mCP:0.5 wt% TBPe and mCP:6 wt% DTPPDDA:0.5 wt% TBPe, even with the addition of TADF material of DTPPDDA to the mCP:0.5 wt% TBPe, due to suppressed RISC of DTPPDDA from strong non-radiative decay even with small ΔE_{ST}.[83] (Table 6.2) Increased delayed emission was observed as Ir complex of $(HFP)_2Ir(pic)$ was implemented in the EML with the delayed decay rate (τ_d) of 974.5 ns in mCP:8 wt% $(HFP)_2Ir(pic)$:0.5 wt% TBPe.

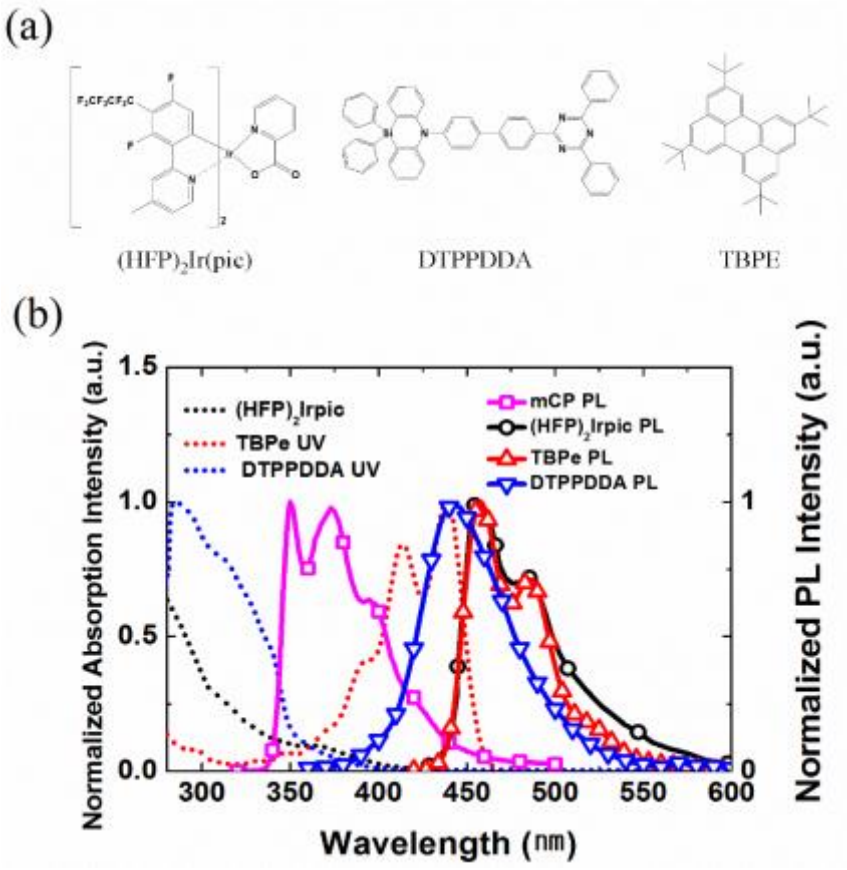

Figure 6.1 (a) Chemical structures of the materials used in this work. (b) Absorption and PL spectra of the materials.

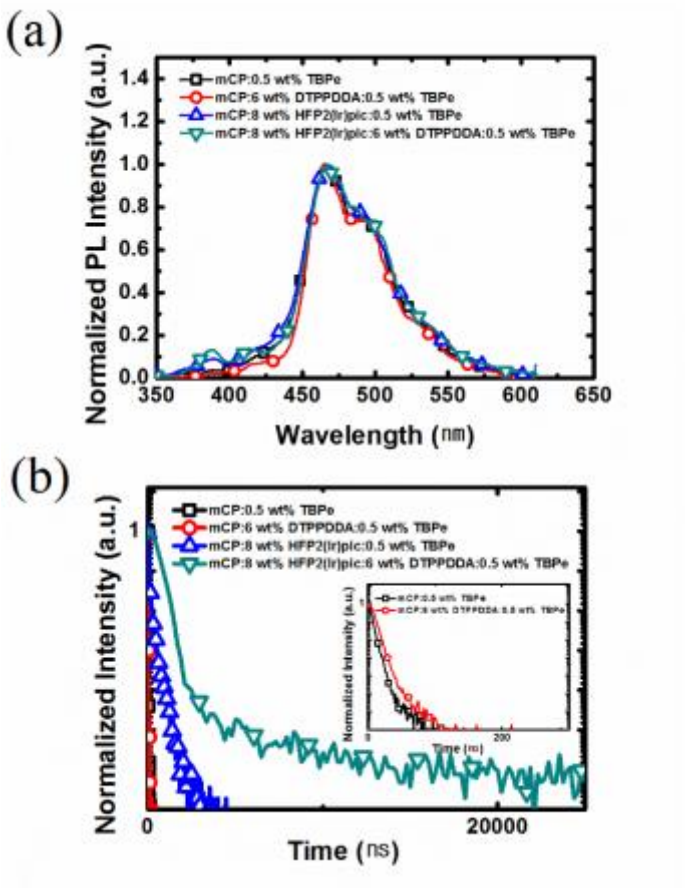

Figure 6.2 (a) Time resolved PL spectra and (b) transient decays of all the samples for the EML. Inset of (b): transient decay of mCP:0.5 wt% TBPe and mCP:6wt% DTPPDDA:0.5 wt% TBPe from the start of excitation to 260 ns.

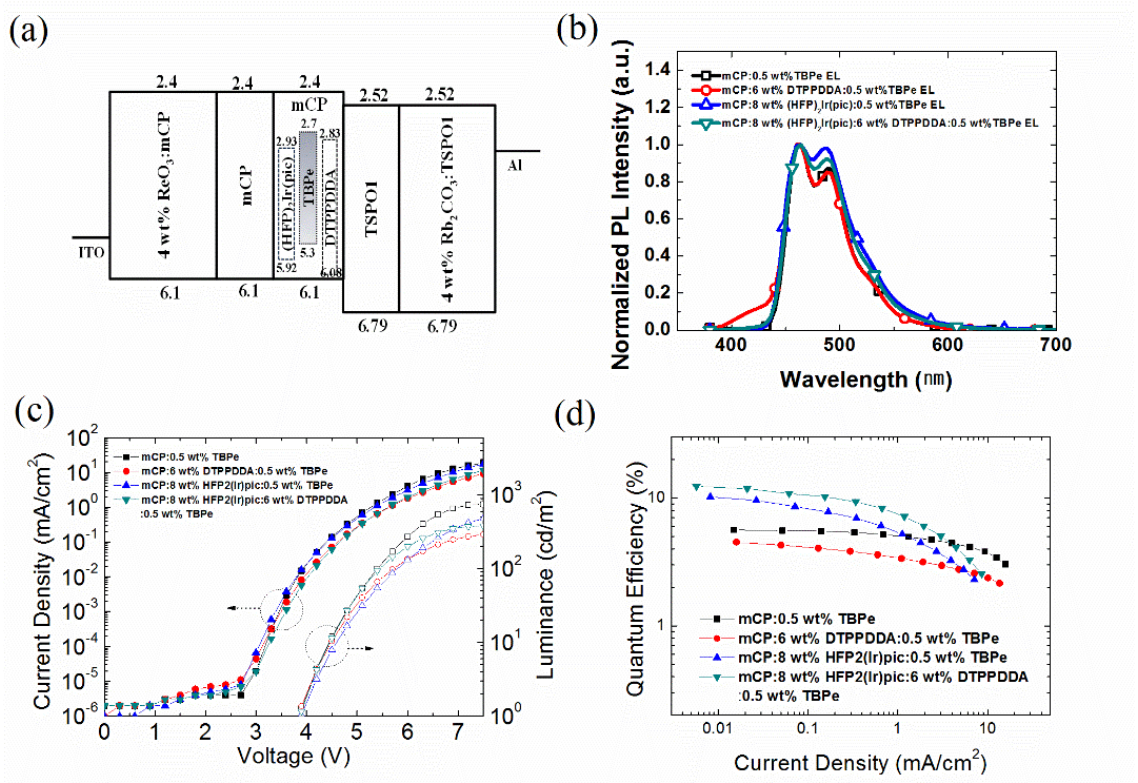

Figure 6.3 (a) Device structure, (b) EL spectra, (c) J-V-L and (d) EQEs of the blue fluorescent OLEDs.

Table 6.1 PLQYs, Estimated Singlet-triplet factors, Achieved and theoretical EQEs of the blue fluorescent OLEDs.

EML	PLQY (%)	Estimated Singlet-Triplet Factor ($\eta_{S/T}$)	Achieved EQE (%)	Theoretical EQE (%)
mCP:0.5 wt% TBPe	84	0.23	5.6	24.4
mCP:6 wt% DTPPDDA:0.5 wt% TBPe	52	0.27	4.5	16.5
mCP:8 wt% $(HFP)_2Ir(pic)$:0.5 wt%TBPe	55.1	0.58	10.1	17.3
mCP:6 wt% DTPPDDA:8 wt% $(HFP)_2Ir(pic)$:0.5 wt%TBPe	41.9	0.94	12.3	13

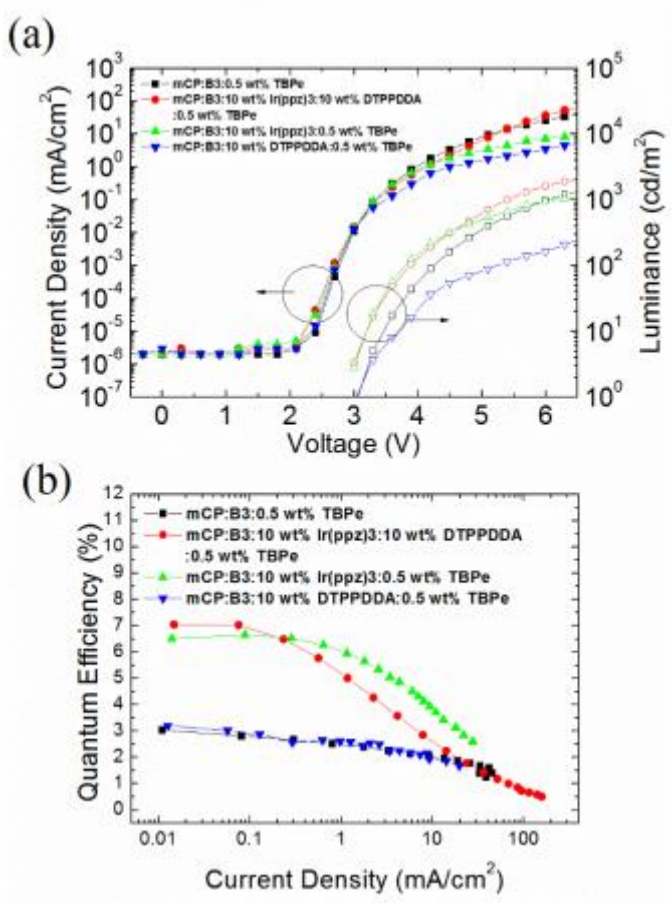

Figure 6.4 (a) J-V-L and (b) EQEs of the OLEDs of mCP:B3PYMPM:0.5 wt% TBPe, mCP:B3PYMPM:10 wt% DTPPDDA:0.5 wt% TBPe, mCP:B3PYMPM:10 wt% Ir(ppz)3:0.5 wt% TBPe and mCP:B3PYMPM:10 wt% Ir(ppz)3:10 wt% DTPPDDA:0.5 wt% TBPe.

And, the delayed emission was the largest in the case of mCP:8 wt% $(HFP)_2Ir(pic)$:6 wt% DTPPDDA:0.5 wt% TBPe (τ_d=3.9 μs). From the equation (1), increase in delayed emission results in enhanced RISC rate (k_{RISC}), where, k_p, k_d, k_{ISC}, Φ_D and Φ_P are prompt decay rate, delayed decay rate, intersystem crossing rate, portion of delayed emission and prompt emission in total photoluminescence quantum yield (PLQY), respectively. Therefore, RISC rate can be assumed to be enhanced from the extended delayed emission in mCP:8 wt% (HFP)2Ir(pic):6 wt% DTPPDDA:0.5 wt% TBPe. The transient decay rates are summarized in Table 6.2

$$k_{RISC} = \frac{k_P \times k_D}{k_{ISC}} \times \frac{\Phi_D}{\Phi_P} \qquad (1)$$

The device structure of the blue fluorescent OLEDs were ITO (70 nm)/6 wt % ReO3:mCP (45 nm)/mCP (15 nm)/mCP : Dopants (15 nm)/TSPO1 (15 nm)/4 wt % Rb2CO3:TSPO1 (50 nm)/Al (100 nm) as shown in Figure 3(a). Hole and electron transporting layers were doped with 6 wt% ReO_3 and 4 wt% Rb_2Co_3 to promote charge injection from the electrodes to the HTL and ETL, respectively.[39-44] The blue fluorescent OLEDs were fabricated on clean glass substrates pre-patterned with 2 × 2 mm^2 active area on the ITO under pressure of 5×10^{-7} Torr by thermal evaporation. Before the deposition of organic layers, the ITO substrates were precleaned with isopropyl alcohol and acetone, and then exposed to ultraviolet (UV)-ozone for 10 minutes. Organic layers were deposited at a rate of 1 Å/s and the deposition rate of the co-deposited layers was 1 Å/s in total. Current density, luminance, and EL spectra were measured using a programmable source meter (Keithley 2400) and a spectrophotometer (Spectrascan PR650, Photo Research). EL spectra of the devices are shown in Figure 6.3b. The spectrum appeared at the early of 400 nm in the sample of mCP:6 wt% DTPPDDA:0.5 wt% TBPe can be assigned to the emission from DTPPDDA. As the phosphorescence material of $(HFP)_2Ir(pic)$ was doped, energy transfer rate (k_{ET}) from DTPPDDA to TBPe became larger than radiative transition rate from

singlet state (k_r) of DTPPDDA, therefore diminishing the emission from DTPPDDA in the spectrum of mCP:8 wt% $(HFP)_2Ir(pic)$:6 wt% DTPPDDA:0.5 wt% TBPe. Second peaks of the spectra at ~490 nm were increased in the samples doped $(HFP)_2Ir(pic)$ from charge trapping on the electrical excitation. The J-V-L characteristics of the OLEDs are shown in Figure 6.3c. The turn-on voltages were the same with 3.9 V in all the OLED devices regardless of the constituents in the host of mCP, indicating that hole transporting property of mCP was governing at low current densities for all the different EML environments here. Figure 6.3d shows EQEs of the OLEDs to current densities. The max EQE was decreased from 5.6% to 4.5% in the OLED of mCP:6 wt% DTPPDDA:0.5 wt% TBPe from addition of 6 wt% DTPPDDA which has low PLQY.[51] However, when the phosphorescent material of $(HFP)_2Ir(pic)$ was added as in mCP:8 wt% $(HFP)_2Ir(pic)$:0.5 wt% TBPe, the EQE was increased from 5.6% to 10.1% from sensitizing effect by having iridium complex in the EML. Due to the low doping ratio of 0.5 wt% of TBPe, only Förster energy transfer from the other constituents to the emitter could be present without having to consider Dexter energy transfer. Maximum EQE was the highest when the both TADF material and Iridium complex were used with CT type material in the EML as in mCP:8 wt% $(HFP)_2Ir(pic)$:6 wt% DTPPDDA:0.5 wt% TBPe. The EQE of 12.3% was achieved in mCP:8 wt% $(HFP)_2Ir(pic)$:6 wt% DTPPDDA:0.5 wt% TBPe from the both HAE and sensitizing effect. Device performances of the blue fluorescent OLEDs are summarized in Table 6.3.

In order to quantitatively judge how much of triplets turned into light on using new concept for EML, optical simulation was performed to compare the theoretical and achieved EQEs were compared for the each OLED structures as shown in Table 1.[5] The horizontal dipole ratio of mCP:0.5 wt% TBPe was measured as 0.73 as shown in Figure 6.6. The photoluminescence quantum yields (PLQYs) and the horizontal dipole ratio were achieved using an integrating sphere and the angle dependent PL spectra, respectively.5.[35-38] $\eta_{s/T}$ increased from the near theoretical singlet exciton production of 0.23 to 0.27 as the TADF material doped into mCP:0.5 wt% TBPe. However, when the iridium complex of $(HFP)_2Ir(pic)$ was doped, $\eta_{s/T}$ increased by almost 2.5

times, showing that sensitizing effect by the heavy metal complex with high PLQY act more strongly than that from the TADF material with low PLQY. On the implementation of the both iridium complex of $(HFP)_2Ir(pic)$ and the CT type material of DTPPDDA, $\eta_{S/T}$ was increased to 0.94, which is 4 times higher than the case of mCP:0.5 wt% TBPe. The result shows that heavy metal complex induced HAE to enhance RISC of the CT type material and the both materials worked as sensitizers, increasing EL efficiency of the blue fluorescent OLED.

Blue fluorescent OLEDs of TBPe in the different kind of host systems were fabricated in order to verify if the combination of TADF and phosphorescent material still enhances EL efficiency of the OLEDs in the other type of host environment. The host material was switched from the single host of mCP to the exciplex of mCP:B3PYMPM in the OLED structure of ITO (70 nm)/6 wt % ReO3:mCP (45 nm)/mCP (15 nm)/mCP:B3PYMPM: Dopants (15 nm)/B3PYMPM (20 nm)/4 wt % Rb2CO3:TSPO1 (55 ㎚)/Al (100 ㎚). For Ir complex, $Ir(ppz)_3$ was selected from the convenience of triplet confinement (Figure 6.7a and 6.7b) and utilized with the same TADF material and fluorescent emitter as in the previous case. The EL efficiencies were similar in the cases of mCP:B3PYMPM:0.5 wt% TBPe and mCP:B3PYMPM:10 wt% DTPPDDA: 0.5 wt% TBPe with maximum EQE of ~3%.

On the doping of 10 wt% of $Ir(ppz)_3$, EQEs were increased to 6.5% and 7% in the cases of mCP:B3PYMPM:10 wt% $Ir(ppz)_3$:0.5 wt% TBPe and mCP:B3PYMPM:10 wt% $Ir(ppz)_3$: 10 wt% DTPPDDA:0.5 wt% TBPe, respectively, The result shows the similar enhancing characteristics in device performance just as in the case of the single host of mCP. Therefore, this shows the possibility of increase in EL efficiency assisted by the both induced HAE and increased energy transfer from sensitizing effect for having both Ir complex and TADF material regardless of host materials. However, $Ir(ppz)_3$ is known to have low PLQY from large non-radiative transition from triplet state, which is probably the reason for relatively lower EQEs compared to the other case of single host. Therefore, optimizing the EML structure with highly efficient heavy metal complex as well as TADF material will further improve device performance of the blue fluorescent OLEDs

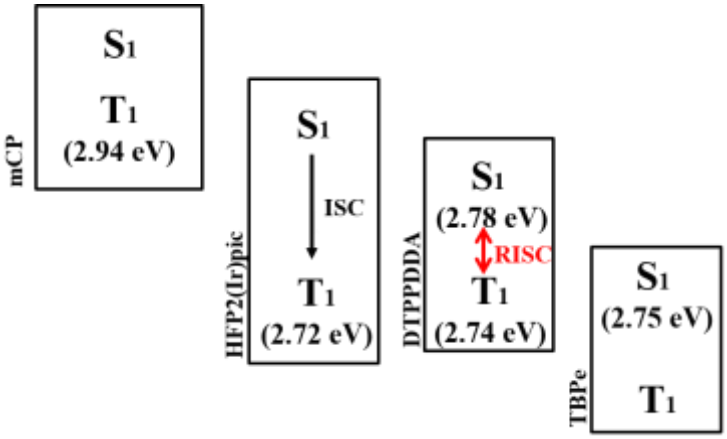

Figure 6.5 Singlet and triplet energy levels of mCP, HFP_2(Ir)pic, DTPPDDA and TBPe.

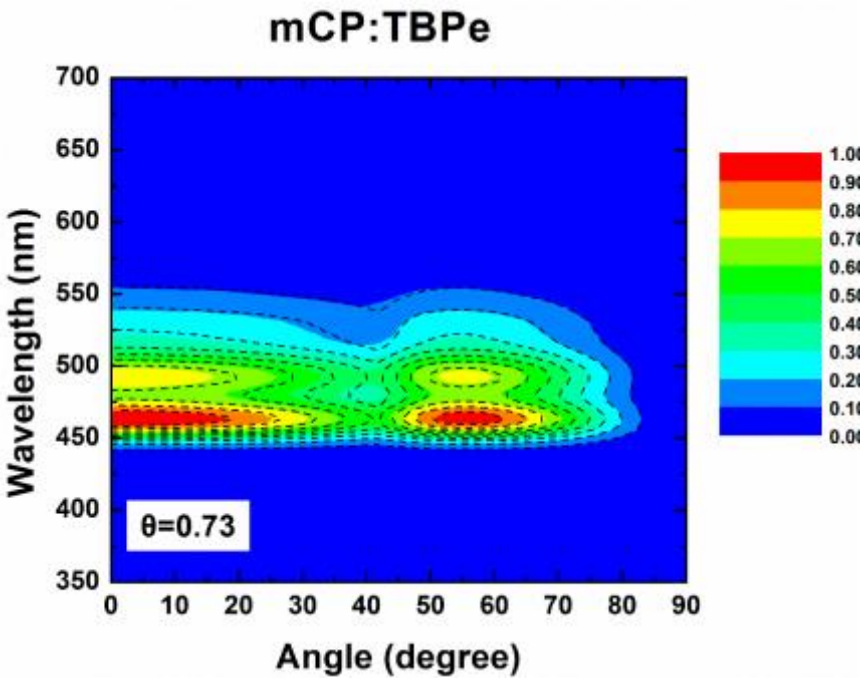

Figure 6.6 Transition dipole moment of TBPe measured with mCP:0.5 wt% TBPe film.

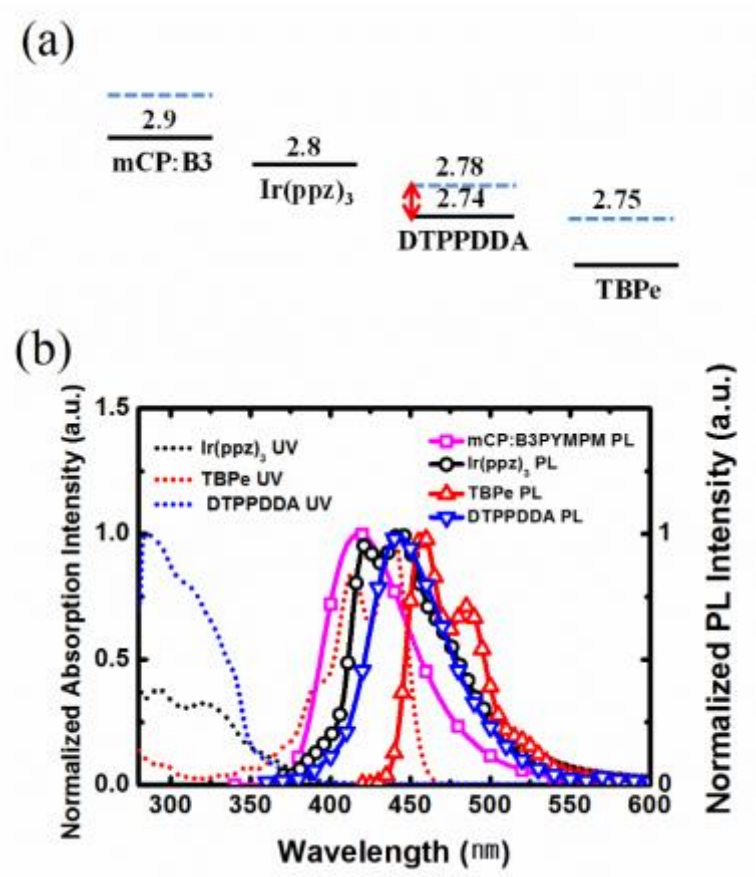

Figure 6.7 (a) singlet(solid line) and triplet levels(dotted line) and (b) absorption and PL spectra of mCP: B3PYMPM, $Ir(ppz)_3$, DTPPDDA and TBPe.

Table 6.2 Transient decay rates of the samples.

EML	Prompt	Delayed
mCP:0.5 wt% TBPe	8 ns	-
mCP:6 wt% DTPPDDA:0.5 wt% TBPe	7 ns	-
mCP:8 wt% $(HFP)_2Ir(pic)$:0.5 wt%TBPe	7.7 ns	51.7 ns, 266.4 ns, 974.5 ns
mCP:6 wt% DTPPDDA:8 wt% $(HFP)_2Ir(pic)$:0.5 wt%TBPe	8.3 ns	64 ns, 331 ns, 3.9 μs

Table 6.3 Device performances of the blue fluorescent OLEDs of mCP:0.5 wt% TBPe, mCP:6 wt% DTPPDDA:0.5 wt% TBPe, mCP:8 wt% $(HFP)_2Ir(pic)$:0.5 wt%TBPe and mCP:6 wt% DTPPDDA:8 wt% $(HFP)_2Ir(pic)$:0.5 wt%TBPe.

Device of	Turn On (V)	Max. EQE (%)	at 300 cd/m^2		
			EQE (%)	Voltage (V)	CIE
mCP:0.5 wt% TBPe	3.9	5.6	4.8	6.2	(0.13, 0.22)
mCP:6 wt% DTPPDDA:0.5 wt% TBPe	3.9	4.5	2.4	6.8	(0.13, 0.20)
mCP:8 wt% $(HFP)_2Ir(pic)$:0.5 wt%TBPe	3.9	10.1	1.7	7.6	(0.15, 0.24)
mCP:6 wt% DTPPDDA:8 wt% $(HFP)_2Ir(pic)$:0.5 wt%TBPe	3.9	12.3	4.8	6.4	(0.15, 0.24)

6.4 Conclusion

Addition to 25% of singlet-exciton production on the electrical excitation, 69% of triplet excitons were harvested by doping iridium complex and CT type material into EML where the conventional blue fluorescent dye of TBPe was used for the emission. The EQEs were increased from 5.6% to 12.3% as Ir complex of $(HFP)_2Ir(pic)$ and TADF material of DTPPDDA were utilized in mCP:0.5 wt% TBPE. $\eta_{s/T}$ was increased from 0.23 to 0.94, showing that nearly all the triplets were harvested in the blue fluorescent OLED system. In the different case of having the exciplex of mCP:B3PYMPM as host materials, by doping both $Ir(ppz)_3$ and DTPPDDA, the blue fluorescent OLEDs show similar enhancing characteristics in EQEs comparable to the case of single host of mCP. The results indicate that both the enhanced RISC induced by HAE and sensitizing effect facilitated to improve EL efficiency of blue fluorescent OLEDs. However, the study shows that there could be margin for further improvement in device performance of blue fluorescent OLED if TADF and phosphorescent material with high PLQY can be utilized.

Chapter 7. Summary and Outlook

In order to replace phosphorescent organic light emitting diodes (OLEDs), which are basically toxic and expensive for containing heavy metal, with fluorescent OLEDs, electroluminescence (EL) efficiency of fluorescent OLEDs need to be greatly improved. Among three primary colors, especially blue fluorescent OLED is being used commercially in spite of its low EL efficiency due to its higher stability than phosphorescent OLEDs. Low efficiency of fluorescent OLEDs are due to their nature of only 25% of exciton taking part into emission on electrical excitation. However, if singlet-triplet splitting (ΔE_{ST}) was small enough then 100% triplets would be able to reverse intersystem cross (RISC) into singlet excited states contributing to radiation.

Even with the importance of blue fluorescent OLEDs, there has been lack of insight or guidelines on either synthetically and in the aspect of designing device structure, possibly due to the difficulty in satisfying wide band gap emitter for blue emission. Therefore, in order to clearly understand the potential of fluorescent OLED, we had to answer to the questions : 1) Is it possible to turn all the triplets into light in a fluorescent OLED ? 2) Can there be efficient host system for blue fluorescent OLED? 3) Is it possible to achieve high EL efficiency and color purity in a same blue fluorescent OLED, simultaneously? 4) Is it possible to achieve high EL efficiency in conventional blue fluorescent OLEDs?

In Chapter 2, We have proposed the exciplex system of mCP:B3PYMPM for green fluorescent OLED where thermally active delayed fluorescent (TADF) emitter of 4CzIPN was utilized, which the emitter showed high photoluminescence quantum yield (PLQY) yet with low external quantum efficiency of ~18%. The exciplex-forming cohosts contributed efficient ET and charge balance in the system. Large distribution of exciton in exciplex cohost lowered exciton density in EML resulting in the smallest efficiency roll-off among the other reported OLEDs using the same fluorescent emitter. This research reported for the first time that 100% triplets can be

harvested to singlet for emission in fluorescent OLED with unprecedented external quantum efficiency (EQE) of 30%.

In Chapter 3, the efficient mixed cohost of mCP:PO15 was suggested for the ideal bipolar host for blue fluorescent OLED to alter the high dependency on single host material with high triplet energy such as DPEPO. The mixed cohost of mCP:PO15 established near perfect charge balance between hole and electron in emitting layer, drawing full potential of the ability of underestimated blue TADF emitter of 2CzPN. As a result, EQE was enhanced from 13% to 21.8% in blue fluorescent OLEDs of 2CzPN.

However, there was no report on blue fluorescent OLED achieving color purity and high EL efficiency at the same time. In Chapter 4, The highly efficient blue fluorescent OLED with deep blue emission was realized by using TADF dopant of DTPDDA in mixed cohost of mCP:TSPO1. The unprecedented EL efficiency of 22.3% and deep blue emission of 0.198 in y-value of Commission Internationale de L'Eclairage (CIE) were reported in this article. The azasiline unit was firstly used for blue electroluminescence as a donor unit in charge transfer (CT) type material. By having silicon in the donor, the level of highly occupied molecular orbital (HOMO) was lowered suitable for deep blue emission. The OLED reported in this article is still one of the most efficient pure blue fluorescent OLEDs.

As azasiline unit was proven to be a solid donor for blue TADF material, so further research was necessary to investigate the ability of the moiety. Three different blue TADF emitters were systematically synthesized and implemented in the mixed cohost of mCP:TSPO1 to investigate the correlation between design parameters of TADF material and OLED device performance, using the azaziline unit, in Chapter 5. DTPPDDA in the formation of donor–connector–acceptor (D–C–A) materials resulted in deep blue emission with CIE coordinate of (0.151, 0.087), close to the blue standard of the National Television System Committee (NTSC) of (0.140, 0.080) with 4.7% EQE. In the donor–acceptor–donor (D–A–D) type materials of BDAPM and SPDDA, carbonyl and sulfone units were used as the acceptors, respectively. The blue fluorescent OLEDs

containing BDAPM and SPDDA demonstrated 11.4% and 2.3% EQEs with CIE y-values of 0.310 and 0.107, respectively.

However, emitting from TADF material itself cause broad EL spectrum and lifetime issues. In order to remove these drawbacks, conventional fluorophore can be used as an emitter, where assisted dopants either phosphorescent or TADF material is strategically implemented to enhance spin mixing of singlet and triplet excited states.). In Chapter 6, almost all the triplets were harvested in the conventional blue fluorescence OLED by promoting both sensitizing and HAE through co-doping TADF material and phosphorescent material into EML. Comparison of the theoretical and experimental data indicates that $\eta_{s/T}$ was increased from 0.23 to 0.94 with increased EQE from 5.6% to 12.3% in blue fluorescent OLED when the both TADF material and phosphorescent material were doped together as assisted dopants, indicating the nearly all the triplets harvested in the conventional blue fluorescent OLED.

Our approach on the development of device structure of fluorescent OLEDs, especially blue, in order to draw full potential of fluorescent OLEDs have been proven to be efficient throughout the works. We believe that the present work will be of interest to engineers and scientist in this field of study, and will even promote the research to enhance efficiency of the fluorescent OLED device. However, lifetime data is not included in this work, which need to be further investigated in order to clear the issue.

Bibliography

[1] C. W. Tang, S. A. VanSlyke, *Appl. Phys. Lett.* **1987**, 51, 913.

[2] M. A. Baldo, D. F. O'Brien, Y. You, A. Shoustikov, S. Sibley, M. E. Thompson, S. R. Forrest, *Nature* **1998**, 395, 151.

[3] H. Uoyama, K. Goushi, K. Shizu, H. Nomura, C. Adachi, *Nature* **2012**, 492, 234.

[4] K. Goushi, K. Yoshida, K. Sato, C. Adachi, *Nat. photon.* **2012**, 6, 253.

[5] S.-Y. Kim, W.-I. Jeong, C. Mayr, Y.-S. Park, K.-H. Kim, J.-H. Lee, C.-K. Moon, W. Brütting, J.-J. Kim, *Adv. Funct. Mater.* **2013**, 23, 3896.

[6] C. K. Chiang, C. R. Fincher, Jr., Y. W. Park, A. J. Heeger, H. Shirakawa, E. J. Louis, S. C. Gau, A. G. MacDiarmid, *Phys. Rev. Lett.* **1977**, 39, 1098.

[7] J.-H. Lee, J.-J. Kim, *Phys. Status Solidi A* **2012**, 209, 1399.

[8] H. Nakanotani, T. Higuchi, T. Furukawa, K. Masui, K. Morimoto, M. Numata, H. Tanaka, Y. Sagara, T. Yasuda, C. Adachi, *Nat. Comm.*, **2014**, 5, 4016.

[9] T.-A Lin, T. Chatterjee, W.-L. Tsai, W.-K. Lee, M.-J. Wu, M. Jiao, K.-C. Pan, C.-L. Yi, C.-L. Chung, K.-T. Wong, C.-C. Wu, *Adv. Mater.* **2016**, 28, 6976.

[10] R. Komatsu, T. Ohsawa, H. Sasabe, K. Nakao, Y. Hayasaka, J. Kido, *ACS Appl. Mater. Interfaces*, **2017**, 9, 4742.

[11] N. J. Turro, *Modern Molecular Photochemistry*, University Science Books, Mill Vally, U.S.A, **1991**.

[12] J.-H. Lee, S. Lee, S.-J. Yoo, K.-H. Kim, J.-J. Km, *Adv. Funct. Mater.* **2014**, 24, 4681.

[13] Y.-S. Park, K.-H. Kim, J.-J. Kim, *Appl. Phys. Lett.* **2013**, 102, 153306.

[14] K. Goushi, C. Adachi, *Appl. Phys. Lett.* **2012**, 101, 023306.

[15] W.-Y. Hung, G.-C. Fang, Y.-C. Chang, T.-Y. Kuo, P.-T. Chou, S.-W. Lin, K.-T. Wong, *ACS Appl. Mater. Interfaces* **2013**, 5, 6826.

[16] J. Li, H. Nomura, H. Miyazaki, C. Adachi, *Chem. Commun.* **2014**, 50, 6174.

[17] W.-Y. Hung, G.-C. Fang, S.-W. Lin, S.-H. Cheng, K.-T. Wong, T.-Y. Kuo, P.-T. Chou, *Sci.*

Rep. **2014**, 4, 5161.

[18] T. Zhang, B. Chu, W. Li, Z. Su, Q. M. Peng, B. Zhao, Y. Luo, F. Jin, X. Yan, Y. Gao, H. Wu, F. Zhang, D. Fan, J. Wang, *ACS Appl. Mater. Interfaces* **2014**, 6, 11907.

[19] X.-K. Liu, Z. Chen, C.-J. Zheng, C.-L. Liu, C.-S. Lee, F. Li, X.-M. Ou, X.-H. Zhang, *Adv. Mater*. **2015**, 27, 2378.

[20] T. Zhang, B. Zhao, B. Chu, W. Li, Z. Su, X. Yan, C. Liu, H. Wu, Y. Gao, F. Jin, F. Hou, *Sci. Rep.* **2015**, 5, 10234.

Chapter 2

[21] S. Park, O.-H. Kwon, Y.-S. Lee, D.-J. Jang, S.-Y. Park, *J. Phys. Chem*. **2007**, A111, 9649.

[22] D. Y. Kondakov, *J. Appl. Phys*. **2007**, 102, 114504.

[23] J. Li, T. Nakagawa, J. Macdonald, Q. Zhang, H. Nomura, H. Miyazaki, C. Adachi, *Adv. Mater*. **2013**, 25, 3319.

[24] V. Jankus, C.–J. Chiang, F. Dias, A. P. Monkman, *Adv. Mater*. **2013**, 25, 1455.

[25] Q. Zhang, B. Li, S. Huang, H. Nomura, H. Tanaka, C. Adachi, *Nature Photonics* **2014**, 8, 326.

[26] D. Tanaka, H. Sasabe, Y.-J. Li, S.-J. Su, T. Takeda, J. Kido, *Jpn. J. Appl.Phys*. **2007**, 46, L10.

[27] M. G. Helander, Z. B. Wang, J. Qiu, M. T. Greiner, D. P. Puzzo, Z. W. Liu, Z. H. Lu, *Science* **2011**, 332, 944.

[28] Y.–S. Park, S. Lee, K.–H. Kim, S.–Y. Kim, J.–H. Lee, J.–J. Kim, *Adv. Funct. Mater*. **2013**, 23, 4914.

[29] S. Lee, K.–H. Kim, D. Limbach, Y.–S. Park, J.–J. Kim, *Adv. Func. Mat.* **2013**, 23, 4105.

[30] S. Lee, D. Limbach, K.–H. Kim, S.–J. Yoo, Y.–S. Park, J.–J. Kim, *Org. Electron*. **2013**, 14, 1856.

[31] C. W. Lee, J. Y. Lee, *Adv. Mater*. **2013**, 25, 5450.

[32] K.–H. Kim, C.–K. Moon, J.–H. Lee, S.–Y. Kim, J.–J. Kim, *Adv. Mater*. **2014**, 26, 3844.

[33] H. Shin, S. Lee, K.–H. Kim, C.–K. Moon, S.–J. Yoo, J.–H. Lee, J.–J. Kim, *Adv. Mater*. **2014**, 26, 4730.

[34] K.–H. Kim, S. Lee, C.–K. Moon, S.–Y. Kim, Y.–S. Park, J.–H. Lee, J. W. Lee, J. Huh, Y. You, J.–J. Kim, 2013, *Nat. Commun*. **2014**, 5, 4769

[35] W.–I. Jeong, S. Y. Kim, J.–J. Kim, and J. W. Kang, *Chem. Phys*. **2009**, 355, 25.

[36] J. Frischeisen, D. Yokoyama, C. Adachi, W. Brütting, *Appl. Phys. Lett*. **2010**, 96, 073302.

[37] P. Liehm, C. Murawski, M. Furno, B. Lüssem, K. Leo, M. C. Gather, *Appl. Phys. Lett*. **2012**, 101, 253304.

[38] L. Penninck, F. Steinbacher, R. Krause, K. Neyts, *Org. Electron*. **2012**, 13, 3079.

[39] D.-S. Leem, H.-D. Park, J.-W. Kang, J.-H. Lee, J. W. Kim, J.-J. Kim, *Appl. Phys. Lett*. **2007**, 91, 011113.

[40] J.-H. Lee, D.-S. Leem, H.-J. Kim, J.-J. Kim, *Appl. Phys. Lett*. **2009**, 94, 123306.

[41] J.-H. Lee, D.-S. Leem, J.-J. Kim, *Org. Electron*. **2010**, 11, 486.

[42] D.-S. Leem, S.-Y. Kim, J.-J. Kim, M.-H. Chen, C.-I. Wu, *ECS Solid State Lett*. **2009**, 12, J8.

[43] M.-H. Chen, Y.-H. Chen, C.-T. Lin, G.-R. Lee, C.-I Wu, D.-S. Leem, J.-J. Kim, T.-W. Pi, *J. Appl. Phys.* **2009**, 105, 113714.

[44] J.–H. Lee, P.–S. Wang, H.–D. Park, C.–I. Wu, J.–J. Kim, *Org. Electron*. **2011**, 12, 1763.

[45] M. J. Frisch, G. W. Trucks, H. B. Schlegel, G. E. Scuseria, M. A. Robb, J. R. Cheeseman, G. Scalmani, V. Barone, B. Mennucci, G. A. Petersson, H. Nakatsuji,M. Caricato, X. Li, H. P. Hratchian, A. F. Izmaylov, J. Bloino, G. Zheng, J. L. Sonnenberg,M. Hada, M. Ehara, K. Toyota, R. Fukuda, J. Hasegawa, M. Ishida, T. Nakajima, Y. Honda, O. Kitao, H. Nakai, T. Vreven, J. A.Jr. Montgomery, J. E. Peralta, F. Ogliaro, M. Bearpark, J. J. Heyd, E. Brothers, K. N. Kudin, V. N. Staroverov, R. Kobayashi, J. Normand, K. Raghavachari, A. Rendell, J. C. Burant, S. S. Iyengar, J. Tomasi, M. Cossi, N. Rega, J. M. Millam, M. Klene, J. E. Knox, J. B. Cross, V. Bakken, C. Adamo, J. Jaramillo, R. Gomperts, R. E. Stratmann, O. Yazyev, A. J. Austin, R. Cammi, C. Pomelli, J. W. Ochterski, R. L. Martin, K. Morokuma, V. G. Zakrzewski, G. A.Voth, P. Salvador,

J. J. Dannenberg, S. Dapprich, A. D. Daniels, O. Farkas, J. B. Foresman, J. V. Ortiz, J. Cioslowski, D. J. Fox, *Gaussian, Inc., Wallingford CT*, **2009**.

[46] K. Masui, H. Nakanotani, C. Adachi, *Org. Electron.* **2013**, 14, 2721.

[47] S. Wu, M. Aonuma, Q. Zhang, S. Huang, T. Nakagawa, K. Kuwabara, C. Adachi, *J. Mater. Chem. C*, **2014**, 421.

[48] S. Hirata, Y. Sakai, K. Masui, H. Tanaka, S. Y. Lee, H. Nomura, N. Nakamura, M. Yasumatsu, H. Nakanotani, Q. Zhang, K. Shizu, H. Miyazaki, C. Adachi, *Nat. Mater*. **2015**, 14, 330.

[49] Q. Zhang, D. Tsang, H. Kuwabara, Y. Hatae, B. Li, T. Takahashi, S. Y. Lee, T. Yasuda, C. Adachi, *Adv. Mater.* **2015**, 27, 2096.

[50] M. Kim, S. K. Jeon, S.-H. Hwang, J. Y. Lee, *Adv. Mater.* **2015**, 27, 2515.

[51] J. W. Sun, J. Y. Baek, K.-H. Kim, C. –K. Moon, J. –H. Lee, S.-K. Kwon, Y.-H. Kim, J.-J. Kim, *Chem. Mater.* **2015**, 27, 6675.

[52] D. R. Lee, M. Kim, S. K. Jeon, S.-H. Hwang, C. W. Lee, J. Y. Lee, *Adv. Mater*. **2015**, 27, 5861.

[53] R. Komatsu, H. Sasabe, Y. Seino, K. Nakao, J. Kido, *J. Mater. Chem. C* **2016**, 4, 2274.

[54] S. Naka, K. Shinno, H. Okada, H. Onnagawa, K. Miyashita, *Jpn. J. Appl. Phys.* **1994**, 33, 1772.

[55] J.-W. Kang, S.-H. Lee, H.-D. Park, W.-I Jeong, K.-M Yoo, Y.-S. Park, J.-J Kim, *Appl. Phys. Lett*. **2007**, 90, 223508.

[56] N. Chopra, J. S. Swensen, E. Polikarpov, L. Cosimbescu, F. So, A. B. Padmaperuma, *Appl. Phys. Lett.* **2010**, 97, 033304.

[57] A. Chaskar, H.-F. Chen, K.-T Wong, *Adv. Mater*. **2011**, 23, 3876.

[58] J. W. Sun, J.-H. Lee, C.-K. Moon, K.-H Kim, H. Shin, J.-J. Kim, *Adv. Mater.* **2014**, 26, 5684.

[59] X. Cai, A. B. Padmaperuma, L. S. Sapochak, P. A. Vecchi, P. E. Burrows, *Appl. Phys. Lett*. **2008**, 92, 083308.

[60] Y. J. Cho, K. S. Yook, J. Y. Lee, *Adv. Mater*. **2014**, 26, 4050.

[61] B. S. Kim, J. Y. Lee, *Adv. Funct. Mater*. **2014**, 24, 3970.

[62] D. R. Lee, B. S. Kim, C. W. Lee, Y. Im, K. S. Yook, S.-H. Hwang, J. Y. Lee, *ACS Appl. Mater. Interfaces*, **2015**, 7, 9625.

[63] Y. Seino, H. Sasabe, Y.-J. Pu, J. Kido, *Adv. Mater*. **2014**, 26, 1612.

[64] M. A. Baldo, C. Adachi, S. R. Forrest, *Phys. Rev. B: Condens. Matter Mater. Phys*. **2000**, 62, 10967.

[65] C. Murawski, K. Leo, M. Gather, *Adv. Mater.* **2013**, 25, 6801.

[66] Q. Zhang, J. Li, K. Shizu, S. Huang, S. Hirata, H. Miyazaki, C. Adachi, *J. Am. Chem. Soc.* **2012**, 134, 14706.

[67] H. Tanaka, K. Shizu, H. Miyazaki, C. Adachi, *Chem. Commun.* **2012**, 48, 11392.

[68] R. H. Young, A. M. Feinberg, J. P. Dinnocenzo, S. Farid, *Photochem. Photobiol*. **2015**, 91, 624.

[69] S. Huang, Q. Zhang, Y. Shiota, T. Nakagawa, K. Kuwabara, K. Yoshizawa, C. Adachi, *J. Chem. Theory Comput.* **2013**, 9, 3872.

[70] H. Sun, C. Zhong, J. L. Bredas, *J. Chem. Theory Comput*. **2015**, 11, 3851.

[71] W. Liu, C.-J. Zheng, K. Wang, Z. Chen, D.-Y. Chen, F. Li, X.-M. Ou, Y.-P. Dong, X.-H. Zhang, *ACS Appl. Mater. Interfaces*, **2015**, 7(34), 18930.

[72] L.-S. Cui, J. U. Kim, H. Nomura, H. Nakanotani, C. Adachi, *Angew. Chem., Int. Ed.* **2016**, 55, 6864.

[73] S. Y. Lee, T. Yasuda, Y. S. Yang, Q. Zhang, C. Adachi, *Angew. Chem*. **2014**, 126, 6520.

[74] M. Numata, T. Yasuda, C. Adachi, *Chem. Commun*. **2015**, 51, 9443.

[75] D. Zhang, M. Cai, Y. Zhang, D. Zhang, L. Duan, *Mater. Horiz*. **2016**, 3, 145.

[76] J. S. Kang, T. R. Hong, H. J. Kim, Y. H. Son, R. Lampande, B. Y. Kang, C. Lee, J.-K. Bin, B. S. Lee, J. H. Yang, J. Kim, S. Park, M. J. Cho, J. H. Kwon, D. H. Choi, *J. Mater. Chem. C*. **2016**, 4, 4512.

[77] T. Hatakeyama, K. Shiren, K. Nakajima, S. Nomura, S. Nakatsuka, K. Kinoshita, J. Ni, Y. Ono, T. Ikuta, *Adv. Mater.* **2016**, 28, 2777.

[78] I. S. Park, J. Lee, T. Yasuda, *J. Mater. Chem. C.* **2016**, 4, 7911.

[79] S. Y. Lee, C. Adachi, T. Yasuda, *Adv. Mater.* **2016**, 28, 4626.

[80] K. Nasu, T. Nakagawa, H. Nomura, C.-J. Lin, C.-H. Cheng, M.-R. Tseng, T. Yasuda, C. Adachi, *Chem. Commun.* **2013**, 49, 10385.

[81] Y. Tao, K. Yuan, T. Chen, P. Xu, H. Li, R. Chen, C. Zheng, L. Zhang, W. Huang, *Adv. Mater.* **2014**, 26, 7931.

[82] M. Inoue, T. Serevičius, H. Nakanotani, K. Yoshida, T. Matsushima, S. Juršėnasc, C. Adachi, *Chem. Phys. Lett.* **2016**, 644, 62.

[83] J. W. Sun, J. Y. Baek, K.-H. Kim, J.-S. Huh, S.-K. Kwon, Y.-H. Kim, J.-J. Kim, *J. Mater. Chem. C.* **2017**, 5, 1027.

[84] I. H. Lee, W. Song, J. Y. Lee, S.-H. Hwang, *J. Mater. Chem. C.* **2015**, 3, 8834.

[85] M. A. Baldo, M. E. Thompson, S. R. Forrest, *Nature*, **2000**, 403, 750.

[86] B. W. D'Andrade, M. A. Baldo, C. Adachi, J. Brooks, M. E. Thompson, S. R. Forrest, *Appl. Phys. Lett.* **2001**, 79, 1045.

[87] X. R. Wang, H. You, H. Tang, G. H. Ding, D. G. Ma, H. Tian, R. G. Sun, *J. Lumin*, **2008**, 128, 27.

[88] H.-G. Kim, K.-H. Kim, C.-K. Moon, J.-J. Kim, *Adv. Optical Mater.* **2017**, 5, 1600749.

[89] J.-B. Kim, S.-H. Han, K. Yang, S.-K. Kwon, J.-J. Kim, Y.-H. Kim, *Chem. Commun.*, **2015**, 51, 58.

초 록

유기발광소자는 현존하는 디스플레이 및 조명을 구현하는 방법중 독보적인 우위를 점하고 있다. 기존 업계에서 내세우던, 단순한 색순도 및 시야각의 장점을 벗어나, 기판의 선택에 따라 유연하게 휘어지고 투명하게 제작될 수 있어, 유기발광소자의 적용범위는 계속 확장되고 있는 실정이다. 이에 따라, 그 어느때보다도 유기발광소자의 효율 및 수명을 증진시키는 연구가 물질 및 소자 측면에서 활발하게 진행되고 있다. 이러한 관점에서, 3원색중 청색 유기발광소자 연구가 가장 활발한데, 그 이유로 인광물질과 형광물질에 기반한 청색 유기발광소자의 장점 및 단점에 기인한 경쟁이 있다. 인광물질에 기반한 청색 유기발광소자는 고효율의 외부양자효율을 구현할 수 있지만 단수명으로 인해 상용화의 한계에 도달해 있어, 낮은 외부양자효율을 보이는 형광물질 기반의 청색 유기발광소자가 상용화 되어 사용되고 있다. 하지만, 이론적으로 형광유기발광소자는 25%의 여기자만이 발광에 사용되어, 인광유기발광소자의 외부양자 효율에 접근할 수 없다.

이러한 형광유기발광소자의 낮은 외부양자효율을 높이기 위한 방법으로, 최근 전하이동 복합체의 역항간 교차를 이용하여 삼중항 여기자를 수확한 연구가 활발히 보고 되었다. 분자내 전하이동 복합체인 열활성화지연형광 (TADF) 발광체는 삼중항-일중항 에너지 차이를 줄여 삼중항 여기자를 발광 가능한 단일항 여기자로 수확할 수 있다. 들뜬상태 분자간 전하이동 복합체인 엑시플렉스도 삼중항-일중항 에너지 차이가 작아서 역항간 교차를 이용하여 효율적인 삼중항 수확을 할 수 있다.

본 논문에서는 이러한 역항간교차 방법을 활용해 형광유기발광소자의 외부양자효율을 증진시키는 방법을 유기발광 소자적 측면에서 연구하였다.

제 2장에서는, 형광유기발광소자의 외부양자효율이 인광유기발광소자에

근접할 수 있는지를 확인하였다. 엑시플렉스는 전술한 바와 같이 삼중항-일중항 차이가 적어 역항간 교차를 이용할 수 있는 장점이외에도, 호스트 물질로 사용시 발광층으로의 주입장벽이 없어져 전하-정공 균형을 맞출 수 있으며, 발광층내 여기자가 넓게 분포하여, 여기자 농도에 의한 급격한 효율감소를 방지할 수 있는 등의 장점이 있다. 엑시플렉스에서 도판트로의 에너지 전이를 고려하여, 발광체로는 기존 높은 절대발광효율에도 낮은 외부양자효율이 보고된 바 있는 녹색 열활성화지연형광 물질을 사용하였다. 제작된 녹색형광유기발광소자는 30%의 외부양자효율을 나타내어, 인광유기발광소자의 외부양자효율과 동일한 외부양자효율이 가능함을 증명하였다.

하지만, 엑시플렉스는 이종의 물질 각각의 최고 점유 분자궤도 (HOMO)와 최저 비점유 분자궤도 (LUMO)에 의해 형성되어, 높은 삼중항에너지가 요구되는 청색 도판트에 적합한 엑시플렉스 호스트의 발견이 용이하지 않다. 이에 따라, 소자에 적용시 엑시플렉스가 갖고 있는 양극성에서 나오는 전하균형의 장점을 사용할 수 있도록, 제 3장에서는 혼합 공동호스트를 사용한 고효율 청색형광유기발광소자를 연구하였다. 고효율의 높은 삼중항에너지의 호스트물질의 부재로, 현재까지 청색형광유기발광소자 연구는 단일호스트인 특정물질에 의존해 왔다. 본 연구에서는 높은 절대발광효율에도 불구하고 낮은 외부양자효율을 보이는 청색 열활성화지연형광 물질을 사용하여, 기존 보고된 ~13%의 외부양자효율 대비 향상된 21.8%의 외부양자효율을 발표하였다. 소자내에서 전기적 손실이 없을때를 가정한 이론적 한계수치와 동일한 외부양자효율이다. 소자적인 측면에서, 기존보고된 청색형광유기발광소자 대비 구동전압은 낮고, 20%가 넘는 외부양자효율을 보여 청색형광유기발광소자용으로 적용된 혼합 공동호스트가 효율적임을 증명하였다.

하지만, 기존 보고된 바에 의하면, 색순도와 소자성능 두가지를 모두 구현한 청색형광유기발광소자는 전무한 실정이었다. 제 4장과 5장에서는, 혼합 공동호스트에 아자질린과 트리아진 물질을 기반으로하는 청색열활성화지연형광 발광체를 적용하여, 발광체의 원활한 역항간 교차와 혼합 공동호스트의 장점을 결합하여, 22.3%의 외부양자효율과 y-색좌표기준 0.2이하의 색 순도 높은 청색형광유기발광소자를 구현할 수 있었다. 이러한 결과를 통해 아자질린 물질이 갖는 열활성화지연형광물질에서의 공여체로서의 장점을 발견할 수 있었다. 아자질린 공여체를 활용한 다른 세가지 열활성화지연형광물질을 공동혼합호스트에 적용하여, 각각의 물질들이 갖는 구조와 수용체의 종류에 따른 현상을 소자 및 광물리적 측면에서 분석하였다.

하지만, 청색 열활성화지연형광 물질을 발광체로 사용시, 물질의 전하이동 특성에 따라 소자의 발광 스펙트럼이 넓어져 색수도가 떨어질 수 있으며, 장수명의 청색 열활성화지연형광 물질이 적어 실질적인 산업체 적용에 한계가 있을 수 있다. 이를 극복하기 위해, 일반 청색형광물질을 발광체로 사용하고, 이를 센시타이징 또는 중원자 효과(heavy atom effect)를 활용하여 외부양자효율을 향상시킬 수 있다. 제 6장에서는, 센시타이징과 중원자효과를 복합적으로 활용하여, 일반 청색형광물질 기반의 청색형광유기발광소자의 외부양자효율을 2.5배 이상 향상시킨 연구 결과이다. 본 연구에서 제안된 방법을 통해, 발광에 사용된 여기자가 기존 ~25%에서, ~94%로 증가하여, 일반청색형광유기발광소자에서 비발광 삼중항 여기자를 거의 모두 수확할 수 있었다.

주요어 : 유기발광소자, 청색형광, 열활성화지연형광, 엑시플렉스, 삼중항 수확, 역항간교차

학번 : 2013-30181

List of Publications

1. **Jin Won Sun**, Jeong-Hwan Lee, Chang-Ki Moon, Kwon-Hyeon Kim, Hyun Shin and Jang-Joo Kim, "A Fluorescent Organic Light-Emitting Diode with 30% External Quantum Efficiency", *Advanced Materials*, **2014**, 26, 5684.
2. **Jin Won Sun**, Jang Yeol Baek, Kwon-Hyeon Kim, Chang-Ki Moon, Jeong-Hwan Lee, Soon-Ki Kwon, Yun-Hi Kim and Jang-Joo Kim, "Thermally activated delayed fluorescence from azasiline based intramolecular charge-transfer emitter (DTPDDA) and a highly efficient blue light emitting diode", *Chemistry of Materials*, **2015**, 27, 6675.
3. **Jin Won Sun**, Kwon-Hyeon Kim, Chang-Ki Moon, Jeong-Hwan Lee and Jang-Joo Kim, "Highly Efficient Sky-Blue Fluorescent Organic Light Emitting Diode Based on Mixed Cohost System for Thermally Activated Delayed Fluorescence Emitter (2CzPN)", *ACS Applied Materials & Interfaces*, **2016**, 8 (15), 9806.
4. **Jin Won Sun**, Jang Yeol Baek, Kwon-Hyeon Kim, Jin-Suk Huh, Soon-Ki Kwon, Yun-Hi Kim and Jang-Joo Kim, "Azasiline-based thermally activated delayed fluorescence emitters for blue organic light emitting diodes", *Journal of Materials Chemistry C*, **2017**, 5, 1027.
5. **Jin Won Sun** and Jang-Joo Kim "Almost All the Triplets Harvested in Conventional Blue Fluorescent OLED", (to be submitted), **2017**.
6. Kwon-Hyeon Kim, Chang-Ki Moon, **Jin Won Sun**, Bomi Sim and Jang-Joo Kim "Triplet Harvesting by a Conventional Fluorescent Emitter Using Reverse Intersystem Crossing of Host Triplet Exciplex", *Advanced Optical Materials*, **2015**, 3(7), 895.

List of Patents

1. 김장주, **선진원**, 이정환, 김권현, "유기발광소자" (출원번호 14-0173253),
2. 김장주, **선진원** "유기발광소자" (출원번호 16-97024),
3. 김장주, 김권현, 김현구, **선진원** "호스트, 인광 도펀트 및 형광 도펀트를 포함하는 유기발광소자" (출원번호 15-24243)
4. Jang-Joo Kim, **Jin Won Sun**, Jeong-Hwan Lee, Kwon-Hyeon Kim "Organic light-emitting device" (US YPL1165 US),.
5. Jang-Joo Kim, **Jin Won Sun,** Organic light-emitting device (US 출원중)

List of Awards

1. "Highly Commended Student Poster Presentation Award", Light, Energy and the Environment Congress, December 3, 2014.

2. “Young Scientist Award”, European Materials Research Society (E-MRS) 2017 Spring Meeting, May 24, 2017.

List of Presentation

International Conference

1. **Jin Won Sun**, Jeong-Hwan Lee, Kwon-Hyeon Kim, and Jang-Joo Kim, "Fluorescent OLED overcoming phosphorescent OLED", SPIE Optics+Photonics 2014, Aug 17-21 (Aug 20), 2014, USA (Poster)

2. **Jin Won Sun**, Jeong-Hwan Lee, Chang-Ki Moon, Kwon-Hyeon Kim, Hyun Shin and Jang-Joo Kim, "A Fluorescent Organic Light Emitting Diode with 100% Internal Quantum Efficiency", OSA Optics & Photonics Congress: Light, Energy and Environment, December 2-5 (December 3), 2014, Australia (Poster)

3. **Jin Won Sun**, Kwon-Hyeon Kim, Yun-Hi Kim, Jang-Joo Kim, "Introducing a thermally activated delayed fluorescence emitter for a highly efficient blue fluorescent organic light emitting diode", SPIE Optics+Photonics 2015, August 9-13 (August 10), 2015, USA (Poster)

4. **Jin Won Sun**, Jang-Joo Kim, “Highly Efficient Fluorescent Organic Light Emitting Diodes by using Thermally Activated Delayed Fluorescence emitters”, E-MRS 2015, May 11~15 (May 13), 2015, France (Oral)

5. **Jin Won Sun**, Kwon-Hyeon Kim, Chang-Ki Moon, Jeong-Hwan Lee, Jang-Joo Kim, “Introducing a thermally activated delayed fluorescence emitter for a highly efficient blue fluorescent organic light emitting diode.” 2015 International Chemical Congress of Pacific Basin Societies (Pacifichem 2015), December 15-20 (December 17), 2015, USA (Poster)

6. **Jin Won Sun**, Jang-Joo Kim "Highly Efficient Blue Fluorscent Organic Light Emitting Diode Based on Intramolecular Charge-Transfer Emitter Using Azasilin Core", 2016 MRS Spring Meeting & Exhibit, March 28-April 1 (March 29), 2016, USA (Poster)

7. **Jin Won Sun**, Jang-Joo Kim, "Introducing a Thermally Activated Delayed Fluorescence emitter for a Highly Efficient Blue Fluorescent Organic Light Emitting Diode", 8th International Conference on Molecular Electronics (ELECMOL16), August 22-26 (August 23), 2016, France (Oral)

8. **Jin Won Sun**, Jang-Joo Kim, "Highly Efficient Sky-Blue Fluorescence from Organic Light Emitting Diode Utilizing Mixed Cohost system for Thermally Actively Delayed Fluorescence Emitter", OSA Light, Energy & Environment Congress, November 14-17 (November 14), 2016, Germany (Oral)

9. **Jin Won Sun**, Kwon-Hyeon Kim, Yun-Hi Kim, Jang-Joo Kim “Highly Efficient Blue Organic Light Emitting Dodes utilizing thermally activated delayed fluorescence material”, E-MRS 2017, May 22~26 (May 24), 2017, France (Oral)

Domestic Conference

1. **Jin Won Sun**, Jeong-Hwan Lee, Chang-Ki Moon, Kwon-Hyeon Kim, Hyun Shin and Jang-Joo Kim, "A Fluorescent Organic Light Emitting Diode with 100% Internal Quantum Efficiency", The 14th International Meeting on Information Display (iMiD 2014), August 26-29, 2014, Korea (Poster)

2. **Jin Won Sun**, Jeong-Hwan Lee, Chang-Ki Moon, Kwon-Hyeon Kim, Hyun Shin and Jang-Joo Kim, "Fluorescent Organic Light Emitting Diode with 100% Internal Quantum Efficiency", The International Workshop on Flexible & Printable Electronics 2014 (IWEFE 2014), November 5-7, 2014, Korea (Poster)

3. **Jin Won Sun**, Jeong-Hwan Lee, Chang-Ki Moon, Kwon-Hyeon Kim, Hyun Shin and Jang-Joo Kim, "Fluorescent OLED overcoming phosphorescent OLED", 2014 Materials Fair, September 25, 2014, Korea (Poster)

4. **Jin Won Sun**, Kwon-Hyeon Kim, Chang-Ki Moon, Jang-Joo Kim, "Highly efficient blue fluorescence from azasiline based thermally activated delayed fluorescence emitter", The 7th International Workshop on Flexible & Printable Electronics 2015 (IWFPE 2015), November 4-6 (November 5), 2015, Korea (Poster)

5. **Jin Won Sun**, Jeong-Hwan Lee, Chang-Ki Moon, Kwon-Hyeon Kim, Hyun Shin, Jang Joo Kim, "A Fluorescent Organic Light Emitting Diode with 100% Internal Quantum Efficiency", The International Symposium on Recent Advanes and Future Issues in Organic Electroluminscence (ISOEL2016), February 17-19 (February 18), 2016, Korea (Poster)

6. **Jin Won Sun**, Kwon-Hyeon Kim, Chang-Ki Moon, Jang-Joo Kim, "Highly Efficient Blue Fluorescent Organic Light Emitting Diode by using Azasiline based Thermally Activated Delayed Fluorescent Emitter", The International Symposium on Recent Advanes and Future Issues in Organic Electroluminscence (ISOEL2016), February 17-

19 (February 18), 2016, Korea (Poster)

7. **Jin Won Sun**, Jang-Joo Kim, "Highly Efficient Sky-Blue Fluorescence from Organic Light Emitting Diode Utilizing Mixed Cohost System", International Conference on Electronic Materials and Nanotechnology for Green Environment (ENGE 2016), November 6-9 (November 07), 2016, Korea (Poster)